

Cellular Selectivity and Kinetics of Clinical Kinase Inhibitors

Dissertation

zur Erlangung des Doktorgrades

der Naturwissenschaften

vorgelegt beim Fachbereich 14

der Johann Wolfgang-Goethe-Universität

in Frankfurt am Main

von

Lena Marie Berger, geborene Kilian

aus Essen

Frankfurt 2023

(D30)

vom Fachbereich 14 der

Johann Wolfgang-Goethe-Universität als Dissertation angenommen.

Dekan: Prof. Dr. C. Glaubitz

Gutachter: Prof. Dr. Stefan Knapp, Prof. Dr. Eugen Proschak

Datum der Disputation: Montag, der 27.02.2023

Acknowledgement/ Danksagung

Table of Contents

Acknowledgement/ Danksagung	V
Table of Contents	VII
1. Summary	1
2. Zusammenfassung (German Summary 5-Page)	5
3. Introduction	11
3.1 Function and dysfunction of protein kinases	11
3.1.1 Human protein kinases share a highly conserved architecture	13
3.1.2 Human protein kinases as key proteins in signalling health and disease	15
3.1.3 Essential eukaryotic pre-mRNA splicing process is controlled by protein kinases	16
3.2 Targeting dysregulated proteins by small molecule inhibition	19
3.2.1 Different types of small molecule protein kinases inhibitors	20
3.2.2 Promiscuity of protein kinases	23
3.2.3 Targeting understudied kinases – the “dark kinome”	23
3.2.4 Classification of small molecule protein kinase inhibitors	24
3.3 Novel protein targeting strategies	26
3.3.1 PROTAC-mediated targeted protein degradation	26
3.3.2 Clinical proof of concept for PROTACs	27
3.3.3 Investigation of new E3 ligases	28
3.4 Methodologies to elucidate drug-protein interactions	30
3.4.1 <i>In vitro</i> profiling assays	30
3.4.2 Cell-based profiling assays	31
3.4.3 Cellular target engagement NanoBRET – an <i>in cellulo</i> method	31
3.5 Objectives of this thesis	32
4. Experimental Procedures	33
4.1 Methods	33
4.1.1 Biochemical methods to determine small molecule potency	33
4.1.1.1 Differential scanning fluorimetry (DSF) assay	33
4.1.1.2 Isothermal titration calorimetry (ITC) assay	34
4.1.2 Cell-based assays	35
4.1.2.1 Mammalian cell culture	35
4.1.2.2 Cell viability assay in living cells	36
4.1.2.3 Cell viability using the IncuCyte	36
4.1.2.4 High content live-cell multiplex assay	36

4.1.2.5 Cellular target engagement assay NanoBRET	37
4.1.2.6 The comparability problem of competition-based assays	39
4.1.3 Compound handling and management	40
4.2 Material	41
5. Results and Discussion	44
5.1 The search for new chemical probes – cellular selectivity as main criteria	44
5.1.1 Selective macrocyclic molecule to investigate understudied kinase STK17A	44
5.1.2 Probe development for Salt-Inducible Kinase (SIK2)	49
5.1.3 The necessity for cellular profiling of on-target and off-target effects for chemical probes and chemogenomics.	52
5.2 Family selectivity for small molecule chemogenomic candidates	54
5.2.1 Development of a small molecule inhibitor to target the PCTAIRE family	54
5.2.2 Characterization of current chemogenomic candidates for splicing kinase family	58
5.2.2.1 Small molecule inhibitor landscape targeting the splicing kinase family	58
5.2.2.2 SGC initial screening library to identify chemical starting points for targeting understudied splicing kinases	68
5.2.3 Cellular selectivity assessment as quality control step for chemogenomics libraries	73
5.3 Assessing the human kinome using the NanoBRET technology	75
5.3.1 Large-scale analysis of <i>in cellulo</i> selectivity against 234 kinases using NanoBRET	75
5.3.2 Comparison of data between published <i>in vitro</i> and <i>in cellulo</i> assay formats	82
5.3.3 Influence of ATP concentration on potency	82
5.3.4 Deviations in selectivity profiles of published kinase inhibitors	83
5.4 Beyond kinases – targeting dysregulated proteins	84
5.4.1 WD-Repeat-Containing Protein 5 (WDR5) Degradable to target transcription factor MYC	84
5.4.2 Cellular family-wide selectivity platform for BIRC proteins	89
5.4.2.1 <i>In vitro</i> affinity assessment of literature BIRC compounds	90
5.4.2.2 BIRC family <i>in cellulo</i> selectivity characterization platform	91
5.4.3 NanoBRET target engagement beyond kinases – challenges and new applications	94
6. General Discussion and Outlook	95
6.1 The future of cellular target engagement assays	95
6.2 Chemical tool compounds are valuable resources, if they are well characterized	96
6.3 Cellular target engagement method as versatile tool to study proteins	97
7. List of Abbreviations	99
8. References	101
9. Appendix	X

9.1 Supplementary Figures	X
9.1 Supplementary Tables	XI
9.2 List of publications and collaboration partners	XLV
9.3 Statutory declarations	LI

1. Summary

Cellular Selectivity and Kinetics of Clinical Kinase Inhibitors

Written by Lena Marie Berger under the supervision of Prof. Dr. Stefan Knapp

Protein kinases are key signalling molecules and transduce intracellular signals via the post-translational phosphorylation of substrate proteins, often other protein kinases. Dysregulation of this protein family has been linked to many diseases including neurodegenerative diseases, inflammation and cancer and amplifications of kinases play important roles as diagnostic biomarkers in a variety of cancers. Various strategies have been developed to treat dysregulated protein kinases. Most commonly, chemical small molecule inhibitors are used to modulate protein kinase activity in cancer cells. Many inhibitor and general research efforts have focused only on a small subset of protein kinases, resulting in a large portion of the kinome, the so-called “dark” kinome, remaining largely unexplored. As part of the strategy to develop inhibitors, it is crucial to understand the structure-activity-relationships (SAR) of small molecules to the activity towards the targets based on understanding small molecule-target affinities as determined by biophysical, biochemical, and cellular methods. However, not always do *in vitro* determined affinities, which are frequently used as basis for SAR considerations, correlate with the cellular affinity. For protein kinases in particular, it has been shown that the cellular concentration of the natural substrate adenosine-triphosphate (ATP) plays a critical role for the resulting small molecule affinity, as substrate and inhibitor frequently compete for the same binding site of the protein kinase. The cellular target engagement assay NanoBRET is a versatile assay that overcomes this problem and can be used to assess binding of a compound to the full-length protein kinase, in the presence of natural binding partners. Another important factor in inhibitor optimization is the selectivity of the molecule within the family of protein kinases. When comparing the selectivity profiles of small molecule kinase inhibitors *in vitro* and in cells, different profiles can be observed. Frequently, a compound, binds fewer protein kinases with high affinity in cells, indicating that cellular profiling of protein kinase inhibitors is necessary to understand the selectivity profile of an inhibitor.

The goal of this work was to understand cellular SARs of inhibitors for kinases and dark kinases in medicinal chemistry projects, and to understand the selectivity profiles of existing

1. Summary

small molecules in cells, including already approved drugs and clinically used kinase inhibitors. The cellular potency and selectivity aspects guided optimization of the inhibitors towards selective small molecules 'chemical probes' or highly validated inhibitors with a narrow selectivity profile as part of 'chemogenomic libraries'. One strategy to improve selectivity has been to use sterically restricted cyclic small molecules, called macrocycles, that allow fewer conformations of the molecule than their non-cyclic parent compound. In this thesis the dark kinase STK17A was investigated. Macrocyclization was used to develop a selective chemical probe molecule that is also selective in the cellular context. For another kinase, SIK2, a rational design approach was used to exclude off-targets bound by the lead structure, resulting in a chemical probe that selectively targets the SIK1/2/3 proteins. Assessing cellular potency of another series of inhibitors, a probe was developed for the PCTAIRE subfamily of the CDK kinases. This required co-expression of the binding partners of CDKs, the cyclins, in cells to obtain a functional assay. To identify new candidates for the neglected family of splicing kinases comprising the CLK, SRPK, DYRK and HIPK protein kinase subfamilies, a literature review was conducted, and the best small molecule candidates were compared for their target engagement in cells. This led to a series of small molecule inhibitors that may be used as a set or single agents to target the CLK proteins and SRPK proteins or in combination to target the remaining proteins. In search of new starting points for this subfamily of kinases, an initial screen with NanoBRET technology was performed using a library of over 2000 inhibitors, and new starting points were identified. Additionally, a set of clinical and approved small molecule kinase inhibitors was assessed for their selectivity in cells. Several highly selective molecules were identified that were much less selective in *in vitro* approaches. The set of data allowed for a comprehensive comparison of cellular potencies with published data using *in vitro* binding, *in vitro* activity and data obtained from cell lysates and identified several protein kinases that would need to be investigated in cells. Beyond conventional kinase inhibitors, a new strategy was to identify and characterize heterobifunctional binders and use them in an approach to attract the cellular ubiquitination dependent degradation machinery of E3 ligases and the proteasome thereby not inhibiting but degrading the target protein. These molecules, called PROTACs, are bivalent, containing a target-specific binder connected via a linker to a binder of an E3 ligase. BIRC-family proteins comprise E3 ligases, which contain beside their BIR domain a RING-domain, which carries

the E3 ligase activity. In order to develop new and characterize existing binders to this family, the literature small molecule landscape of BIRC binders was assessed to identify tools to use for the development of PROTACs, revealing several suitable small molecules as starting points.

This thesis focused on the development and characterization of small molecule inhibitors in cells using the method NanoBRET. These projects have targeted kinases and dark kinases in medicinal chemistry projects, identified several new starting points when comparing literature inhibitors and tool compounds and new starting points for future projects, enabling the development of chemical probes and chemogenomic libraries to study the role of specific kinases in biology and disease.

2. Zusammenfassung (German Summary 5-Page)

Zelluläre Selektivität und Kinetik von klinischen von Klein-Molekularen Kinase Inhibitoren

Geschrieben von Lena Marie Berger unter der Leitung von Prof. Dr. Stefan Knapp.

Proteinkinasen wirken als Signalmoleküle und leiten intrazelluläre Signale über die posttranslationale Phosphorylierung von Substratproteinen, häufig anderen Proteinkinasen, weiter. Zur Behandlung desregulierter Proteinkinasen wurden verschiedene Strategien entwickelt; am häufigsten werden chemische niedermolekulare Inhibitoren zur Modulation der Proteinkinaseaktivität in Krebszellen eingesetzt. Viele Hemmstoff- und allgemeine Forschungsbemühungen haben sich nur auf eine ähnliche Gruppe von Proteinkinasen konzentriert, was dazu führt, dass ein Teil des Kinoms, das so genannte "dunkle" Kinom, weitgehend unerforscht bleibt. Als Teil der Strategie für den Einsatz von Inhibitoren ist es von entscheidender Bedeutung, die Struktur-Aktivitäts-Beziehungen zwischen kleinen Molekülen und ihren Zielmolekülen zu verstehen, und zwar auf der Grundlage des Verständnisses der Affinitäten zwischen niedermolekularen Molekülen und Zielmolekülen, wie sie durch biophysikalische, biochemische und zelluläre Techniken bestimmt werden. Während eine *in vitro* ermittelte Affinität häufig mit der zellulären Affinität korreliert, müssen bei manchen anderen Substanzen zusätzliche Faktoren im zellulären Kontext berücksichtigt werden. Bei Proteinkinasen hat sich gezeigt, dass die zelluläre Konzentration des natürlichen Substrats Adenosintriphosphat (ATP) eine entscheidende Rolle für die resultierende Affinität kleiner Moleküle spielt, da Substrat und Inhibitor um die Bindungsstelle der Proteinkinasen konkurrieren. Weitere Faktoren, die bei dem zellulären Target-Engagement-Assay, auch NanoBRET genannt, berücksichtigt werden, sind die Verwendung von transient exprimierten Proteinkinasen in voller Länge, posttranslationale Modifikationen beim Menschen, die subzelluläre Lokalisierung und das Vorhandensein natürlicher Bindungspartner. Ein weiterer wichtiger Faktor bei der Optimierung kleiner Moleküle ist die Selektivität des Moleküls innerhalb der Familie der Proteinkinasen. Beim Vergleich der Selektivitätsprofile von niedermolekularen Kinase Inhibitoren *in vitro* und in Zellen wurde festgestellt, dass die Selektivitätsprofile kleiner werden, also weniger Proteinkinasen mit hoher Affinität gebunden werden, was darauf hindeutet, dass eine

zelluläre Profilierung von Proteinkinase Inhibitoren notwendig ist, um die Zielprofile zu verstehen.

Ziel dieser Arbeit war es, die zellulären Struktur-Aktivitäts-Beziehungen von Proteinkinasen und dunklen Proteinkinasen in Projekten der Medizinalchemie zu verstehen, hochselektive kleine Moleküle zu entwickeln und die Selektivitätsprofile bestehender niedermolekularer Moleküle in Zellen zu untersuchen, einschließlich bereits zugelassener Medikamente und klinisch verwendeter Kinase-Inhibitoren. Eine Strategie zur Verbesserung der Selektivität war die Verwendung sterisch eingeschränkter zyklischer kleiner Moleküle, so genannter Makrozyklen, die weniger Bindungszustände des Zielproteins zulassen als ihre nicht-zyklische Ausgangsverbindung. Die aus dieser Arbeit resultierenden zellulären Daten halfen bei der Identifizierung neuer Kandidaten auf der Suche nach chemischen Sonden oder chemogenomischen Verbindungen, die für künftige Studien zur Identifikation neuer Zielmoleküle von Bedeutung sein können, da kleine Moleküle, die ein einziges Zielmolekül oder nur wenige Zielmoleküle hemmen, in phänotypischen Assays zur Identifizierung neuer Zielmoleküle verwendet werden können.

Die in dieser Arbeit hauptsächlich verwendete Methode, NanoBRET, wurde dabei ausgehend von veröffentlichten Protokollen so weiterentwickelt, dass im Hochdurchsatzverfahren viele Projekte mit wichtigen Daten bereichert werden konnten. Bei NanoBRET wird eine Zielproteinkinase innerhalb eines DNA-Plasmids an eine kleine Luciferase fusioniert und diese über transiente Transfektion exprimiert. Durch ein an die Zielkinase bindendes fluoreszierendes Molekül, dem Tracer, und der Zugabe von einem Substrat der kleinen Luciferase kommt es zu einem Energieübertrag der Biolumineszenz der kleinen Luciferase an den Tracer. Der so beobachtbare Signalanstieg kann durch konkurrierende Kleinmoleküle der Zielkinase dosisabhängig reduziert werden. In Kleinmolekültitrationen kann so auf die Affinität der Kleinmoleküle im zellulären Kontext geschlossen werden.

Ein Beispiel für eine dunkle Kinase, die in dieser Arbeit untersucht wurde, ist STK17A. Für STK17A wurde die Strategie der Makrozyklisierung genutzt, um ein selektives chemisches Sondenmolekül zu entwickeln, das auch im zellulären Kontext selektiv ist. Dabei wurden initiale *in vitro* Daten der Selektivität im zellulären System selektiver im Vergleich zum Zielmolekül STK17A. Für eine andere Kinase, SIK2, wurde ein rationaler Designansatz

verwendet, um unerwünschte Zielmoleküle nichtmehr zu inhibieren, die die Leitstruktur zeigte, wodurch am Ende eine chemische Sonde entwickelt werden konnte, die selektiv für die SIK1/2/3-Proteine ist. Die initiale *in vitro* Affinität hat sich dabei im zellulären Kontext bestätigt.

Zur Identifizierung neuer Kandidaten für die vernachlässigte Familie der Spleißkinasen, die die Unterfamilien der CLK-, SRPK-, DYRK- und HIPK-Proteinkinasen umfasst, wurde eine Literaturrecherche durchgeführt, und die besten niedermolekularen Kandidaten wurden unter zellulären Bedingungen verglichen. Dies führte zu einer Reihe von niedermolekularen Inhibitoren, die als Set oder einzelne Wirkstoffe gegen die CLK-Proteine und SRPK-Proteine oder in Kombination gegen die übrigen Proteine eingesetzt werden können. Auf der Suche nach neuen Ansatzpunkten für die in diesem Set noch nicht vollständig durch chemische Sonden analysierbaren Spleißkinasen, wurde an repräsentativen Vertretern der Familien ein initiales Screening mit einer Bibliothek von über 2000 Inhibitoren durchgeführt, und es wurden neue Ansatzpunkte identifiziert, die zukünftig weiterentwickelt werden können.

Innerhalb der Familie der CDK-Kinasen führte das Verständnis der Struktur-Aktivitäts-Beziehung zu einem für die Unterfamilie selektiven Inhibitor, der für das Screening von CDKs als Targets in neuen phänotypischen Assays verwendet werden kann. Beim Überprüfen der Selektivität des Moleküls innerhalb der CDK Familie fiel auf, dass vorrangig die CDKs des phylogenetischen Asts der sogenannten TAIRE Familie, also CDK14/15/16/17/18 mit guter Affinität in Zellen gebunden werden. Entsprechend kann das entwickelte Molekül für Zielidentifikationsstudien als chemogenomisches Kleinmolekül verwendet werden.

Innerhalb der Gruppe der klinischen und zugelassenen niedermolekularen Kinase Inhibitoren wurden mehrere hochselektive Moleküle in Zellen identifiziert, die in *in vitro* Ansätzen weit weniger selektiv waren. Der Datensatz ermöglichte einen umfassenden Vergleich der zellulären Potenzen mit veröffentlichten Daten unter Verwendung von *in vitro* Bindung, *in vitro* Aktivität und aus Zelllysaten gewonnenen Daten und identifizierte mehrere Proteinkinasen, die in Zellen untersucht werden sollten. Für dieses Projekt wurden neue Tracer Titrationen für 238 Proteinkinasen durchgeführt und jedes Testsystem an vier Kontroll-Kleinmolekülen getestet. Mithilfe dieser Plattform wurden folgend 189 Kleinmoleküle profiliert. Es wurde dabei festgestellt, dass mehrere klinische

Kleinmoleküle unerwartet unselektiv waren, wobei sich diese Selektivität im zellulären Kontext verbesserte. Ein Vergleich der zellulären Daten mit publizierten Daten eines *in vitro* Bindungsassays zeigte eine generelle Korrelation der Bindungsaffinitäten, die jedoch um den Faktor 10-100 unpotenter waren als vorher. Diese Differenz kann mit der natürlichen Konkurrenz des Substrates ATP erklärt werden, da dieses in Zellen in hohen Konzentrationen vorliegt. Ein weiteres Subset an Proteinkinasen zeigte jedoch besonders hohe Verschiebung der Affinität um den Faktor 1000. Hier werden weitere biologische Gründe vermutet, wie das Vorhandensein posttranslativer Modifikationen oder subzellulärer Lokalisation der getesteten Proteine. Diese Untersuchungen dienen als Grundlage für folgende Studien.

Eine weitere Methode um deregulierte Proteine zu behandeln ist der gezielte Proteinabbau. Niedermolekulare Binder werden dabei verwendet, um die zelluläre ubiquitinierungsabhängige Degradationsmaschinerie der E3-Ligasen und des Proteasoms anzuziehen und dadurch das krebserregende Zielprotein abzubauen. Bei dem als PROTACs bezeichneten Ansatz wird ein bivalentes Kleinmolekül entwickelt, das einen zielspezifischen Binder enthält, der über einen Linker mit einem Binder für eine E3-Ligase verbunden ist.

In einem Projekt wurde das MYC-bindende Protein WDR5 mit Hilfe eines PROTAC-Moleküls ins Visier genommen, um nicht nur WDR5, sondern auch MYC selbst abzubauen, wobei ein Literaturligand, eine Linker-Optimierung und Thalidomid als Angriffsmodalität für die E3-Ligase Cereblon zur Polyubiquitinierung von WDR5 verwendet wurden. Der PROTAC Homer zeigte, dass das Molekül in Zellen WDR5 gebunden hat und WDR5 abgebaut wird. Die Degradation von MYC konnte leider nicht untersucht werden. Um sicherzustellen, dass das Zielmolekül, hier WDR5, vom PROTAC in Zellen gebunden wird, kann als erste Indikation für einen späteren Proteinabbau gesehen werden.

Eine weitere Familie von E3-Ligasen sind die RING-Domänen enthaltenden Proteine der BIRC-Familie. Es gibt 8 BIRC Proteine mit jeweils 3 BIR-Domänen. Auffallend ist hier, dass ein BIRC-Protein mehr als eine BIR-Domäne enthalten kann und somit auch Verbindungen denkbar sind, die bivalent an mehrere BIR-Domänen binden. 5 BIRC-Proteine enthalten eine RING-Domäne und sind somit als E3 Ligasen aktiv. Zur Untersuchung der Affinität der BIRC Proteine wurden zelluläre NanoBRET Testsysteme neu entwickelt. Dafür wurden die BIRC-

Proteine sowohl in voller Länge als auch jeweils als einzelne BIR-Domänen als NanoBRET Plasmide hergestellt und eine Titration des vorhandenen Tracers durchgeführt. Die Literaturlandschaft der Kleinmoleküle von BIRC-Bindern wurde in einem Projekt dieser Arbeit gescreent, um Werkzeuge für die Entwicklung von PROTACs zu identifizieren, wobei mehrere geeignete kleine Moleküle als Ausgangspunkte gefunden wurden. Die Liganden wiesen auch im zellulären Kontext Affinitäten von weniger als 1 μM auf, was für die Entwicklung neuer PROTACS ein ausreichendes Maß ist. Leider wiesen die getesteten Moleküle keine Selektivität innerhalb der BIRC-Proteine auf, was für die Entwicklung chemischer Sonden essentiell wäre. Mithilfe der Charakterisierung der Kandidaten können nun medizinalchemische Entwicklungsprojekte gestartet werden, deren Ziel die Verbesserung der Selektivität der Kleinmoleküle ist. Durch die Entwicklung der einzelnen Testsysteme für die BIRC-Proteine können auch zukünftige Kandidaten charakterisiert werden.

Diese Arbeit konzentrierte sich auf die Entwicklung und das Verständnis von niedermolekularen Inhibitoren in Zellen unter Verwendung verschiedener Strategien zur Bekämpfung von Krebs oder zur Entwicklung von Werkzeugen zur Identifizierung neuer potenzieller Ziele in der Krebstherapie. Ein Schlüsselement in den Entwicklungsprojekten war die Bewertung von Kleinmolekülen im Kontext der lebenden Zelle mit der Methode NanoBRET. Im Rahmen dieser Projekte wurden sowohl bereits erforschte Kinasen als auch dunkle Kinasen in Projekten der Medizinalchemie ins Visier genommen, mehrere neue Ansatzpunkte beim Vergleich von Inhibitoren aus der Literatur sowie Werkzeugverbindungen ermittelt und neue Ansatzpunkte für künftige Projekte vorgeschlagen.

3. Introduction

3.1 Function and dysfunction of protein kinases

Human protein kinases are key players in nearly all aspects of cellular function and are involved in almost all cellular processes. They are organized in signalling cascades and transmit external and internal stimuli to regulate cell growth, division, development and death by regulating the activity of effector proteins or other kinases. Protein kinases are enzymes that catalyse the transfer of the terminal phosphate group of adenosine triphosphate (ATP) to a specific substrate resulting in the formation of phosphate ester linkage through a nucleophilic substitution reaction. During the phosphorylation, the phosphoanhydride bond between the β - and γ -phosphate of ATP is cleaved and free energy is released which is the driving force of this reaction. Depending on the chemical properties of the substrates, kinases can be categorized into protein kinases, lipid kinases, carbohydrate kinases or even nucleoside-phosphate kinases or nucleoside-diphosphate kinases. Due to their proven involvement in different cancer types, this work will focus on protein kinases. For eukaryotic protein kinases, the main phosphorylatable sites are serine (Ser), threonine (Thr) and tyrosine (Tyr); whereas in prokaryotes, the main sites are aspartic acid (Asp), glutamic acid (Glu) and histidine (His). Other phosphorylatable amino acid residues include arginine (Arg), lysine (Lys) and cysteine (Cys)¹.

The process of phosphorylation is dependent on a tight interplay between kinases and phosphatases, catalysing dephosphorylation. It enables a flexible and rapid response for diverse extra- and intra-cellular stimuli and cellular networks². Protein phosphorylation performed by protein kinases as a regulatory mechanism of cellular function was first described by Edwin G. Krebs and Emil Fischer in the 1950s³. The importance of phosphorylation as a mechanism for cellular signalling is reflected by the fact that 2% of the human genome is encoded for kinases⁴. Because of its advantages, reversibility and versatility, phosphorylation is a key posttranslational modification that introduces a negative charge to a serine, threonine or tyrosine residue of a protein. This in turn can affect the conformation of a protein, alter the protein activity and modulate protein-protein interactions, especially sub-cellular localization⁵.

The first comprehensive study of all human kinases has been performed in 2002 by Manning *et al.*, who identified 518 protein kinases and classified them into nine distinct groups, according to their sequence similarity in the kinase domain⁶. Generally, protein kinases are grouped, depending on their amino acid residue they phosphorylate - as serine/ threonine kinases, tyrosine kinases or dual-specificity kinases. The total number of protein kinases included in the kinome is still under debate, since some kinases phosphorylate non-protein substrates or are so called atypical kinases⁷. The subgroups defined by Manning *et al.* are defined as such: AGC family containing PKA, PKG and PKC, calcium/ calmodulin dependent kinase (CAMK), casein kinase1 (CK1), a group of cyclin dependent kinases, MAP kinases, glycogen synthase kinase and casein kinases (CMGC), sterile 20-like kinases (STE), tyrosine kinases (TK) and tyrosine kinase like (TKL), and others⁶. Around 10% of the described protein kinases lack key catalytic function, due to a lack of catalytic residues, hence these kinases are termed pseudokinases⁸. Sometimes a kinase can contain both an active kinase domain and a pseudokinases domain, like e.g. the Janus Kinases (JAKs)⁹. Almost all of the kinases play an important role in cellular signalling pathways and transduction¹⁰ and are located in various parts of the cell. Receptor tyrosine kinases are transmembrane proteins localized in the plasma membrane of the cell and transduce external signals, like the well-known oncogene called epidermal growth factor receptor (EGFR) which belongs to the ErbB family of tyrosine kinases. Activation mutations in EGFR and overexpression of EGFR proteins results in dysregulated signalling and confer growth advantage to the tumour cells by stimulating proliferation, survival and metastasis¹¹. Other kinases have very different subcellular locations, *e.g.* the nucleus or the cytoplasm. Kinases that are currently targeted by approved drugs are for example kinases involved in several hallmarks like proliferation, *e.g.* MEK1 and MEK2 in the MAPK pathway, mTOR in the PI3K-Akt pathway or RSK in the FGFR dependent proliferation pathway¹². Also, other important cellular regulation processes are regulated by kinases, like *e.g.* energy homeostasis and metabolic stress. The salt-inducible kinases (SIK1-3) for example are members of the AMP activated protein kinase (AMPK) subfamily of the CAMK group and play a major role in these processes. SIK2 is activated in cells, that recover from starvation and activate the transcription factor cAMP response element-binding protein (CREB1) by phosphorylation¹³. In contrast SIK family members can also repress CREB1-mediated gene expression by phosphorylating the associated transducer of CREB1 TORC¹⁴.

¹⁵. An imbalance of SIK has been observed in the context of several diseases, especially cancer, with both tumour-promoting and tumour-suppressive roles being reported¹⁶. The SIK family members are dysregulated in many different cancer types. For example, SIK2 is downregulated or completely deleted in breast cancer and has been linked to a tumour suppressor role¹⁷. SIK3 on the other hand is highly overexpressed in breast cancer, with an effect on the inflammation process¹⁸. The SIK kinase family is a good example of a kinase with complex roles in different types of cancer, which makes them important therapeutic targets for many different drug discovery processes.

3.1.1 Human protein kinases share a highly conserved architecture

Protein kinases share an evolutionarily conserved tertiary structure, sharing a common catalytic mechanism. The catalytic kinase domain is highly dynamic and flexible and allows the binding of ATP and the substrate in the active state (Figure 1). The kinase domain can switch between two different states, the active and the inactive conformation, during the process of phosphorylation¹⁹. The active conformation is highly conserved within the protein family, because all kinases catalyse the same reaction. The inactive conformation on the other hand can vary between the different kinase subfamilies²⁰. Overall, the kinase domain is a bi-lobal structure and contains conserved regions most of which are very flexible and can adopt different states: The N-terminal lobe consists primarily of beta sheets and at least one alpha helix called α C. The C-terminal lobe consists primarily of alpha helices. The N- and C-terminal lobes are connected by the hinge region that is involved in ATP binding via polar backbone hydrogen bonds with the adenosine ring of ATP.

3. Introduction

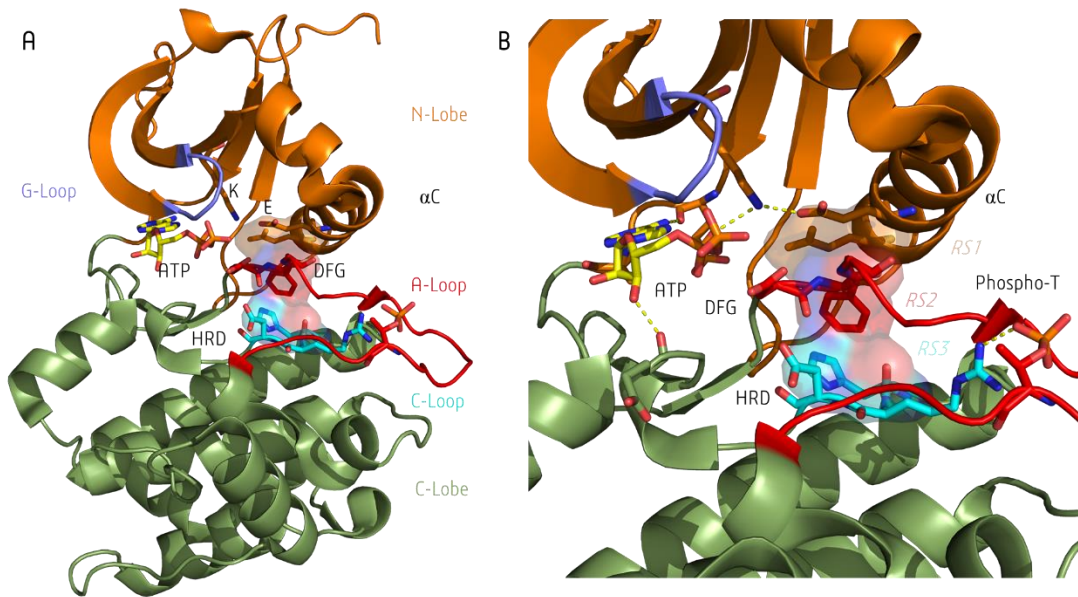


Figure 1 | Structure of the protein kinase domain modified from AURKA (PDB code: 1OL5). **A** The kinase domain is a bi-lobal structure and shows an upper N-terminal lobe (orange) and a lower C-terminal lobe (green) connected by the hinge region. The ATP binding site (ATP is depicted in yellow stick model) is positioned at the interface between the two lobes. The αC helix is positioned to the right of the ATP binding site and is part of the N-lobe. Below the ATP binding site, the activation loop (A-loop) containing the DFG motif forms part of the protein substrate-binding site. The G-Loop is positioned on top of the ATP binding site including the GxGxxG motif that coordinates the ATP-phosphates. The catalytic loop (C-loop) including the HRD motif form a second part of the protein substrate-binding site. **B** Magnified view of the interface between the lobes, showing key interactions. A Lysine (K) residue of $\beta 3$ and a glutamic acid (E) residue of the C-helix form a salt bridge that connects the ATP site to the C-helix tightening the pocket into its final form. A crucial connection between the two lobes is formed by the R-spine residues (RS). RS3, a side chain originating from the αC and RS2, also the central residue in the highly conserved 3-amino acid sequence, the DFG motif, located at the N terminus of the Activation-loop interact as shown by the surface representation. The HRD motif is positioned in the C-loop where the phosphorylation of the substrate takes place. Adapted from Arter *et al*¹.

The DFG (aspartic acid, phenylalanine, glycine) motif is a key player in the activation mechanism of a kinase. This highly conserved motif can flip between the DFG-in confirmation, where the kinase is active, and the DFG-out confirmation, where the kinase is inactive. During the flip, the hydrophobic phenylalanine flips towards the ATP active site and the necessary interaction with the regulatory spine disrupts. In order to obtain the conserved kinase structure, each kinase contains two so called spines that stabilize the kinase domain. The catalytic spine consists of polar residues that align upon binding of ATP. The regulatory spine consists of hydrophobic residues alongside the DFG-motif. During the activation of a kinase, many kinases are phosphorylated on the activation loop that also contains the DFG motif. After phosphorylation, the newly negatively charged phosphate residue interacts with the positively charged arginine of the HRD (histidine, arginine, aspartate) motif that is positioned in the catalytic loop (C-loop). In the reaction, ATP binds to the kinase with polar

interactions of its adenosine core to the hinge region and its phosphates being coordinated by the GxGxxG motif in the G-Loop or P-Loop which usually connects $\beta 1$ and $\beta 2$ sheets. The P-Loop also positions the AxK motif to form a salt bridge with the conserved glutamate in the αC which tightens the binding pocket into its active form. Only if all motifs interact as described, the kinase is fully active and can phosphorylate a substrate peptide that usually binds alongside the C-lobe where the residue to be phosphorylated points into a cleft along the catalytic loop. After the reaction is catalysed, the resulting ADP and phosphorylated substrate peptide dissociate from the protein kinase.

In order to become fully active, some kinases are dependent on interaction partners. One prominent example that was investigated in more detail in this thesis are the serine-threonine cyclin-dependent kinases (CDKs), that require an activation via binding to so called cyclins to establish a catalytically active ATP binding pocket. The eukaryotic CDK family consists of 21 kinases that are characterized by a highly conserved ATP binding pocket, the so called PSTAIRE-like binding domain and an activation loop. Upon binding of cyclin, the activation loop shifts to expose the substrate-binding site and the kinase is activated. CDKs have key roles in regulating the cell cycle but they also perform diverse other cellular functions, such as regulation of mRNA processing and transcription^{22, 23}. Dysregulation of these kinase involved in mRNA processing play important roles in tumorigenesis and could be potential therapeutic targets.

3.1.2 Human protein kinases as key proteins in signalling health and disease

Kinases are important signalling molecules that play key roles in biology ranging from developmental roles, cell-cell communication, growth and movement and many other roles of multicellular organisms. Accordingly, dysregulation or mutation of these enzymes is associated with a plethora of diseases and in particular to cancer. Kinases play key roles in most if not all of the hallmarks of cancer.

In 2000 Hannahan and Weinberg²⁴ proposed six hallmarks of cancer, which aimed to describe the complexity of the difference between healthy cells in comparison to cancerous cells. They added two emerging hallmarks and two enabling characteristics in the year 2011²⁵. Cancer cells show selective growth and proliferation advantage, altered stress response favouring overall survival, vascularization, invasion and metastasis, metabolic rewiring, an abetting

environment and immune modulation²⁵. Hallmarks can be developed by dysregulated control mechanisms in biochemical signalling pathways that alter the gene expression due to genomic mutations. Mostly, this genetic alteration of the DNA leads to a dysregulated transcriptome, altered protein expression and function and thereby end in the initiation and survival of a cancerous cells.

3.1.3 Essential eukaryotic pre-mRNA splicing process is controlled by protein kinases

Pre-mRNA splicing is an essential process during which transcripts of DNA containing alternative exons are included or removed from mature mRNA. Frequently, transcripts contain several alternative exons and their incorporation into the mRNA can be combined, largely increasing the diversity of the mRNA expressed from the genome, making alternative splicing a central element in forming complex organisms. Alternative splicing patterns constantly change under physiological conditions, allowing an organism to respond to changes in the environment by determining which part of the genome it expresses²⁶. Alternative splicing that is not precisely controlled has a great probability to result in erroneous splicing events, generating aberrant transcripts and functionally altered proteins, thereby promoting the onset and progression of diseases, including cancer, neurodegenerative diseases, cardiovascular diseases, and muscular dystrophy²⁷. Hundreds of mis-splicing events have been reported in various types of human solid tumours, which are associated with malignant progression and treatment-resistance of tumours. Among these tumours, the expression and activity of dysregulated splicing factors vary in different models^{28, 29}. Therefore, regulating proteins relevant for alternative splicing, such as RNA binding proteins (RBPs) and related kinases associated with miss-splicing events in specific cancer models is considered as an effective strategy for the development of anticancer drugs³⁰. RNA binding proteins (RBPs) form a large family of proteins that play essential roles at all steps of RNA metabolism, including splicing, transcription, transport, stability and translation³¹. Among the RBPs, serine/ arginine-rich splicing factor (SR) proteins constitute a conserved family of 12 proteins in humans that are capable of regulating the alternative splicing process^{32, 33, 34}. SR proteins share some common domains such as one or more RNA-recognition motif (RRM) at their N-terminus and a region, rich in serine-arginine and/or serine-proline dipeptides (RS) at their C-terminus³³. Reversible phosphorylation of serine residues within the RS motif of SR proteins constitutes an essential mechanism that regulates

their intra-cellular and intra-nuclear localization and their splicing activities³². Not surprisingly, the RS domain of SR proteins is also extensively modified by phosphorylation. Several kinases have been reported to phosphorylate SR proteins in a consecutive manner. All of these kinases belong to the CMGC (cyclin-dependent kinase [CDK], mitogen-activated protein kinase [MAPK], glycogen synthase kinase [GSK3], CDC-like kinase [CLK]) family that includes eight families of highly inter-connected kinases that regulate a variety of processes and, in particular, transcription and RNA processing³⁵. The main kinases reported to phosphorylate SR proteins are SR protein kinases (SRPKs) and CLKs^{36, 37}. Additionally, some kinases, in particular dual-specificity tyrosine-regulated kinases (DYRKs)^{38, 39} and pre-mRNA processing 4 (PRP4)^{40, 41}, which were initially described for their function in other biological processes, appear to be equally able to phosphorylate SR proteins. SRPK1 was the first SR protein kinase discovered and remains the best studied among them⁴². Serine-arginine protein kinases are highly specific for RS repeats and phosphorylate serine residues that are adjacent to arginine⁴³. SRPKs thus regulate cellular splicing via phosphorylation of SR proteins. SRPKs are the first kinases phosphorylating newly translated SR proteins in the cytoplasm, as documented in the case of SRSF1. This activity has been well-documented for SRPK1 and to a lesser extent for SRPK2. Besides their direct effect on splicing, SRPKs also have additional roles potentially linked to their capacity to phosphorylate SR-like domains that are present in a variety of cellular proteins. The CLK kinases (Cdc2-Like Kinases) represent the second important family of kinases that control the activity of SR proteins. The CLK family includes four members (CLK1-4) with CLK1 and CLK4 being considered almost identical, whereas CLK3 is most distantly related with the most relevant difference being the DFG-1 residue that changes from a valine to an alanine residue⁴⁴. CLKs are defined as dual-specificity kinases because they can phosphorylate both serine/threonine and tyrosine residues. However, while auto-phosphorylation occurs at tyrosine residues, phosphorylation of other substrates seems to target uniquely serines or threonines^{45, 46}. CLKs play a role in pre-mRNA splicing by regulating serine-arginine-rich (SR) proteins. When the SR proteins are phosphorylated by CLKs they relocate to the spliceosome and interact with pre-mRNA to facilitate exon recognition in the splicing machinery. Cancer can gain a survival advantage when the splicing machinery is “hijacked”, hence, splicing machinery proteins are often mutated or overexpressed in cancers. CLK1, CLK2, and CLK4 for example are overexpressed in

renal cancer, breast cancer, colorectal cancer, liver cancer, and glioblastoma, while CLK3 is mainly expressed in mature spermatozoa⁴⁷. The DYRK subfamily of kinases is encoded by two groups of paralog genes (DYRK1A/B and DYRK2/3/4) that are conserved in all animal species. Their common feature is their function as priming kinases, in particular for glycogen synthase-3 (GSK-3) and Polo-like (PLK) kinases⁴⁸. In contrast to the other two main families of SR protein kinases, SRPKs and CLKs, DYRK enzymes are mostly known for their activities in a wide variety of processes such as cell growth, differentiation and transcription and only a few studies have indicated that some of these enzymes, in particular DYRK1A, can regulate the activity of SR proteins⁴⁸. The kinases were discovered in 1996 as highly expressed in the brain and their overexpression was shown to be associated to some pathological traits of neurodegenerative syndromes, in particular Down syndrome⁴⁹. Several studies further indicated a dosage dependent effect of DYRK1A on neuronal development with haploinsufficiency leading to intellectual disability, microcephaly, and autism whereas overexpression confirmed the association with clinical manifestations of trisomy 21⁵⁰. DYRK kinases are described as constitutively active kinases and their activation was thought to occur by co-translational autophosphorylation at tyrosine residues within their activation loop⁵¹. The PRP4 kinase was initially identified in yeast as a temperature-sensitive factor involved in pre-mRNA processing and as a component of the U4/U6 snRNP⁵². Later on, the protein was characterized as a kinase able to phosphorylate SRSF1 *in vitro*⁴¹. The PRP4 kinase displays some homologies with CLKs, in particular, a N-terminal RS domain. In interphase cells, the protein localizes in nuclear speckles and interacts with CLK1 which can phosphorylate the RS domain of PRP4 *in vitro*⁴¹. However, despite these initial strong homologies, no further evidence reported a role of PRP4 in SR protein phosphorylation. Rather, studies conducted in yeast and mammalian cells, suggest that this kinase is involved in spliceosome assembly by directly phosphorylating its components. In humans, PRP4 associates with the U5 snRNP and phosphorylates several components of the human spliceosome B complex^{53, 54}.

3.2 Targeting dysregulated proteins by small molecule inhibition

The essential role of human protein kinases in cell signalling and transcription factors and the relevance of their dysregulation was discussed in a previous chapter. Given the crucial role of kinases, targeting them is in the focus of many drug discovery companies and academia over the last three decades. Two major molecular approaches have emerged for targeting protein kinases: antibodies and small molecules. Antibodies are large biomolecules that bind to the extracellular domain of receptor tyrosine kinase and thereby preventing the binding of the ligand that activates or inactivates the kinase⁵⁵. In contrast, small molecules can penetrate the cells and therefore can inhibit the intracellular kinase domain by inhibiting the target kinase or a downstream kinase of the receptor tyrosine kinase⁵⁶. Both therapeutic strategies have proven to be successful in various drug campaigns and have led to 28 monoclonal antibody-drugs and 72 small molecule inhibitor-drugs targeting protein kinases approved by the U.S. Food and Drug Administration (FDA) in 2022⁵⁷ (Figure 2). In this work the focus will be on small molecule kinase inhibitors, hence, the next chapters will provide a more detailed insight into small molecules as class of therapeutics.

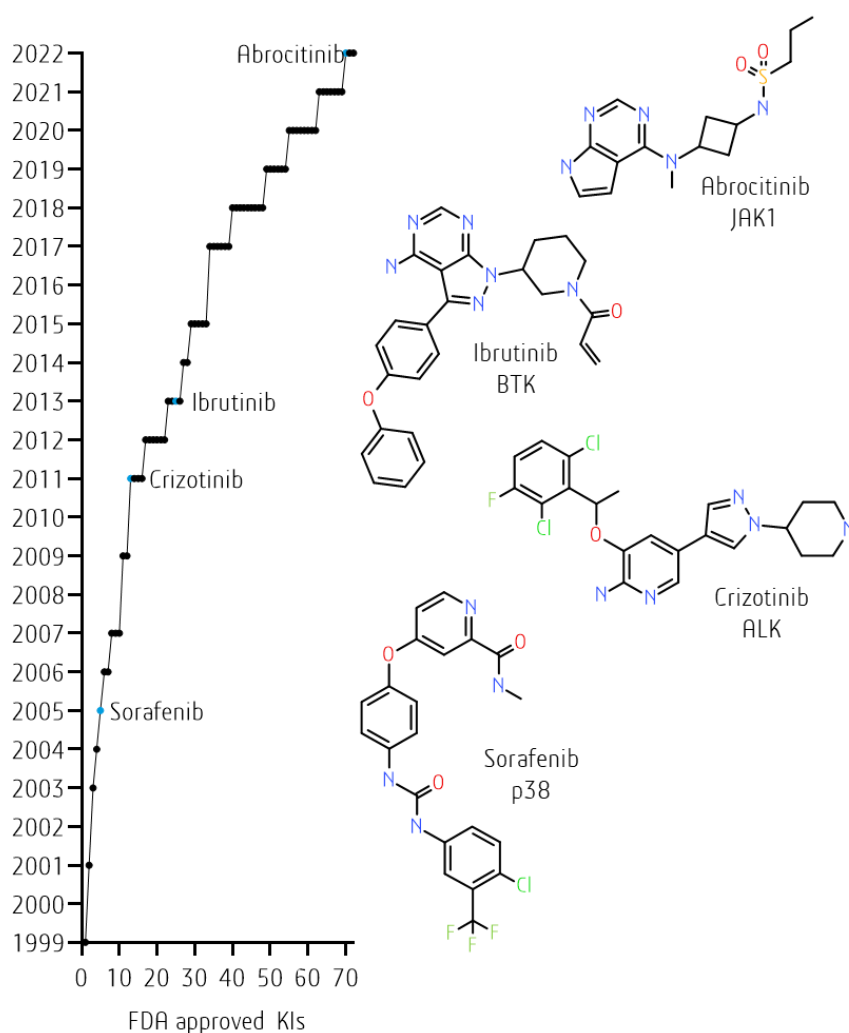


Figure 2 | FDA approved kinase inhibitors from 1999 to date. 72 small molecules that mainly target kinases have been approved by the FDA. Depicted next to the chart are exemplary chemical structures of four inhibitors, sorafenib, crizotinib, ibrutinib and abrocitinib. The main kinase target is indicated below the inhibitor.

3.2.1 Different types of small molecule protein kinases inhibitors

Protein kinases, like all enzymes, are defined by catalysing a reaction that requires binding to a specific substrate. This binding can be inhibited by multiple mechanisms, in the drug discovery field most often by competitive inhibition. Usually during competitive inhibition, a small molecule inhibitor is binding to the active site of the enzyme thereby blocking binding of the substrate, which ultimately leads to the inhibition of the enzyme and a temporary loss of function of this protein. In recent decades, numerous small molecule kinase inhibitors have been developed and revolutionized the cancer treatment landscape. Despite their great potential, challenges remain in developing effective and selective kinase inhibitors⁵⁸. Protein kinase domains have a high structural flexibility and can adapt different conformation. Small molecules can bind in various states of the kinase and are classified according to the state

their target exhibits during binding and by the pocket they bind. Several classifications have been developed in the past decades, but the currently most acknowledged and detailed classification is based on Roskoski's⁵⁹ work and divides kinase inhibitors into following seven sub-types: Type I, I ½, II, III, IV, V and VI (Figure 3).

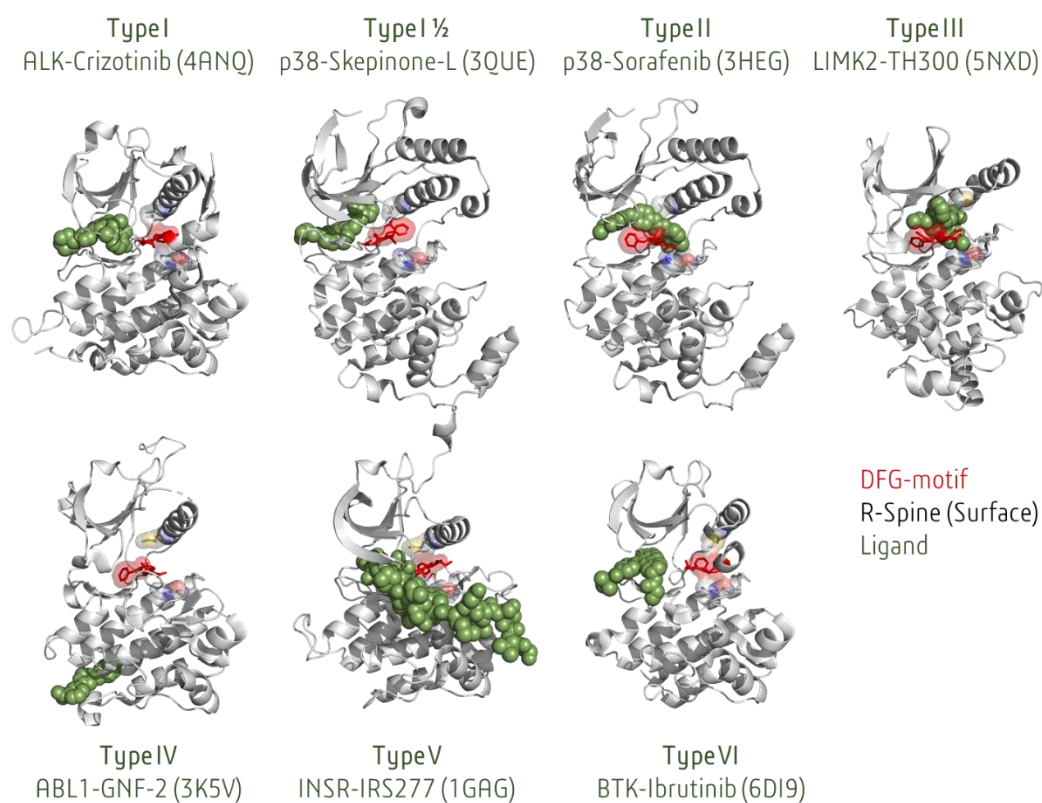


Figure 3 | Binding modes of small molecule kinase inhibitors. Kinase inhibitors are categorized into seven different mechanisms of binding. Type I, I ½ and II molecules bind to the ATP-binding site competitively and are distinguished by the inactive or active confirmation of the DFG-motif. Type III inhibitors target the neighbouring phosphor-acceptor site of the kinase and type IV an allosteric site remote from the catalytic center. Bivalent inhibitors targeting both the ATP pocket and an allosteric binding site are categorized into type V. The last class defines inhibitors that bind irreversibly via a covalent bond, irrespective of the location of the binding on the kinase. The target and exemplary ligand are shown in the figure and the corresponding PDB code is stated in brackets.

Type I inhibitors are ATP-competitive and bind to the catalytic site of a target kinase in an active confirmation. The active state confirmation is defined by an active "in" confirmation of the conserved DFG motif and an intact hydrophobic regulatory spine⁶⁰, whereby the conserved DFG motif on the activation loop is oriented towards the interior of the kinase and aligned with the ATP-binding site, so called DFG-in. An example for a type I inhibitor is the approved drug crizotinib that binds its main target ALK. A subtype to the type I inhibitor, type I ½ binds to the ATP binding region and extends into the back pocket (DFG-in confirmation and C-helix is out). An example would be the inhibitor Skepinone-L. Type II

inhibitors are also ATP competitive and bind to the hinge region of the kinase, but additionally are extending into the adjacent hydrophobic pocket which is made accessible through the conformational change of the DFG-motif in the activation loop, the DFG-out confirmation. This confirmation breaks the regulatory spine, which is important for the activity of the kinase and therefore keeps the kinase in an inactive state. The interaction of the inhibitors with the kinase leads to the formation of single or multiple hydrogen bonds with the protein in the hinge region that forms part of the ATP binding pocket⁶¹. An example for a type II inhibitor would be the approved drug sorafenib binding to its main target p38⁶². Type III inhibitors are non-competitive allosteric inhibitors and bind only to the adjacent hydrophobic pocket opening because of the DFG-out confirmation and thereby remotely modulate kinase activity in an allosteric manner. An example would be the inhibitor TH300 binding its target LIMK2⁶³. Type IV inhibitors are non-competitive allosteric inhibitors that are binding to a site remote from the ATP binding site. This kind of inhibitor is most frequently of high selectivity as it exploits a unique site in the kinase activity. An example would be the inhibitor GNF-2 binding an allosteric site of ABL1⁶⁴. Type V inhibitors are bivalent inhibitors that bind to two regions of the kinase domain. They bind to the active kinase sites and peptide motifs representing the substrate targeted by the kinases⁶⁵. Because they bind to both the ATP-binding site and a structural feature of a specific kinase, bivalent kinase inhibitors are highly selective and potent. This type of inhibitor class is still under investigation and has not yet been approved for clinical application. Another class of kinase inhibitors are the covalent inhibitors, which can be included in Type VI inhibitors. They can bind reversible, but most often irreversible. Covalent inhibitors are forming a bond to the kinase active site typically by interaction with reactive electrophilic groups with primarily the nucleophilic cysteine residue. An example would be the approved drug ibrutinib binding its target BTK⁶⁶. Most of the 72 FDA approved small molecules inhibitors⁶⁷ target the receptor tyrosine kinase (RTK) family.

Typical ATP-mimetic kinase inhibitors are flat hydrophobic molecules with many flexible rotatable bonds. To improve the drug design and develop more bioactive inhibitors many other strategies have emerged, one especially promising is the macrocyclization⁶⁸. Most macrocyclic kinase inhibitors contain an ATP-mimetic pharmacophore, which is connected by a linker of 12 or more atoms that connects flexible moieties. The controlled shape leads to

conformational restriction in the binding pocket and the entropic costs during binding can be reduced, which could lead to an increased binding affinity to the target protein. This compound design strategy has been proven to be effective when the first macrocyclic kinase inhibitor lorlatinib was approved in 2018 by the FDA for treatment of ALK positive non-small cell lung cancer (NSCLC)⁶⁹.

3.2.2 Promiscuity of protein kinases

When designing new small molecule kinase drugs, achieving selectivity for the very conserved and similar kinase domain architecture is a major challenge⁷⁰. Most of the small molecules developed today are targeting the ATP binding pocket that is highly conserved within the human kinome, because allosteric inhibitor sites are rare. Accordingly, designing highly selective ATP competitive kinase inhibitors is a challenging task. Overall, drug discovery has much to gain from knowing the full target profile and the selectivity of small molecule kinase inhibitors which allow to better estimate risks and opportunities of off-target engagement. Promiscuity is often perceived negatively because of side-effects that can occur when the drug modulates the activity of off-targets⁷¹. Side-effects associated with common off-targets are well documented and these targets are often screened during drug development to decrease the risks of side-effects during subsequent development phases⁷². In cancer treatment, a larger number of off-targets may be tolerated because of short treatment cycles performed during chemotherapy. With larger screening panels becoming available in the past decade much was learned about the selectivity of protein kinase inhibitors. However, the cellular selectivity profile of these inhibitors was not investigated yet which will be a focus of this work.

3.2.3 Targeting understudied kinases – the “dark kinome”

More than ten years ago, 75% of all research was focused on only 10% of the human kinome^{73,74}. Although most of the kinases in the human kinome are associated with at least one disease as revealed by disease-gene association databases, cancer mutation data, text mining and genome wide association studies, industrial and academical pharmaceutical research mainly focused on a few well-studied kinases with known function on cellular signalling. Especially, tyrosine kinases and a few other kinases, that are important for cell survival and proliferation, are of great interest for most research groups. From this

perspective it is not surprising that the function of approximately one third of the kinome is still poorly understood or completely unknown⁷³. One example for an understudied kinase family are the death associated protein kinases (DAPKs) that are part of the CAMK subfamily. The best studied kinase in this branch is DAPK1, which is involved in many different cellular processes, such as autophagy and apoptosis⁷⁵. The DAPKs are highly conserved compared to the other part of the DAPK subfamily the DRAKs (death-associated protein kinase-related apoptosis-inducing protein kinase 1, also called serine/ threonine kinase 17A and B [STK17A/B]). The C-terminal regulatory domains of the DAPKs differ substantially. For example, in testicular cancer cells, cell death is induced by DRAK1 as a result of reactive oxygen species, induced by cisplatin in a p53-dependent manner⁷⁶. DRAK1 is mainly localized in the nucleus where it interacts with p53. Nevertheless, DRAK1 can translocate into the cytosol upon the activation of protein kinase C (PKC) and DRAK1 can also be found in mitochondria interacting with the anti-apoptotic oncoprotein adenine nucleotide translocator 2 (ANT2)⁷⁷. Compared to the normal brain tissue, DRAK1 is overexpressed in multiple gliomas, with the highest expression levels occurring in glioblastoma multiform (GBM), promoting cell proliferation, migration, and resistance to genotoxic agents in GBM⁷⁸. Other functions of the DAPKs are unknown, which makes it harder to treat cancer related to these kinases.

3.2.4 Classification of small molecule protein kinase inhibitors

Apart from pharmaceutical drug discovery research, small molecule kinase inhibitors also play a major role in basic research for exploring the function of a kinase in a defined biological context. A chemical tool compound must meet strict criteria that were debated within the chemical biology community. A so-called chemical probe should address the designated target with sufficient *in vitro* potency of < 100 nM or cellular potency of <1 μ M and must be able to penetrate the cell (<https://www.sgc-ffm.uni-frankfurt.de/#!donateview>). Furthermore, the chemical probe must be selective within >30-fold selectivity in the subfamily such that the effect can be assigned to the designated target protein. Besides these on-target-related criteria, the physicochemical properties, like solubility in different solvents (aqueous or organic solvents) and chemical stability should also be considered. Additionally, an inactive analogue of the chemical molecule in an inactive form should be provided, which is beneficial in experimental testing. The highly selective compounds that meet these criteria

facilitate the functional annotation of the human proteome and help to understand physiological and pathological processes in the cell. Selectivity and known target profile is a special requirement for chemical probe compounds. Indeed, high selectivity and potency are prerequisite for compounds to be classified as chemical probes. Only when the function of a single kinase is pharmacological disrupted the cellular effect can unambiguously be assigned to the specific kinase. In addition, if the survival and proliferation of a cancer cell is dependent on a single over-activated kinase, inhibition of this kinase has dramatic biological and clinical effect. In this case, a highly selective inhibitor for this kinase would be beneficial and would minimize off-target effects. The search for these highly specific and selective chemical probes is tedious and expensive, which is why a new idea of so called chemogenomic inhibitors focuses on less strict criteria. Here, a chemogenomic inhibitor may inhibit up to ten different targets but needs to show exceptional selectivity beyond these. By creating a library of inhibitors with overlapping target spectra, it is possible to deconvolute the target causing the phenotypical response observed experimentally⁷⁹.

The ultimate goal of consortia, like the Structural Genomics Consortium (SGC), is it to build a chemogenomic set that consist of chemical probes and chemogenomic tool compounds for all human kinases. Despite the success of small molecules as drug treatment and probe programs, there are a large quantity of proteins, including human protein kinases, that cannot be targeted so far. For these, the investigation and development of orthogonal strategies for altering protein functionality are essential.

3.3 Novel protein targeting strategies

Targeted protein degradation is attracting substantial interest owing to its potential to therapeutically modulate proteins that have proved difficult to target with conventional small molecules. Some targets have been undruggable so far because their active site is too broad, contain shallow pockets that are difficult to bridge or simply have no surface for a small molecule to bind. Many of these targets have remained of great therapeutic interest, because they have key roles in cancer and other diseases. Through a rather unintentional discovery, the first molecular glue, thalidomide, was found. Used in the late 1950s as treatment for morning sickness in pregnant women, thalidomide was causing severe physical abnormalities in thousands of children through the exposure in the uterus⁸⁰. Many years later in 1994 thalidomide was found to be effective in treating multiple myeloma⁸¹, although it was not yet discovered that it was through its function as a so-called molecule glue. Molecules that act as molecular glue stick two proteins together, first a target protein that causes a specific phenotype, like a disease, and secondly an E3 ubiquitin ligase that later is responsible for the polyubiquitination and subsequent degradation of the first target by the ubiquitin-dependant cellular protein-degradation machinery. Such destruction of a protein function has advantages over the more common protein-targeting strategy of inhibition. Once its target protein is degraded, a molecular glue can catalytically bind to another protein and repeat the process as a cycle⁸². Furthermore, while a more traditional small molecule needs to actually bind to its target and inhibit it in order to stop the protein's activity, a molecular glue only requires binding which may be achieved with much lower doses.

3.3.1 PROTAC-mediated targeted protein degradation

Beyond molecular glues like thalidomide, induced targeted protein degradation through proteolysis-targeting chimeras (PROTACs) by the ubiquitin-proteasome system represent a new therapeutic modality and owing the potential advantages with respect of dosing, side-effect, drug resistance and modulating un-targetable proteins⁸³. At least 15 designed degraders are in clinical phases in the beginning of 2022⁸⁴, with Arvinas Therapeutics in 2019 being the first company that introduced heterobifunctional degraders in two clinical trials⁸⁵. This chapter will focus on the emerging class of small molecule drugs that do not inhibit protein activity but destroy it by degradation. These degrader small molecules consist of two moieties: one binds a target of interest (POI) while the other binds a cellular E3-

ubiquitin ligase such as CEREBLON (CRBN) or the von Hippel-Lindau tumour suppressor (VHL), that are connected with each other via a linker. Degraders produce proximity between the target and the E3 ligase, resulting in ubiquitination of the target of interest and thereby inducing the proteasome system.

3.3.2 Clinical proof of concept for PROTACs

To date no heterobifunctional degrader molecules are approved by the FDA. The question remains if PROTACs compared to traditional occupancy-based inhibitors would have drug-like properties and are safe for humans⁸³. There are positive reports for the first PROTACs in phase I trials that answered these foundational questions. In 2019, the first PROTAC molecules ARV-110 and ARV-471 have entered clinical testing. In 2020 the trials showed modality against two well-established cancer targets: the oestrogen receptor (ER) and the androgen receptor (AR) (Table 1).

Table 1 | Selected degraders in and approaching the clinical, adapted from Mullard⁸⁵.

Drug	Company/ Sponsor	Target, Indication	Clinical Phase (2021)
ARV-110	Arvinas	AR, Prostate cancer	Phase II
ARV-471	Arvinas	ER, Breast cancer	Phase II
ARV-766	Arvinas	AR, Prostate cancer	Phase I
AR-LD	Bristol Myers Squibb	AR, Prostate cancer	Phase I
DT2216	Dialectic	BCL-XL, Liquid and solid cancers	Phase I
KT-474	Kymera/ Sanofi	IRAK4, Autoimmune	Phase I
KT-413	Kymera	IRAK4, MYD88-mutant DLBCL	Phase I
KT-333	Kymera	STAT3 Liquid and solid tumors	Phase I
NX-2127	Nurix	BTK, B cell malignancies	Phase I
NX-5948	Nurix	BTK, B cell malignancies and autoimmune	Phase I
CG001419	Cullgen	TRK, Cancer and other diseases	Phase I
CFT8634	C4 Therapeutics	BRD9, Synovial sarcoma	Phase I
FHD-609	Foghorn	BRD9, Synovial sarcoma	Phase I

AR = Androgen receptor, ER = Oestrogen receptor, DLBCL = diffuse large B cell lymphoma

So far, the heterobifunctional degraders currently in the clinic have focused only on proteins with well-characterized biological and biochemical properties and previously established clinical efficacy. To expand the toolbox of PROTACs it will be necessary for academia and

pharmaceutical industry to focus on the investigation of new E3 ligases and especially the establishment of the proof of concept, because it induces a completely new variable in the design of PROTACs.

3.3.3 Investigation of new E3 ligases

After the development of ARV-110 and ARV-471 it was disclosed that both PROTACs recruit CRBN as their E3 ligase to catalyse their target ubiquitination and proteasome degradation⁸³. The first molecular glue thalidomide and its close analogues lenalidomide and pomalidomide have been identified as ligands for CRBN, and hence it appears that CRBN is the preferred E3 ligase for the first wave of targeted protein degradation therapeutics in clinical trials, with the exception of BCL-XL that recruits VHL as 3L ligases. Academia and the pharmaceutical industry have realized that CRBN and VHL supplanted as the initial workhorses and that it might be useful to explore the more than 600 human ubiquitin E3 ligases⁸⁶. Resistance mechanisms play a major role in targeting proteins with small molecules and using the same E3 ligase creates concerns that tumour cells could mutate to evade degraders that rely on non-essential ligases, such as CRBN and VHL. Preclinical studies suggest that degraders that use CRBN and VHL to target multiple protein classes have detected emerging resistance that occurs via mutation and/ or downregulation of components of the ubiquitin ligases machinery⁸⁷. The development of novel E3 ligases involved practical considerations such as structural enablement, druggability and mechanistic understanding of the ligase. However, ligases have other key characteristic, like tissue and cell-type specificity, tumour enrichment or tumour essentiality. Several new emerged E3 ligases have been identified so far: tripartite motif-containing protein 24 (TRIM24)⁸⁸, DCAF 15⁸⁹, GID4⁹⁰ and RING (Really Interesting New Gene) containing proteins⁹¹ and many others⁹².

The family of human inhibitors of apoptosis (IAP) proteins, also called baculoviral IAP repeat containing proteins (BIRCs) consists of five RING type E3 ligases and 3 non-E3 ligases (BIRC1, BIRC5 and BIRC6) and share a homologous domain, called baculoviral IAP repeat (BIR) domain. All BIRC E3 ligases contain next to the C-terminal RING domain a BIR3 domain, which are both required for their protein degradation activity⁹³. BIRC2/3 E3 ligases are involved in the modulation of diverse pathways including TNF α regulation through TRAF2 degradation and the regulation of the NF κ B pathway⁹⁴. BIRC4 has been reported to activate

the NF κ B pathway but plays additional roles in TGF β signalling, mammary gland development and maturation of T-cells. Deficiency of BIRC4 in humans causes defects in immunity such as susceptibility to infections, splenomegaly, cytopaenias, and auto inflammatory disease⁹⁵. BIRC7 acts as an activator of non-apoptotic functions of caspases such as spermatogenesis. BIRC8 was reported to be active in immune deficiency response as a result of *E. coli* infection⁹⁶. BIRCs have been shown to inhibit apoptosis of cells, while uncontrolled BIRC activity leads to resistance of regulated cell death, an acquired property that constitutes one of the hallmarks of cancer²⁵. Biological roles of BIRCs have been extensively reviewed^{97, 96, 98}. X-linked IAP (XIAP/ BIRC4) is one of the best characterized family members and is considered a target for therapeutic intervention in several cancers⁹⁹. The natural inhibitor of XIAP is the so called Second Mitochondria-derived Activator of Caspases/Direct IAP Binding with Low pI (SMAC/Diablo), an N-terminal tetrapeptide (AVPI) which inspired IAP antagonists, called "SMAC mimetics" binding to the IAP binding motif (IBM) groove of some BIR domains^{97, 98} and have potential to function as the E3 ligase handle when designing PROTAC molecules to recruit the E3 ligase machinery to degrade different proteins of interests. Despite the increasing number of SMAC mimetic inhibitors including a number of compounds in clinical evaluation, no comprehensive assay platforms have been established to characterize the selectivity of BIRC inhibitors within this family of protein interaction domains.

3.4 Methodologies to elucidate drug-protein interactions

Investigating the interaction between small molecules and proteins can be approached from different perspectives and is important for the advancement of both basic science and drug discovery.

3.4.1 *In vitro* profiling assays

Biochemical methods, especially ones that can be used in a high-throughput approach, have proven to be beneficial in the discovery of small molecule kinase inhibitors. Using these enzymatic and binding assays enables to screen large compound sets in a short period of time and give important information about the compound's potency. Besides confirming the on-target affinity it is important to screen additional targets to determine the compounds selectivity profile. Many different screening technologies have been proven suitable for the high throughput assessment of selectivity, in general these technologies can be divided in activity/ enzymatic based assays and binding assays. Both formats need the purified protein, either the kinase domain or the full-length kinase, meaning that they do not accomplish close-to-physiological conditions and are far from the cellular environment. Enzymatic assays are mainly used to directly or indirectly measure the activity of the kinase, often the product production such as the consumption of ATP, the production of ADP or the amount of converted phosphorylated substrate. Radioactivity, fluorescence or luminescence are common detection methods. Competition binding assays are capable of measuring the binding of a small molecule kinase. Although binding to a kinase does not automatically alter the kinase activity, both are in good correlation with each other. An example for a binding assay is the KinomeScan™ technology developed by Ambit, now licensed by DiscoverX¹⁰⁰. The method uses DNA-tagged kinases and quantifies them by immobilized kinase inhibitors on streptavidin-coated magnetic beads and subsequent PCR readout¹⁰⁰. The DNA tagged kinase is combined with an inhibitor of interest which will prevent its target kinase from binding to the beads. The quantity of bead bound protein is analysed by qPCR and compared between the control and test sample. This commercially available assay is commonly used to determine the selectivity of probe molecules and chemogenomics on around 350 kinases. The assay uses purified proteins and is limited by the capability of a kinase to bind to an inhibitor-immobilized bead. An example for a commercial kinase activity assay is the radioactivity-based assay of Reaction Biology. Here, a ³³Phosphor labelled ATP is used as a

substrate and the resulting transfer of the radioactive phosphate onto the peptide or protein substrate is quantified via membrane spotting. A competing inhibitor prevents the transfer of the radioactive phosphate in a dose-dependent manner and the resulting affinity can be calculated. The assay is limited by finding a suitable substrate for a given kinase, a task that is challenging for assaying the dark kinome.

3.4.2 Cell-based profiling assays

Biochemical assays such as mentioned above help to determine possible targets and give important information of the selectivity of a small molecule and the drug's mode of action. Unfortunately, these methods do not consider cellular features like posttranslational modification, complex partners, target localization, cellular compartments or intracellular ATP concentration. An important aspect which can be investigated in cell-based assay is the cell permeability of a test molecule, which is particularly important for larger molecules like macrocyclic compounds and bivalent PROTAC molecules. A method taking some of these cellular features into account is called Kinobeads^{101, 102}. In this method, a mixture of lysates from six different cell lines, expressing the maximum amount of endogenous proteins without diluting the individual protein concentrations beyond detectability, is used to form a panel of assays covering most of the human kinome. The lysates are mixed with a set of kinase ligand immobilized beads that bind the kinases and enrich them after a wash-out. If in a test sample a compound binds the kinase it competes with the Kinobeads and the kinase no longer is enriched. The dose-dependent reduction in signal later is quantified to determine the compounds binding potency using mass spectrometry. The Kinobeads assay used endogenous human expressed proteins with human PTMs as present in the six cell lines. About 400 protein kinases are detectable with the limitations being the expression of the target kinase in the lysates used, the ability to be bound by Kinobeads and the kinases ability to get ionized for mass spec detection.

3.4.3 Cellular target engagement NanoBRET – an *in cellulo* method

The NanoBRET target engagement assay determines the binding potency of a small molecule in the environment of a living cell¹⁰³. A full-length protein kinase is fused to a NanoLuc luciferase and that construct is transiently transfected into a suitable host cell for protein expression. In this setup, the kinase is overexpressed and will carry human post translational

modification. Usual binding partners are present in the cell as well as a cellular concentration of the kinase's substrate ATP. If a suitable tracer molecule, often a promiscuous kinase inhibitor fused to a BODIPY fluorophore, is added to the cells a bioluminescence resonance energy transfer (BRET) can be observed for the luciferase and BODIPY upon furimazine substrate addition. Because of a competition for the binding site of both test compound and tracer molecule, this BRET is reduced in a dose-dependent manner when test compound is added and the affinity can be determined. The method is limited by finding a matching kinase-tracer pair.

3.5 Objectives of this thesis

The aim of this thesis is to assess and investigate the cellular selectivity of small molecules inhibitors.

- The first aim was to support medicinal chemistry SAR projects using the cellular target engagement method and determine on-target activity as well as off-target profiles for different chemical probes and chemogenomics compounds (Chapter 5.1).
- The second aim was to evaluate current literature compounds regarding their potency and family selectivity and potential use as a chemical tool compound of two specific understudied subfamilies of the human kinome, the splicing kinase family and the CDK family (Chapter 5.2).
- The third aim was to evaluate a large library of published FDA approved and clinical small molecule kinase inhibitors regarding their selectivity using an optimized target engagement method in cells (Chapter 5.3).
- The last aim was to enable the design of PROTACs with novel E3 binders by investigating published small molecules for the WDR5 and BIRC proteins and test them in prospect of their potency and family selectivity (Chapter 5.4).

4. Experimental Procedures

4.1 Methods

In this chapter general techniques used in the thesis will be described. If not stated otherwise all experiments were conducted as described below. This chapter will be divided into biochemical methods and cell-based methods. Biochemical methods allow the detection, quantification or the activity of molecules, while cell-based assays allow the determination of health of cells in response to a biological active molecule. The main method in this thesis, the NanoBRET cellular target engagement assay, allows the determination of the molecule binding in an intact living cell environment, and hence is a combination of these two methods.

4.1.1 Biochemical methods to determine small molecule potency

The biochemical methods used in this thesis require purified protein and were mainly used to determine the potency of a test molecule and rank chemical SAR projects. The purified proteins used for the projects described in thesis were purified by different colleagues, namely Dr. Andreas Krämer, from the SGC Frankfurt and are part of our in-house T_M panel. A full list of all purified proteins can be found in SI Table 1.

4.1.1.1 Differential scanning fluorimetry (DSF) assay

Most of the DSF data collected for the projects used in this thesis, especially the characterization of the chemical probes (Chapter 5.1) and the splicing kinases set (Chapter 5.2.1) was performed by Lewis Elson. The DSF data measured for the kinome-wide clinical inhibitor analysis (Chapter 5.3) was performed by Martin P. Schwalm.

DSF measurements were performed as described previously¹⁰⁴. In more detail: During the DSF assay the protein denaturation process over a temperature gradient from 25°C to 99°C is monitored using a fluorescent probe, namely SYRPO-Orange. The dye is binding to the hydrophobic parts of the protein which are usually located inside of the protein, but become solvent exposed once the protein gets denaturized. Upon temperature increase the now hydrophobic solvent exposed protein molecules aggregate and thereby reduce the fluorescence of the dye, which results in the well-known protein melting curve. If a small molecule is binding to the protein it is believed to increase the melting temperature proportional to the binding affinity of the compound and thereby thermally stabilize the

protein. The shift in the temperature is the shift of the melting temperature of non-treated protein and small molecule treated protein and is often used as an assay parameter to guide a SAR. The comparison for single proteins to a set of small molecule inhibitors gives comparable results and the thermal shift can serve as ranking parameters, while it could be difficult to compare different temperature shift of proteins, because the stabilization of each protein can vary. A comparison of these different thermal shifts between different proteins could be leading to false conclusions regarding the selectivity profile of inhibitors.

For the projects described in detail in this thesis DSF measurements were performed on the QuantStudio5, if not stated otherwise. The purified proteins were buffered in DSF buffer (25 mM HEPES pH 7.5, 500 mM NaCl) and assayed in a 384-well plate with a final protein concentration of 2 μ M in 10 μ L final assay volume. Small molecule inhibitors were added in excess to a final concentration of 40 μ M, using the ECHO 550 acoustic dispenser. SYPRO-Orange was used at five times final concentration. Filters for excitation and emission were set to 465 and 590 nm, respectively. The temperature was increased from 25°C with 3°C/min to a final temperature of 99°C, while scanning. Data was analysed using Boltzmann-equation in the Protein Thermal Shift software.

4.1.1.2 Isothermal titration calorimetry (ITC) assay

The ITC data collected for the projects used in this thesis, especially the investigation of the current BIRC inhibitor landscape (Chapter 5.4.2) were performed by Martin P. Schwalm.

Isothermal titration calorimetry is a technique by which thermodynamic parameters as ΔG , ΔH and $T\Delta S$ and the reactions stoichiometry can be determined¹⁰⁵. ITC determines the binding heat upon protein titration into test compound solution in comparison to a reference cell. Based on the signal upon this titration of the analyte solution to the test solution the thermodynamic parameters are calculated.

For the projects described in detail in this thesis ITC measurements were performed using a NanoITC instrument at 25°C. Purified protein at a concentration of 116 μ M was titrated into the reaction cell containing 10 μ M inhibitor dissolved in gel filtration buffer. For this protocol, the chamber was pre-equilibrated with the test compound, and the protein was titrated in while continuously measuring the rate of exothermic heat evolution. The heat of binding was integrated, corrected, and fitted to an independent single-binding site model based on the

manufacturer's instructions, from which thermodynamic parameters (ΔH and $T\Delta S$), equilibrium association and dissociation constants (K_A and K_D , respectively), and stoichiometry (n) were calculated. Data was analysed and displayed using GraphPad Prism 9.3 software.

4.1.2 Cell-based assays

Cell-based assays do not have the need to purify protein, but rather use the endogenous protein level from a human cell or transfect the protein directly in an intact cell environment.

4.1.2.1 Mammalian cell culture

Human cancer derived cell-lines used in projects described in this thesis are embryonic kidneys cells HEK293T (ATCC CRL-3216), epithelioid carcinoma PANC1 (ATCC CRL-1469), adenocarcinoma/ cervical carcinoma HeLa (ATCC CCL-2), osteosarcoma U-2OS (ATCC HTB-96), bipenotypic B myelomonocytic leukemia MV4-11 (ATCC CRL-9591) and acute monocytic leukemia THP-1 (ATCC TIB-202). In general mammalian cells can be separated into adherent and suspension cells. The information for the appropriate growth media can be found on the ATCC website.

Adherent cell lines. The cells were cultured using DMEM supplemented with 1% Penicillin/Streptomycin and 10% FBS in a 75 cm² flask. The old culture medium was removed and the cell layer was briefly rinsed with PBS and 0.05% Trypsin EDTA solution was added to disperse the thin cell layer. The Trypsin mixture is incubated for a few minutes at 37°C/ 5% CO₂, till the cells are detached. After incubation DMEM is added to inactivate the Trypsin-EDTA solution. The cells were distributed to a new flask at an appropriate concentration or the cell number was counted and diluted to use for experiments. Cells were counted by using a Cell Counter and Counting Slides. To measure the cells, they were stained using 0.4% trypan blue.

Suspension cell lines. Suspension cell lines do not adhere to the culture flask and thereby do not need to be trypsinized, before used in an experiment. The cells were mixed and centrifuged at 200g for 1 min to separate the old growth media from the cells. The old media was removed and fresh media was added to the cells. The cells were distributed to a new flask, or the cell number was counted, to be used in further experiments. The cell number was counted as the adherent cells described above.

4. Experimental Procedures

4.1.2.2 Cell viability assay in living cells

The assay for cell viability which was used in chapter 5.4.1 was the alamarBlue assay. A resazurin-based reagent that functions as a cell healthy indication can be used to quantitatively measure the cell viability. Living cells have a natural metabolic reducing power to convert the added non-fluorescent dye resazurin to bright red-fluorescent resorufin. To readout the fluorescence a PHERAstar plate reader is used at 560/590 nm (excitation/emission) filter settings.

4.1.2.3 Cell viability using the IncuCyte

The cell viability assay data for the projects used in this thesis, especially the investigation of the splicing kinase family (Chapter 5.2.1) were performed by Lewis Elson.

Viability assessment was performed using the IncuCyte S3 in U2OS and HEK293T cells. HEK293T and U2OS were cultured in DMEM supplemented by 10% FBS and 1% Penicillin/Streptomycin. For every cell line, 1500 cells per well were seeded in 384- well plates in culture medium. Confluence was measured before compound treatment and 12 h, 24 h as well as 48 h after 10 μ M of compound exposure. Staurosporine 10 μ M was used as a positive control and DMSO 0.1% as a negative control. Growth rate was calculated as described previously by Hafner *et al*¹⁰⁶. Two biological duplicates were performed.

4.1.2.4 High content live-cell multiplex assay

The multiplex assay data for projects used in this thesis, especially the investigation of the splicing kinases families (Chapter 5.2.1) were performed by Amelie Tjaden.

The Multiplex live-cell high-content assay was performed as described previously described by Tjaden *et al*¹⁰⁷. In brief, U2OS were cultured in DMEM supplemented by 10% FBS and Penicillin/Streptomycin. MRC-9 fibroblasts were cultured in EMEM plus L-glutamine supplemented by 10% FBS and Penicillin/Streptomycin. For every cell line, 1500 cells per well were seeded in 384- well plates in culture medium. Cells were stained with 60 nM Hoechst33342, 75 nM Mitotracker red, 0.3 μ L/well Annexin V Alexa Fluor 680 conjugate and 25 nL/well BioTracker 488 green microtubule cytoskeleton dye. Each compound was tested at two different concentrations (1 and 10 μ M), n = 4. Staurosporine 10 μ M was used as a positive control. Cellular shape and fluorescence were measured before compound treatment and 12 h, 24 h as well as 48 h after compound exposure using a CQ1 high-content confocal

microscope. The following setup parameters were used for image acquisition: Ex 405 nm/Em 447/60 nm, 500 ms, 50%; Ex 561 nm/Em 617/73 nm, 100 ms, 40%; Ex 488/Em 525/50 nm, 50 ms, 40%; bright field, 300 ms, 100% transmission, one centered field per well, 7 z-stacks per well with 55 μm spacing. Images were analysed using the CellPathfinder software. The cells were detected as described previously, gated using a machine learning algorithm and divided in different categories. Normal cells were further gated in cells showing healthy, fragmented or pyknotic nuclei. The program was trained using a training set of five compounds with known effects (staurosporine, paclitaxel, digitonin, milciclib, and daunorubicin). Data was normalized against the average of DMSO (0.1%) treated cells. Significance was shown using a two-way ANOVA analysis. Two biological duplicates were performed.

4.1.2.5 Cellular target engagement assay NanoBRET

The NanoBRET target engagement assay determines the binding potency of a chemical molecule in the environment of a living cell¹⁰³ and is described in Figure 4. For that, a full-length protein kinase is fused to a NanoLuc luciferase and that construct is transiently transfected into a suitable host cell for protein expression. In this setup, the kinase gets mildly overexpressed and will carry human post translational modifications. Usual binding partners are present in the cell as well as a cellular concentration of the kinase substrate ATP. If a suitable tracer, here a promiscuous kinase inhibitor fused to a BODIPY fluorophore, is added to the cells a bioluminescence resonance energy transfer (BRET) can be observed for the luciferase and BODIPY upon furimazine substrate addition¹⁰⁸. Because of a competition for the binding site of both test compound and tracer, this BRET reduces in a dose-dependent manner when test compound is added.

4. Experimental Procedures

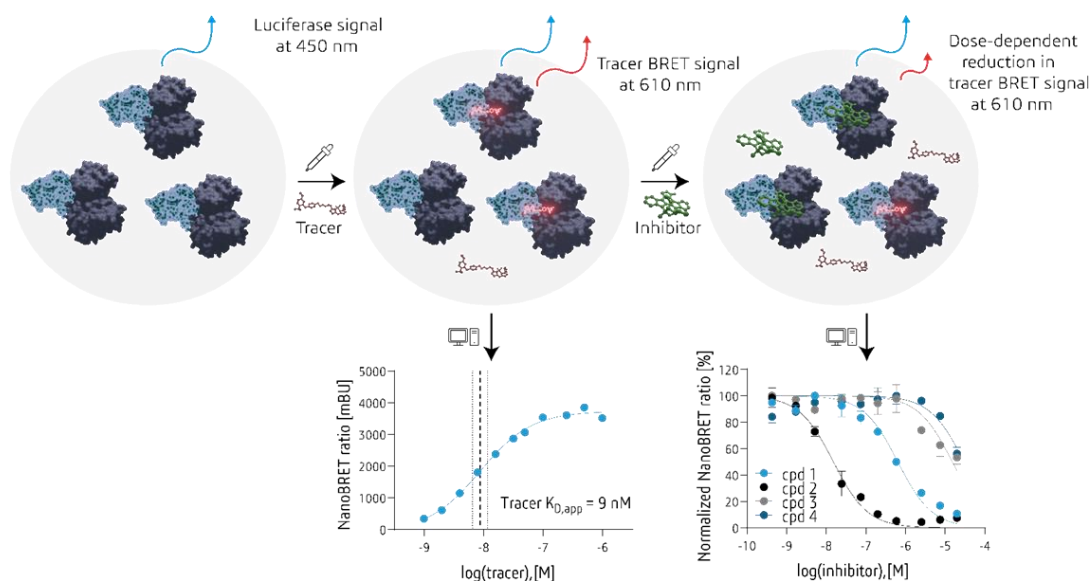


Figure 4 | Cellular target engagement NanoBRET assay. Transiently overexpressed kinase of interest is fused to a NanoLuc construct. Upon addition of the substrate, the luciferase emits light at 450 nm. After addition and binding of the tracer molecule a second signal at 610 nm can be measured. If the test small molecule is binding to the kinase of interest, it displaces the tracer molecule thereby decreasing the tracer BRET signal at 610 nm. This dose-dependent reduction in the signal can be plotted against the inhibitor concentration used and an EC₅₀ can be determined. Figure adapted from cellinib.com (<https://www.cellinib.com/technique/>).

The NanoBRET target engagement assay was performed as described previously^{103, 109}. Full-length kinases plasmids containing N- or C-terminal placements of NanoLuc were obtained by the manufacturer. See full list of constructs used in this thesis in SI Table 2. To lower intracellular expression levels of the reporter fusion, the NanoLuc/kinase fusion constructs were diluted into carrier DNA (pGEM3ZF-) at a mass ratio of 1:10 (mass/mass), prior to forming FuGENE HD complexes according to the manufacturer's instructions. DNA and FuGENE complexes were formed at a ratio of 1:3 (µg DNA/µL FuGENE). One part of the transfection complexes was then mixed with 20 parts (v/v) of HEK293T cells suspended at a density of 2 × 10⁵ cells /mL in DMEM + 10% FBS seeded into T75 flasks and allowed to express for 20h. For target engagement both serially diluted test compound and NanoBRET Kinase Tracer as specified in SI Table 2 at the indicated final concentration were pipetted into white 384-well plates. The corresponding transfected cells were added and reseeded at a density of 2 × 10⁵ cells /mL after trypsinization and resuspending in Opti-MEM without phenol red. The system was allowed to equilibrate for 2 hours at 37°C /5% CO₂ prior to BRET measurements. To measure BRET, NanoBRET NanoGlo Substrate and Extracellular NanoLuc Inhibitor was added as per the manufacturer's protocol, and filtered luminescence was measured on a PHERAstar plate reader equipped with 450 nm BP filter (donor signal) and

610 nm LP filter (acceptor signal). Competitive displacement data was then graphed using GraphPad Prism 9 software using a 3-parameter curve fit with the following equation:

$$Y = \frac{100}{(1 + 10^{(x - \log IC_{50})})}$$

The data was normalized to background and tracer only control signal. To perform the NanoBRET assay in lysed assay mode digitonin a non-ionic detergent is added to the cells after the incubation time of cells and transfection mix after 20h, while adding the tracer molecule and the small molecule inhibitor. The cell-tracer-digitonin mixture is then incubated at 1h at room temperature, instead of the 2h at 37°C from the standard protocol.

4.1.2.6 The comparability problem of competition-based assays

In this work, a kinase cellular profiling panel was developed. The signal of the respective assays is dependent on the match of kinase and tracer and a BRET will be more efficient if the proximity of the tracer and luciferase are smaller. The signal can be increased by using a higher tracer concentration but when determining the potency of a kinase inhibitor, the reagents used may disturb the determination of an inhibitor affinity because of a competition of the reagent, here the tracer, and the inhibitor for the binding site are related to the concentrations of tracer and compound used in the respective assay. The relation of the influence of the reagent used to the resulting K_D is given by the Cheng-Prusoff-Relation¹¹⁰:

$$K_D = \frac{IC_{50}}{1 + \frac{[tracer]}{tracer K_{D,app}}}$$

If a tracer concentration is now used at a previously determined $K_{D,app}$ of the tracer molecule, 50% of the kinases are bound by that tracer. According to the Cheng-Prusoff-Relation, the "true" K_D of the inhibitor in this competition assay would be described as:

$$K_D = \frac{IC_{50}}{1 + \frac{[tracer]}{tracer K_{D,app}}} = \frac{IC_{50}}{1 + 1} = \frac{IC_{50}}{2}$$

If a tracer is used at higher concentration, e.g. 10-times the $K_{D,app}$, this would shift to:

$$K_D = \frac{IC_{50}}{1 + \frac{10 \times tracer K_{D,app}}{tracer K_{D,app}}} = \frac{IC_{50}}{1 + 10} = \frac{IC_{50}}{11}$$

4. Experimental Procedures

This would result in a dramatic underestimation of the IC_{50} because of a very high tracer concentration. In the other case, when a concentration lower as the tracer $K_{D, app}$ is used, e.g. 0.1-times the tracer $K_{D, app}$:

$$K_D = \frac{IC_{50}}{1 + \frac{0.1 \times \text{tracer } K_{D, app}}{\text{tracer } K_{D, app}}} = \frac{IC_{50}}{1 + 0.1} = \frac{IC_{50}}{1.1}$$

When a lower tracer concentration is used in relation to the tracer $K_{D, app}$, the EC_{50} is a better estimate for the “true” K_D . In the panel set-up to make each kinase as comparable to the other as possible, each tracer and kinase are used at their respective $K_{D, app}$ if possible but because of solubility limitations of the tracer-coupled BODIPY fluorophore a maximum concentration of 1 μM may be used. In a tracer titration this may result in an overestimation of the tracer $K_{D, app}$ but as observed above, if a lower tracer concentration is used than the tracer $K_{D, app}$, the effect of the reagent is lower and hence closer to the true K_D . This means, the maximum error of a potential “underestimation” of the true K_D would be 2-fold as used at tracer $K_{D, app}$ and the minimal error would be 1-fold. Between these two points is the estimated error created in this panel set-up which is deemed within the normal margin of error for cell-based assay.

4.1.3 Compound handling and management

Small molecule inhibitors used for this thesis were purchased from different vendors. For the analysis of the kinase panel a set of clinical and FDA approved kinase inhibitors was purchased from Selleckchem (SI Table 6). A list of all compounds used in this thesis and they suppliers can be found in SI Table 3.

4.2 Material

Listed below are the different devices (Table 2), materials (Table 3) and reagents (Table 4) used for this thesis.

Table 2 | List of devices used.

Description	Name	Company (Location Headquarter)
Cell Counter	TC20 Automated Cell Counter	Bio-Rad (US, CA)
Cell culture hood	HeraSafe 2025	Thermo Fisher (US, MA)
Confocal microscope	CQ1	Yokogawa (Tokio)
DSF instrument	QuantStudio5	Applied Biosystems (US, MA)
Heat Sealer	PlateLoc	Agilent Technologies (US, Santa Clara)
Incubator	CellXpert® C170i	Eppendorf AG (GE, Hamburg)
ITC instrument	NanoITC	TA Instruments (US, DE)
Liquid Handler	ECHO 550 acoustic dispenser	Labcyte (US, CA)
Liquid Handler	Multidrop Combi	Thermo Fisher (US, MA)
PCR machine	Thermo cycler	Biometra (GE, Göttingen)
pH meter	3510 pH Meter	Jenway Bibby (UK, Straffordshire)
Pipettes	Eppendorf Research Plus 0.1-2.5	Eppendorf AG (GE, Hamburg)
Pipettes	Eppendorf Research Plus 2-20	Eppendorf AG (GE, Hamburg)
Pipettes	Eppendorf Research Plus 20-200	Eppendorf AG (GE, Hamburg)
Pipettes	Eppendorf Research Plus 100-1000	Eppendorf AG (GE, Hamburg)
Pipettes	Thermo E1 Clip-Tip 200	Thermo Fisher (US, MA)
Pipettes	Thermo E1 Clip-Tip 12.5	Thermo Fisher (US, MA)
Plate Reader	PHERASTAR FS	BMG labtech (GE, Offenburg)

Table 3 | List of materials used.

Description	Name	Company (Location Headquarter)
Assay plate	1536-well, black, #782900	Greiner Bio-One (Austria)
Assay plate	96-well 2 mL #780270	Greiner Bio-One (Austria)
Cell Viability assays	384-well #781 091	Greiner Bio-One (Austria)

4. Experimental Procedures

Counting Slides	Cell Counting Slides #145-001	Bio-Rad (US, CA)
DSF plate	384-well #BC3384	Thermo Fisher (US, MA)
ECHO plate	PP 384-well #LBCYPP-0200	Labcyte Inc. (US, Sunnyvale)
ECHO plate	LDV 384-well # LBCYLP-0200	Labcyte Inc. (US, Sunnyvale)
NanoBRET plate	384-well #781 207	Greiner Bio-One (Austria)
PCR plate	Standard PCR plate for LC480	4titude Ltd. (US, Sacramento)
Seals	Nunc Aluminium Acrylate	Thermo Fisher (US, MA)

Table 4 | List of reagents used.

Description	Name	Company, Location Headquarter
Agar	Agar, pure, powder	Sigma-Aldrich Corp. (US, St. Louis)
Antibiotic cell culture	Penicillin/Streptomycin	Thermo Fisher (US, MA)
Antibiotics	Kanamycin	Sigma-Aldrich Corp. (US, St. Louis)
Antibiotics	Chloramphenicol	Sigma-Aldrich Corp. (US, St. Louis)
Antibiotics	Ampicillin	Sigma-Aldrich Corp. (US, St. Louis)
Buffer ingredients	Bovines Serum Albumin #A-7906	Invitrogen AG (US, Carlsbad)
Buffer ingredients	DL- Dithiothreitol >98% (DTT)	Sigma-Aldrich Corp. (US, St. Louis)
Buffer ingredients	Glycerol	Melford Laboratories (UK, Chelsworth)
Buffer ingredients	HEPES buffer solution	Sigma-Aldrich Corp. (US, St. Louis)
Buffer ingredients	Imidazole, 99+%, crystalline	Thermo Fisher (US, MA)
Buffer ingredients	KCl	Thermo Fisher (US, MA)
Buffer ingredients	MgCl ₂	VWR Chemicals (US, Radnor)
Buffer ingredients	MnCl ₂	Thermo Fisher (US, MA)
Buffer ingredients	MOPS >99.5%	Sigma-Aldrich Corp. (US, St. Louis)
Buffer ingredients	Sodium chloride	Sigma-Aldrich Corp. (US, St. Louis)
Buffer ingredients	TCEP	Thermo Fisher (US, MA)
Buffer ingredients	TRIS Base	Merck KGaA (GE, Darmstadt)
Buffer ingredients	Tween 20	Cisbio Bioassays (FR, Codolet)
Cell Culture	Trypsin 0.1% EDTA	Thermo Fisher (US, MA)

Cell Culture	Phosphate Buffered Saline (PBS)	Thermo Fisher (US, MA)
DNA Loading Dye	5x DNA Loading Buffer, Blue	Bioline (GE, Luckenwalde)
DNA staining dye	Hoechst33342	Thermo Fisher (US, MA)
Dye	Mitotracker red	Thermo Fisher (US, MA)
Dye	Annexin V Alexa Fluor 680	Thermo Fisher (US, MA)
Dye	BioTracker 488	Merck Millipore (GE)
<i>E.coli</i> cells	MACH1 cells	Thermo Fisher (US, MA)
Fluorescent probe DSF	SYPRO-Orange #S6651	Thermo Fisher (US, MA)
Growth Medium	DMEM, Gibco	Thermo Fisher (US, MA)
Growth Medium	Opti-MEM wo phenol red	Thermo Fisher (US, MA)
Luciferase Inhibitor	Extracellular NanoLuc Inhibitor	Promega (US, WI)
Media	LB broth (MILLER)	Sigma-Aldrich Corp. (US, St. Louis)
Media	Peptone from casein (Tryptone)	Merck KGaA (GE, Darmstadt)
Media	Yeast Extract Granulated	Sigma-Aldrich Corp. (US, St. Louis)
Midi Prep Kit	MidiPrep Kit Qiagen	Qiagen N.V. (NL, Venlo)
Midi Prep Kit	MidiPrep Kit Promega	Promega (US, WI)
NanoBRET substrate	NanoGlo Substrate	Promega (US, WI)
NaOH	Sodium hydroxide – pellets	Merck KGaA (GE, Darmstadt)
Solvent	DMSO, Dimethyl sulfoxide	Sigma-Aldrich Corp. (US, St. Louis)
Supplement Medium	FBS, Gibco	Thermo Fisher (US, MA)
Transfection Reagent	FuGene HD	Promega (US, WI)
Transfection Reagent	Transfection Carrier DNA	Promega (US, WI)

5. Results and Discussion

The results presented in the thesis were generated by me as well as by internal and external collaboration partners. The exact distribution of the contributions is listed in Appendix 9.2 List of publications and collaboration partners, 9.3 Statutory declarations and in the author contributions from the respective publications.

5.1 The search for new chemical probes – cellular selectivity as main criteria

During my thesis, I contributed to the characterization of several chemical probes and chemogenomic tool compounds. Next to the potency of below 100 nM *in vitro* and below 1 μ M in cells, the narrow selectivity profile for probes is essential, because they are used to question a specific targets biology. Per definition, the closest off-target needs to show a 30-fold window to allow for using the chemical probe at a concentration where the on-target effect is still observable but any off-target effects are negligible. Chemogenomic tool compounds are less strict when it comes to their selectivity, they are allowed to have up to ten “on-targets”, but the knowledge about the on-targets and their respective affinity is indispensable. Using a set of chemogenomic tool compounds with overlapping target spectra allows for target identification within phenotypical assays. Within these projects, we frequently investigated the selectivity profile derived from *in vitro* assay technologies as basis for their profiling in living cells and assessed the cellular target affinity for these molecules. A selection of these projects will be presented during the next chapter.

5.1.1 Selective macrocyclic molecule to investigate understudied kinase STK17A

(In the following subchapter, parts of the publication “Illuminating the Dark: Highly Selective Inhibition of Serine/Threonine Kinase 17A with Pyrazolo[1,5- α]pyrimidine-Based Macrocycles” are included¹¹¹).

In this study, we investigated the apoptosis inducing protein kinase DRAK1, also called serine/threonine kinase 17A (STK17A) which is part of the dark kinome. The cellular function of DRAK1 and its involvement in different physiological processes is widely unknown. Although DRAK1 has been identified as an off-target for several kinase inhibitors - for example the multi kinase inhibitor AT9283¹¹² as well as the FDA approved drug tomivosertib¹¹³ - no selective DRAK1 inhibitor has been reported yet to study the targets biology. A reported DRAK2 isoform selective compound SGC-STK17B-1, shows only weak

activity on the DRAK1 isoform of $4.7 \mu\text{M}^{114}$, which is surprising because both isoforms share a sequence similarity of 66% in the kinase domain. The starting point for the development of a selective DRAK1 inhibitor was the published non-selective macrocyclic inhibitor IC19, which is based on a pyrazolo[1,5- α]pyrimidine scaffold¹¹⁵. Interestingly the initial starting compound (14) was not exclusively selective for DRAK1, but it showed no activity against the closely related DAPKs. To further optimize the SAR, we solved the structure of DRAK1 bound to 14¹¹¹ (PDB ID: 7QUE). The structure revealed an activation loop exchange with a second kinase domain located in the asymmetric unit. This has been also described for the auto-activated DAPK family member DAPK3¹¹⁶. Whether DRAK1 requires phosphorylation at this position to be fully activated is not known. In the observed conformation, DRAK1-T226 is positioned in the substrate-binding site of the interaction protomer. Indeed, DRAK1-T226 is conserved in DRAK2 (T198). A phosphorylation at this tyrosine would stabilize the interaction with a lysine residue in the catalytic loop next to the HRD (HLD in DRAK1) motif resulting in a stabilization of the substrate-binding site. The initial compound 14 is interacting with DRAK1 in a type I binding mode. A structural alignment of the DAPKs confirmed that DAPK1–3 differed significantly from DRAK1 and DRAK2, whereas the ATP-binding pocket of DRAK1 shared high similarity with DRAK2.

5. Results and Discussion

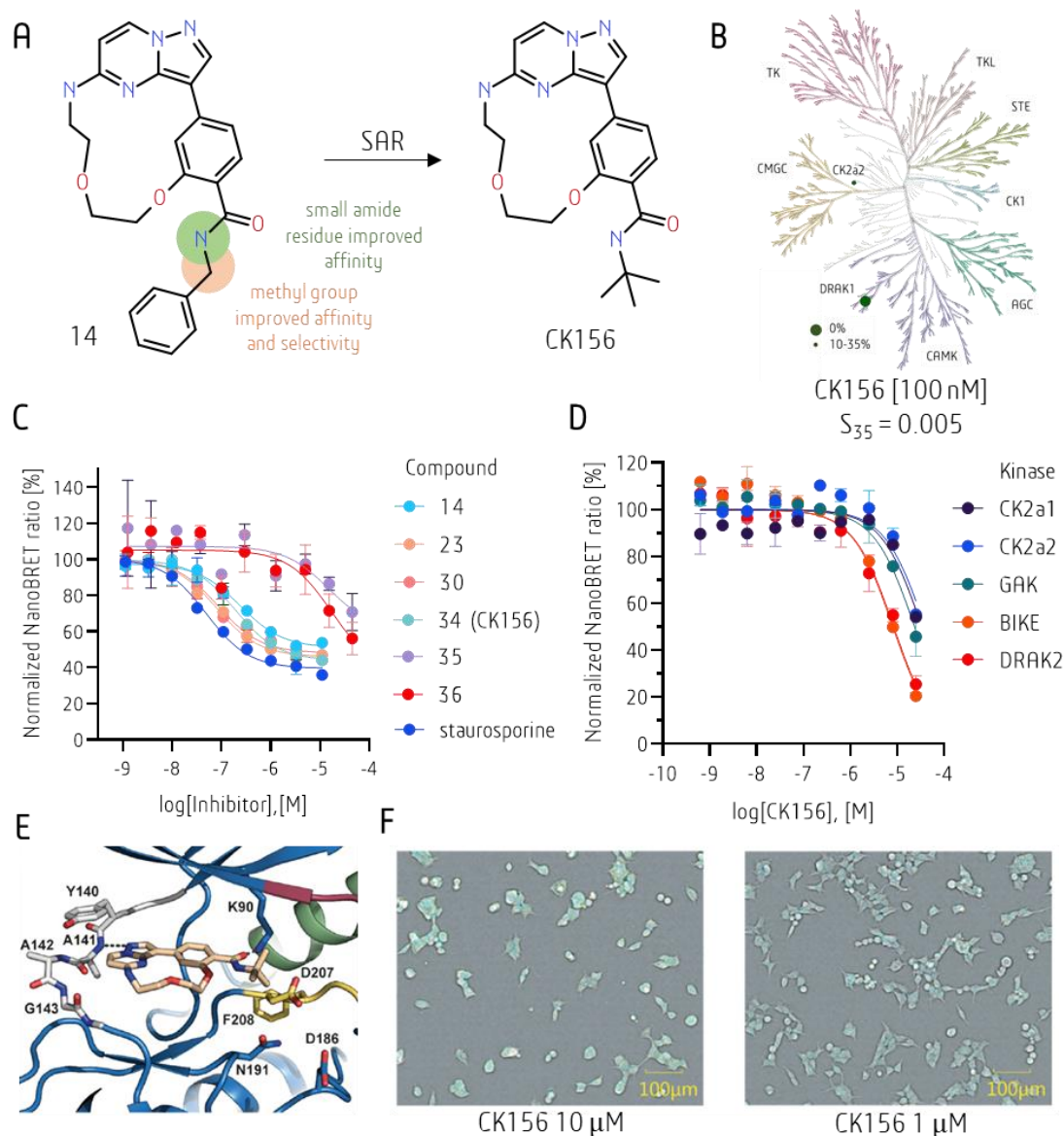


Figure 5 | Structure activity relationship (SAR) of a pyrazolo[1,5- α]pyrimidine series. **A** Chemical starting point of the SAR series resulting in **CK156** with improved potency and selectivity. **B** Selectivity profile of pyrazolo[1,5- α]pyrimidine-based macrocycle **CK156** measured in the KINOMEScan assay (Eurofins) at 100 nM. Green circles represent the displacement of the control and their size corresponds to the % displacement (small value corresponds to high potency) as indicated in the figure. The S -score quantifies the selectivity at the measured concentration – here S_{35} calculates the ratio of kinases hit below 35% displacement and the total amount of kinases tested. **C** Cellular potencies of macrocyclic pyrazolo[1,5- α]pyrimidine series on DRAK1 using NanoBRET. **D** Cellular potencies of **CK156** on potential off-targets CK2a1, CK2a2, GAK, BIKE and DRAK2 determined by NanoBRET. **E** Binding mode of **CK156** to DRAK1 determined by x-ray crystallography. **F** Brightfield confocal image of stained HEK293T cells after 18h of 10 and 1 μM compound exposure (blue: DNA/nuclei, green: microtubule, red: mitochondria, and magenta: Annexin V apoptosis marker). Figure compiled and modified from Kurz *et al*¹¹¹.

To rank the synthesized compounds accordingly to the binding affinity to DRAK1 and obtain an overview of the selectivity, a DSF assay against 44 kinases, including DRAK1, was performed (final protein concentration: 2 μM ; final inhibitor concentration: 10 μM). CK156 and CK228 showed an excellent thermal stabilization of DRAK1, of 12.3 and 11.3 K, and

therefore were the most promising candidates for a sufficiently potent DRAK1 molecule. The chemical structure of CK156 is shown in Figure 5A. The *in vitro* binding affinity was confirmed using isothermal titration calorimetry (ITC) and revealed a low K_D value of 9 nM and 21 nM for both compounds, respectively. The enthalpic contribution for binding of DRAK1 were comparable for CK156 and CK228, showing a large negative enthalpy and therefore suggest that macrocyclization has reduced the compounds flexibility and stabilizes the conformation of DRAK1. The on-target potency was further validated by an orthogonal radioactivity-based enzyme kinetic assay provided by ProQinase (reaction biology). The IC_{50} values from the kinetic assay of 15 nM (CK228) and 49 nM (CK156) are in good correspondence with the ITC values and confirmed the potency against DRAK1. After confirming the on-target potency in DSF, ITC and the enzymatic assay, the selectivity profiles of the two most promising compounds were verified using the kinome-wide KINOMEScan assay by Eurofins. For comparison, the parental compound 14 was also assessed. The initial selectivity was tested using a DSF assay of 44 kinases and five targets (CK228) and three targets (CK156) with T_M -shifts higher than 5 K. The selectivity profile of CK156 at 100 nM screening concentration is shown in Figure 5B and revealed next to the on-target DRAK1 only one off-target CK2a2 with a selectivity score (35%) of 0.005. The off-target detected in the KINOMEScan assay was 20-fold weaker than the potency measured on DRAK1, which correlates well with the measured weak thermal shifts for CK2a2 from the DSF panel. The crystal structure of compound CK156 bound to DRAK1 (Figure 5E) revealed an excellent complementarity with the active binding site of the kinase, which explains the exceptional selectivity determined in DSF and the KINOMEScan assay. In comparison to the other tested compounds from the SAR study the smaller *tert*-butyl moiety of CK156 was able to bind deeper into the hinge region, compared to other larger moieties, which is only possible due to a conformational rearrangement in the hinge region. DRAK1-G143, which belongs to a subsequent linker region, was twisted in the binding mode of CK156 in comparison to the parental compound 14. This flexibility in the back pocket is unusual for a kinase, but could explain the promiscuity of DRAK1 to other kinase inhibitors. In the next step the most promising compound CK156 was assessed in the NanoBRET target engagement assay to verify the *in vitro* on-target potency as well as the promising kinome-wide selectivity data in living cells. Especially interesting is the cell permeability of the molecule, because so far, the

compound was only analysed in *in vitro* assays and macrocyclic compounds tend to be bulkier and have a higher molecular weight than traditional kinase inhibitors and therefore could potentially be less cell penetrant. CK156 showed good cellular potency of 182 ± 22 nM, which is in good correlation with the *in vitro* data with about 4-fold change and suggested excellent cell penetration of these inhibitor (Figure 5C). Furthermore, all potential identified off-targets CK2a1, CK2a2, GAK, BIKE and DRAK2 were investigated using the NanoBRET assay. All EC_{50} were more than 30-fold higher than compared to potencies measured for DRAK1 and CK156 (8 μ M for BIKE – 39 μ M for CK2a2) as shown in Figure 5D. It has been described in the literature that DRAK1 is highly overexpressed in gliomas compared to other cancer cells¹¹⁷. A knockdown of DRAK1 results in decreased proliferation, clonogenicity and cell migration¹¹⁷. To assess this effect of DRAK1 and test our highly selective and potent chemical probe CK156 we tested its cytotoxicity in glioma cells. As a control experiment, we investigated the general cell viability using a multiplex high content assay simultaneously allowing the observation of phenotypic effects. CK156 showed no cytotoxicity at 1 μ M in the tested cell lines (U2OS, HEK293T and MRC-9), whereas at 10 μ M some toxicity was observed. It cannot be ruled out that this cytotoxic effect at the higher tested concentration is due to unspecific off-target effects. The brightfield confocal image for HEK293T cells treated with CK156 at 1 μ M and 10 μ M is shown in Figure 5F. After a general cytotoxic effect of CK156 at its intended concentration was excluded, the effect in glioma cells was tested. The expression levels of five different glioblastoma multiforme (GBM) cell lines were tested revealing that LN-229 and D-247MG showed the highest expression levels of DRAK1. A DRAK1 knock-out was reported to alter glioma cell line morphology but surprisingly, only minor changes in the morphology of the cell lines upon treatment of up to 20 μ M CK156 were observed, indicating that an inhibition of the DRAK1 kinase activity alone may not lead to the observed phenotype in GBM.

In this study we made modifications on a pyrazolo [1,5- α]pyrimidine-based macrocyclic scaffold that resulted in a highly selective and potent DRAK1 inhibitor. Our selective chemical probe CK156 will help to elucidate the biological role of DRAK1 although its effect in glioma cells was surprisingly not sufficient to induce a knock-out indicated phenotype pointing to additional scaffolding roles of this kinase.

5.1.2 Probe development for Salt-Inducible Kinase (SIK2)

(In the following subchapter, parts of the publication “Structure-Based Design of Selective Salt-Inducible Kinase Inhibitors” are included¹¹⁸).

In this study we investigated the salt-inducible kinases 1,2 and 3 (SIKs) which are key metabolic regulators. Dysregulation of SIK is associated with the development of diverse cancer types, including breast, gastric and ovarian cancer. Known SIK and pan-SIK inhibitors have been reported, for example HG-9-91-01, YKL-05-099, ARN-3236 and G-5555, but all display significant off-target activity, limiting their use as a chemical tool compound. The aim of this study was to develop a well-characterized chemical tool compound for the SIK family that lacks the activity on other kinases and hence reduced the number of off-targets compared to the currently available SIK inhibitors. The p-21-activated kinase (PAK) inhibitor G-5555¹¹⁹ has a reported dual activity against STE kinase, including PAKs and MSTs, but also potent activity against SIK2. This is intriguing, because these kinases share little sequence homology, such as the gatekeeper residue and therefore we hypothesized that selectivity against the targets of the STE family towards SIK can be achieved. To validate G-5555 as a suitable scaffold for the development of a selective SIK chemical probe, we assessed its selectivity *in vitro* using the KINOME scan technology from Eurofins at 100 nM and 1 μ M. After identifying G-5555 as an attractive starting point a crystallization effort was made to guide the SAR using a structure of a SIK family member bound G-5555. Unfortunately, it has been challenging to crystallize any isoform of the SIK family, due to poor expression yields in insect cell expression and general instability of the resulting proteins. To be able to rationally design the chemical molecule with high selectivity for the SIK kinases, the crystal structures of two off-targets MST3 and MST4¹¹⁸ (PDB ID: 7B30 and 7B36) bound to G-5555 were solved. These structures served as surrogate models and as a template for generating a SIK2 family homology model. The binding mode of G-5555 revealed that the pyridine ring is positioned to the catalytic residue MST3-K65 and that the serine located in the P-loop (MST3-S46) is linked with the catalytic MST3-L65 and the pyridine ring of G-5555, through the formation of a water-mediated hydrogen-bond network. MST3 and MST4 in comparison to PAK1 contain a bulkier residue at the glycine-rich loop which has been moved out in the ATP-binding pocket of PAK1. When comparing these off-targets to the SIK family model it became apparent that MSTs and PAK1 contain a bulky methionine gatekeeper and the SIK family

members in contrast a smaller threonine residue. Based on the crystal structures of MSTs and PAK1 and *in silico* simulations on SIK we designed a series of compounds in order to explore the potential of the pyrido[2,3-*d*]pyrimidin-7-one scaffold for the development of selective SIK inhibitors. The proposed modifications are depicted in Figure 6.

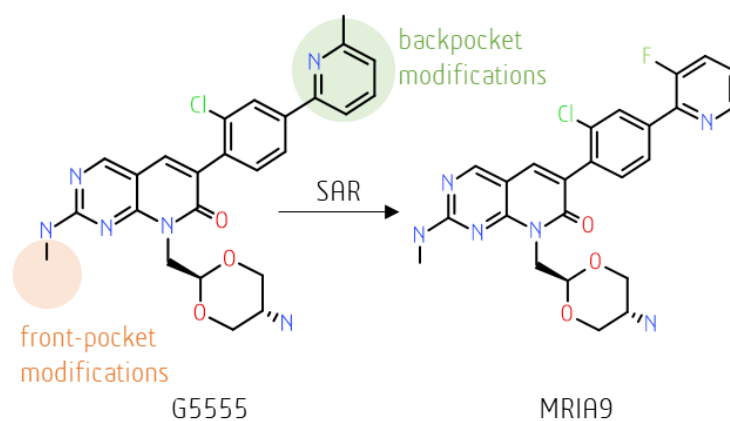


Figure 6 | Design of a focused series of pyrido[2,3-*d*]pyrimidin-7-one analogues based on the PAK1 inhibitor G-5555 with complete SAR characterization resulted in the selective compound MRIA9. Figure modified from Rak and Tesch *et al*¹¹⁸.

The activity on the proposed on-targets SIK2 and SIK3 were evaluated using the cellular target engagement assay NanoBRET, while the off-target effect on other kinases, especially MSTs and PAK1 was evaluated using a DSF assay. G-5555 was used as a positive control. The DSF data correlated well with reported literature data¹¹⁹. G-5555 showed melting temperature shifts (ΔT_M) of 9.9 K, 6.6 K, and 6.6 K for MST3, MST4, and PAK1, respectively. Removing the methyl group in the ortho-methoxyphenyl ring of the backpocket modification lead to much lower potency against SIK2 ($IC_{50} = 777$ nM) and SIK3 ($IC_{50} = 117$ nM), and ΔT_M of 5.7 K and 3.9 K for MST3 and MST4, respectively, indicating that the methyl group is important for MST binding. We were able to increase the cellular potency on the SIK family by adding a fluorine atom at position 3 in the methoxyphenyl ring, but still retained activity against the off-targets. By removing the methyl group, which we observed to be important for the MST binding, we observed reduced ΔT_M values for MST3/4 by 5.9 K and 3.4 K compared with G-5555. Introducing another halogen atom at the fluorine position led to a similar cellular potency of 139 nM confirming that a halogen substitution at position 3 can account for high potency toward both SIK2 and SIK3. These data highlight the role of

substitutions at positions 3 and 6 of the G-5555 core scaffold for modulating SIK2 and SIK3 activity. In conclusion MIRA9, the compound with the fluorine in 3-position in the methoxyphenyl ring showed the best SIK2/3 cellular potency and lowered potency on the known off-targets of G-5555. The compound was therefore screened at 1 μ M concentration against 443 kinase in the 33 PanQinase radioactivity-based activity assay from reaction biology. The selectivity score (35%) of MIRA09 was with 0.018 much lower than compared to the selectivity score of G-5555 with 0.12, confirming that designing a focused series on SIK inhibitors based on the G-5555 scaffold was successful. The next step was to follow-up the kinome-wide screening data by determining IC₅₀ values in an enzymatic assay as well as testing the same off-targets in our cellular screening platform NanoBRET. The data is shown in Table 5.

Table 5 | Selectivity profile of G-5555. Results of screening of MIRA9 against 443 as percent control >50% at 1 μ M as well as *in vitro* IC₅₀ (radiometric protein kinase assay, reaction biology) and *in cellulo* EC₅₀ (NanoBRET data, duplicates) data for the main targets. Table adapted from Rak and Tesch *et al*¹¹⁸.

Targets	Percent of control (%)	IC ₅₀ (nM)	EC ₅₀ (nM) NanoBRET
SIK2	1	48	180 \pm 40
SIK3	2	22	127 \pm 23
SIK1	4	55	516 \pm 5
KHS1	8	210	13000 \pm 280
PAK3	9	140	n.d.
PAK2	10	41	n.d.
NLK	13	250	3100 \pm 160
PKN3	35	1400	6700 \pm 750
PAK1	36	580	n.d.
MAP2K4	37	830	n.d.
TIE2	39	3100	6000 \pm 1800
MST4	45	1600	34000 \pm 14000
MELK	48	2200	n.d.

MIRA9 showed IC₅₀ against its main targets SIK1-3 of 48, 22 and 55 nM, with similar potencies in a cellular environment of 180, 127 and 516 nM. Unfortunately, MIRA9 showed relatively low IC₅₀ for PAK1-3 of 580, 140 and 41 nM and it was not possible to determine

the cellular PAK activity in the NanoBRET assay due to a lack of suitable tracer molecules for this kinase. Hence, MRIA9 shows sufficient cellular potency of below 1 μM and good overall selectivity except a PAK1 off-target activity within the required 30-fold selectivity window. However, combining MRIA9 with a known PAK1 chemical probe NVS-PAK1¹²⁰, MRIA9 can be used as a chemical probe for elucidating the complex biology of SIK kinases. Other targets that showed up in the kinome-wide selectivity screening like MST4 showed larger selectivity in cells ($\text{IC}_{50} = 2200 \text{ nM}$ and cellular $\text{IC}_{50} = 34 \mu\text{M}$), as well as KHS1, NLK and PKN3.

After identifying MRIA9 as a potent SIK2 inhibitor with narrowed and well characterized off-target profile compared to its lead scaffold we decided to further investigate the compound as a chemical tool compound to better understand the mechanism and phenotype of the SIK family, specifically SIK2. It is known that SIK inhibitors can sensitize ovarian cancer cells to paclitaxel treatment^{120, 121}. We selected SKOV3 ovarian cancer cells as a model and monitored them over 9 days with low concentration of MRIA9 in presence and absence of paclitaxel, and observed that cells that were treated with paclitaxel in combination with MRIA09 showed a strong reduction in cell viability. A general cytotoxic effect of MRIA9 without paclitaxel treatment could be excluded.

The *in vitro* and *in cellulo* screening results showed that MRIA9 is a highly potent pan-SIK and PAK2/3 inhibitor with excellent cellular activity, especially against SIK3 and we also showed that a combination treatment with paclitaxel and SIK inhibitors may result in improved therapeutic effects for ovarian cancer and that MRIA09 can be used as a chemical tool compound to elucidate the cellular function of the SIK subfamily.

5.1.3 The necessity for cellular profiling of on-target and off-target effects for chemical probes and chemogenomics.

The first aim of this thesis was to support different medicinal chemistry SAR projects using the cellular target engagement method NanoBRET and to determine on-target activity as well as off-target profiles for different chemical probes and chemogenomics. The two projects explained in more detail in the chapter above are good examples for medicinal chemistry projects that benefited from the *in cellulo* potency data as well as the profiling of determined off-targets in a cellular context. Sometimes, the protein was simply not available to perform *in vitro* measurements like DSF or an activity assay because the protein is unstable or hard to

obtain, like e.g. SIK2. Therefore, it is useful to have a complementary method the NanoBRET assay where proteins are transiently expressed in mammalian cells with post-translational modifications and potential chaperones present in the cellular environment. Other times the selectivity profile which we obtain from commercially available kinome-wide screening platforms like ProQinase from Reaction Biology can be further evaluated by looking at the inhibitor in a cellular context. Sometimes targets and/ or off-targets found to be potent *in vitro* are significantly less potent in a cellular context, due to for example the presence of the high cellular ATP concentration as described for crizotinib and dasatinib¹⁰⁹. It can be beneficial to use a cellular screening method to determine on-target effects as well as off-target effects, especially when developing and characterizing chemical probe molecules and chemogenomics compounds that are intended to be used in a cellular phenotypic assay.

5.2 Family selectivity for small molecule chemogenomic candidates

When developing a chemical tool compound or a chemogenomic compound many things need to be taken into consideration. Next to the on-target potency of below 1 μM in cells the selectivity is most important. Developing a selective small molecule can be challenging, especially in the kinase field where the sequence similarity inside the kinase domain is very high. This similarity is even higher for closely related kinases and kinases in the same subfamily. Due to this reason, chemical probes are often pan-family or dual probes, because it is nearly impossible to develop family selective small molecules (MRIA9 is a pan-SIK probe [<https://www.thesgc.org/chemical-probes/mria9>], T3-CLK is a pan-CLK probe [<https://www.thesgc.org/chemical-probes/T3-CLK>] or TH-257 is a LIMK1 and LIMK2 probe [<https://www.thesgc.org/chemical-probes/TH-257>]). Thus, to complement exclusively selective chemical probes, the idea of a chemogenomic tool compound was developed. These molecules are very well characterized, but a lesser selectivity is acceptable (having up to 10 close on-targets). Using a set of chemogenomic compounds with overlapping target spectra it may be easier to target subfamilies of kinases and still be able to assign a phenotypic effect to a specific kinase. In the next chapter, two subfamilies of kinases will be examined in more detail. The first part focused on an attempt to develop a subfamily-specific inhibitor for the PCTAIRE family and the second part explains an attempt to cover an entire subfamily with a set of well characterized published molecules.

5.2.1 Development of a small molecule inhibitor to target the PCTAIRE family

(In the following subchapter, part of the publication "Discovery of 3-amino-1H-pyrazole-based kinase inhibitors to illuminate the understudied PCTAIRE family" are included¹²²).

In this study we investigated an understudied subfamily of the cyclin-dependent kinases (CDK), which are activated by binding of cyclin Y, the so-called TAIRE family (CDK14-16) (Figure 7A). CDKs have key roles in regulation of the cell cycle and also perform diverse other cellular functions, such as regulation of mRNA splicing and transcription. There are many drugs reported and approved for CDK4/6 for the treatment of cancer¹²³, but so far, no family-selective inhibitor is published and the majority of this kinase family is still understudied. The high similarity of the kinase domain within the TAIRE family makes it challenging to develop family-selectivity kinase inhibitors¹²⁴. Although it was shown by Dixon-Clarke *et al* in 2017

after solving the crystal structure that CDK16 can be bound by type I and type II inhibitors and known FDA approved drugs like rebastinib and dabrafenib, no selective compound has been developed yet¹²⁵. In this study we developed a set of small molecule inhibitors based on a 3-aminopyrazole-scaffold that is based on kinase inhibitors that were previously published as promiscuous kinase inhibitors, targeting over 300 kinases in a 360 wild-type kinome-wide screen at a concentration of 1 μM ¹²⁶. The flexibility of these small molecules in the binding pocket, that was disclosed looking at the structure in complex with VRK1 and STK17B, could be an explanation for the various targets and the promiscuous behaviour¹²⁶. Using the knowledge of the high on-target potency in the CDK family in combination with the solved crystal structure makes the 3-aminopyrazole moiety (Figure 7B) an excellent starting point for an extensive SAR study to better explore the TAIRE subfamily.

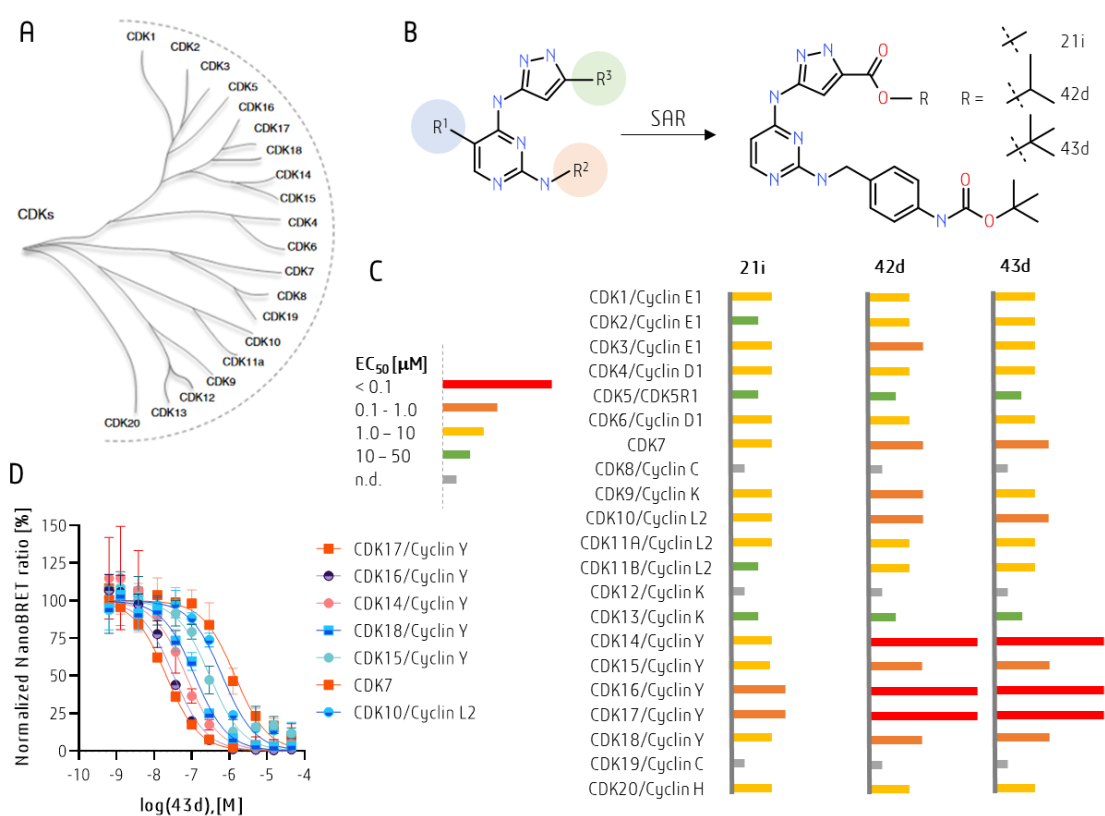


Figure 7 | Family selectivity of pyrazole-based kinase inhibitors. **A** Phylogenetic tree of CDK family based on sequence similarity. Figure adapted from Wells *et al*¹²⁴. **B** Summary of modifications made on the 3-aminopyrazole scaffold. On position R¹ different smaller and bulkier residues were introduced, on position R² different linkers that vary in length were introduced and on position R³ the influence of the head group was investigated. Optimization of the molecule led to three favoured molecules 21i, 42d and 43d. **C** Cellular EC₅₀ values of molecules 21i, 42d and 43d against the CDK family were determined using the NanoBRET technology in a 11-point-dose-response curve in duplicates. **D** Cellular target engagement of 43d as a bar chart representation against the seven main targets inside the CDK family. B-D adapted and modified from Amrhein *et al*¹²².

The hinge binding moiety present in the 3-aminoopyrazole scaffold represents a known scaffold for targeting kinases in different medicinal chemistry approaches. Previous publications highlighted the inhibitory proliferation and anticancer potential of pyrazole-based small molecules. Three different positions were selected for improving the inhibitor selectivity and potency for CDK16. First, the head group on the pyrazole was varied, different smaller and bulkier alkyl groups were added and amide groups were tested. To investigate the selectivity profile and obtain first insights into the potency of the compound sets, a DSF assay was used. We determined thermal stabilization using an in-house panel of 89 kinases, including CDK16 and other CDK proteins and included the parental compound as promiscuous control. We identified several molecules from the series, which showed strong stabilization of CDK16, but also other targets that are favoured by the scaffold, like CDK2, JNK3 and GSK3B, which are potential off-targets of this compound series. The overall selectivity was indicated by the number of kinases with thermal shifts higher than 5 K. The lead structure was highly promiscuous as indicated by stabilizing up to 60 kinases with ΔT_M shifts >5 K. An introduction of a methyl ester at the pyrazole led to a reduction in the stabilization of CDK16 in comparison to the lead structure, however the thermal shift of 6.5 K was still high compared to the shift of staurosporine (9.1 K) which translates to an IC_{50} of 24 nM¹²⁷. A cleavage of the Boc group which was introduced as R² showed no significant influence on compound selectivity. Introducing a tert-butyl ester at the pyrazole increased the thermal shifts on CDK16 to up to 9.3 K. These moieties can be found in various approved drugs indicating that these groups have valuable pharmacokinetic properties^{128, 129}. The other common off-targets for the scaffold, CDK2 and GSK3B, were in a moderate range. Only two other kinases beside CDK16 exhibited a DSF shift >5 K on 43d, MAPK15 and PLK4, however, these shifts were comparatively small compared to the staurosporine reference, suggesting that these compounds did not bind strongly to these kinases. The most favourable thermal shift was observed in 43d with no addition in position R¹, the introduction of a tert-butyl after a pyrazole at position R² and a tert-butyl at position R³.

To validate the DSF data in an orthogonal assay method and to obtain insight into the cellular potency of the compound series, a NanoBRET cellular target engagement assay was performed. The lead structure exhibited the highest shift against CDK16 with 10.3 K and a corresponding cellular EC_{50} of 18 nM. Compound 42d and 43d showed comparable DSF shifts

to the lead structure that was also reflected in cellular EC₅₀ values of 44 and 33.4 nM, respectively. Having these on-target potencies from the DSF and NanoBRET assay in mind and including the information about the selectivity, 42d and 43d were selected as the best candidates for a more comprehensive selectivity study within the CDK subfamily. To assess the CDK family-wide selectivity we profiled the 3 most promising compounds 21i, 43d and 43d in the NanoBRET assay. As expected the lead structure showed high potencies on most of the CDKs, but no selectivity towards a specific kinase. 21i exhibited an interesting profile by targeting only CDK16 and CDK17 with 380 and 673 nM) (Figure 7C). However, a much higher potency was observed for 42d and 43d. Additionally 43d exhibited the best selectivity profile within the CDK family with nanomolar values only for the PCTAIRE (CDK16-18) and the PFTAIRE (CDK14-15) subfamily (Figure 7D).

Although CDK16 is considered to be part of the understudied dark kinome, some cellular functions of the kinase are known. CDK16 expression has been linked to be cell cycle dependent¹³⁰ and that a knockdown of CDK16 leads to late G2/ M phase cell cycle arrest that is followed by apoptosis¹³¹. To assess the cellular function of CDK16 using our newly characterized chemogenomic molecule we performed a cell-based assay in liver cells using the fluorescent ubiquitination-based cell cycle reporter (FUCCI) system^{131, 132}. This technology enables the detection of cell cycle states (G1, G2/M, or S phase) on a single cell level. 43d, the most potent and family selective inhibitor of our SAR series, led to the accumulation of cells in G2/M phases at all three concentrations tested (1 μM, 5 μM, 10 μM) demonstrating the biggest influence on the cell cycle. Milciclib, a published CDK2 inhibitor that was used a control compound¹³³, led to G1 cell cycle arrest at both tested concentrations. In comparison, the lead structure compound, which displays no family or kinome wide-selectivity, had no effect on the cell cycle at all three concentrations tested.

Dysregulation of CDK16 has been described in many cancers such as breast, prostate, cervical cancer and melanomas^{134, 130, 131}, and with 43d we found a two-digit nanomolar potent and family selective molecule to investigate the biology of the TAIRE family.

5.2.2 Characterization of current chemogenomic candidates for splicing kinase family

(Parts of the following chapter will be included in the in the publication “Evaluation of current chemogenomic candidates for splicing kinase subfamily”, which manuscript is currently in draft.)

Industrial and academical drug discovery research efforts have focused only on a small subset of kinases of the human kinome. As mentioned above, chemogenomic compound libraries which consist of well-characterized small molecules that target a small number of kinases have emerged as a method to explore the biological relevance and therapeutic potential of yet underexplored kinases. In this project, we focus on a small branch of the kinome tree consisting of 17 closely related kinases of the CMGC branch involved in various RNA metabolism functions. The goal was to identify the best inhibitors available and to characterize them in *in vitro* and *in cellulo* systems for their efficacy and kinome-wide selectivity as well as their subfamily-wide selectivity. In this project, we selected published small molecule inhibitors, focusing on the compounds that have the potential to be utilized as quality chemical biology probes and assembled them into a high-quality chemogenomics set. Moreover, the selected compounds provide chemical starting points for further optimisation of more selective compounds for the so-called splicing kinase subfamily. Despite the good general knowledge of some functions of the splicing kinase subfamily, specific functions of these proteins, which often act in concert to regulate splicing, are still underexplored. In order to study their biological mechanisms in more detail, potent and selective small molecules, like chemical probe molecules, could be used to question the targets function in phenotypic assays. In this project we analysed the current landscape of kinase inhibitors of the splicing kinases and tested the best candidates form the literature for their *in vitro* and cellular potency and their kinome-wide selectivity to identify a set of chemogenomic compounds.

5.2.2.1 Small molecule inhibitor landscape targeting the splicing kinase family

In the kinase inhibitor literature, many compounds have been developed and described for the CLKs, DYRKs, HIPKs and SRPKs. However, the data presented are often incomplete and critical assessments of *e.g.* the kinome-wide selectivity are missing. These data are needed to be able to assess the inhibitors usefulness to interrogate the biology of a specific splicing

kinase and subsequent inclusion in our chemogenomic library. We therefore mostly relied on reported on-target potencies from various assay formats (SI Table 4) and identified 29 promising candidates that were selected based on their suitability to be used as tool compounds to study the proteins' biological functions. Compounds that show high potency and are currently in clinical trials, but do not show a comprehensive reported selectivity towards one kinase or subfamily of the splicing kinases were not included. An overview of the chemical structures of the tested compounds we selected, grouped based on their reported main target, can be found in Figure 8. A problem often observed in the 29 candidates is a cross-activity between different subfamilies. For all the proteins, crystal structures have been reported. However, the 3D-structures of the splicing kinases overall is nearly identical, with only minor opportunities to gain selectivity windows as e.g. described in targeting the DFG-1 residue for CLK1/2/4 versus CLK3⁴⁴.

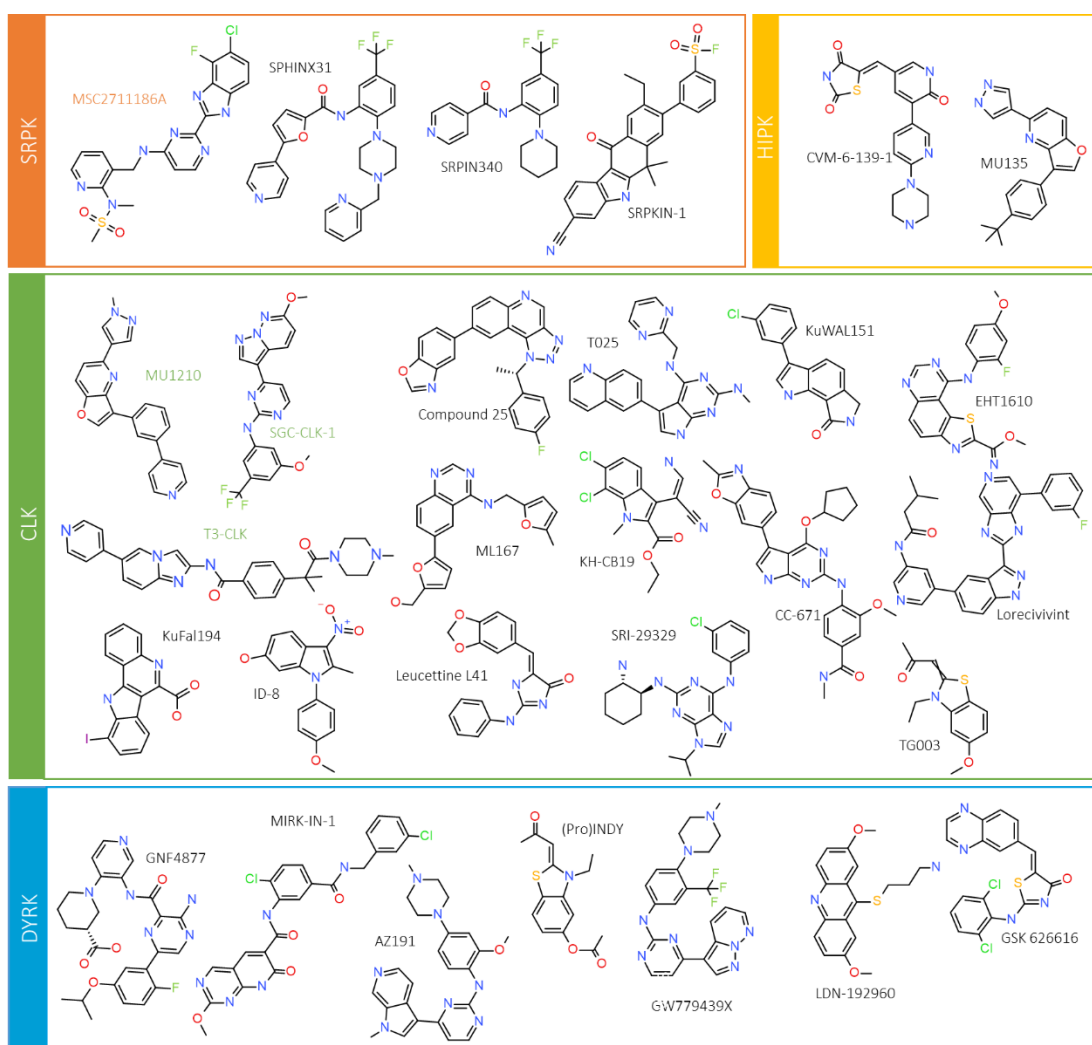


Figure 8 | Literature reported small molecule inhibitors targeting the splicing kinases. The compounds are grouped based on their literature-reported main target. There are no sufficient compounds reported for PRP4,

which is why PRP4 is not included in this overview. Highlighted in green are MU1210, SGC-CLK-1 and T3-CLK and highlighted in orange is MSC2711186 which are already approved chemical probes by the Structural Genomics Consortium (<https://www.thesgc.org/chemical-probes>) for their respective targets SRPK (orange), HIPK (yellow), CLK (green) and DYRK (blue).

Before testing the compound set on their splicing family-wide potency and selectivity *in vitro* as well as their potency and selectivity in cells, we evaluated the chemical integrity of each of the commercially obtained compounds, by performing a quality control HPLC. Also, cell viability was assessed in osteosarcoma cells (U2OS) and human embryonic kidney cells (HEK293). All described compounds (29 candidates and 4 negative controls) were tested in a first screen using brightfield microscopy at 10 μM over 24 h. Based on the growth rate¹⁰⁶ as well as image evaluation, we observed effects on cell viability for four tested compounds in U2OS and ten in HEK293T cells. Exemplarily shown in Figure 9A are two compounds (AZ191 and KuWAL151) that showed different cell morphology at 10 μM in comparison to the negative control 0.1% DMSO in both cell lines. To evaluate generic effects regarding basic cell properties and cell viability, we performed a live-cell multiplex high-content assay¹⁰⁷ (Figure 9B-D) in U2OS, HEK293T and MRC-9 cells at two different compound concentrations (1 μM and 10 μM). To investigate autofluorescence or precipitation, Hoechst High Intensity Objects were used as described by Tjaden *et al*¹³⁵. One compound (Leucettine L41) showed an increase in Hoechst High Intensity Objects at both tested concentrations (Figure 9B), indicating that the compound has autofluorescent properties at a concentration of 1 μM . This compound property can influence further evaluation, *e.g.* explaining the following low healthy cell count (< 50%), that was observed in the next evaluation step for Leucettine L41 at 1 μM (Figure 9C). At the same concentration, only one compound (GW779439X) showed a healthy cell count of less than 50%, next to the assay controls (Figure 9D). GW779439X is a reported DYRK inhibitor¹³⁶ also binding to all splicing kinases presented. The healthy cell proportion was around 30%, the pyknosed at around 20% and the fragmented at 50%. The main targets of GW779439X are CLKs and DYRKs and both are also involved in many different cellular processes explaining the effect on cell viability even at lower concentrations¹³⁷. None of the other tested compound showed an effect on general cytotoxicity at 1 μM , regardless of which target they mainly inhibit, indicating that impairment of single kinases which alter the splicing function has no crucial survival function for the tested cell lines U2OS, HEK293T and MRC-9.

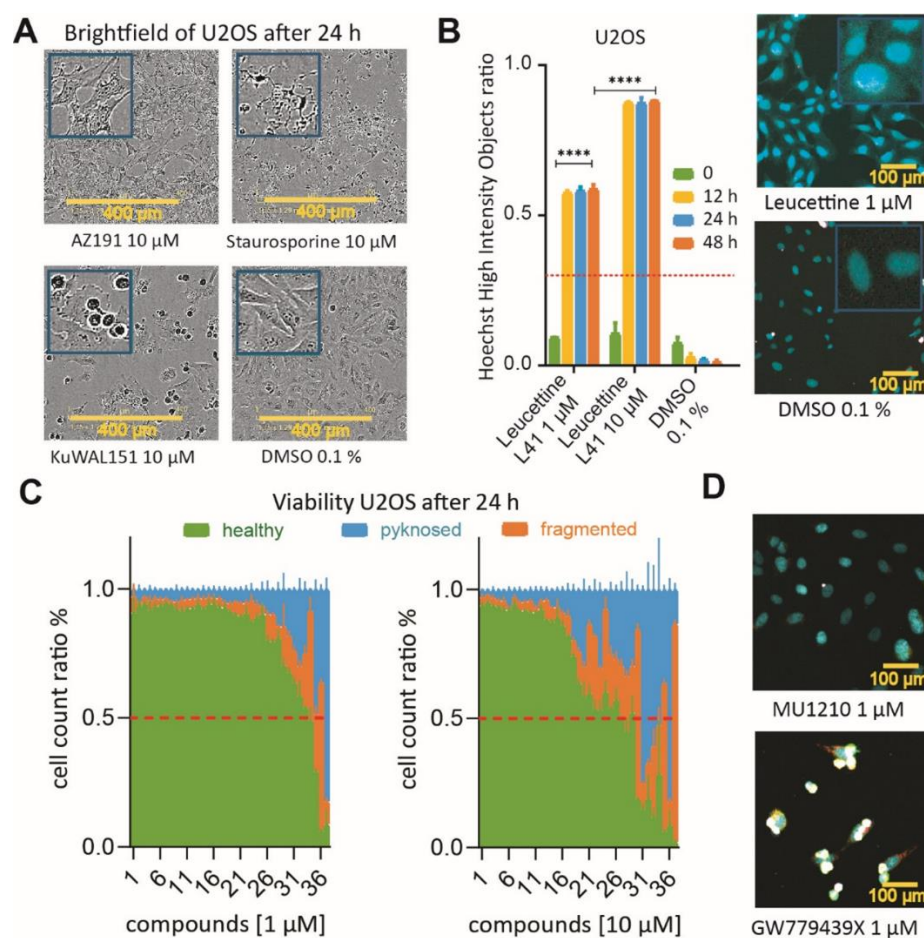


Figure 9 | Viability Assessment and live-cell high content screen of the candidates in U2OS cells. **A** Brightfield image of U2OS cells after 24h of 10 μM compound exposure (CLK inhibitors AZ191 and KuWAL151) in comparison to Staurosporine (10 μM) and 0.1% DMSO control measured in the IncuCyte. **B** Hoechst High Intensity Objects after 0, 12, 24 and 48 h compound exposure. Error bars show standard error of the mean of biological triplicates. Significance was calculated using a two-way ANOVA analysis. Brightfield confocal image of stained U2OS cells after 24 h at 1 μM compound exposure of Leucettine in comparison to 0.1% DMSO (blue: DNA/nuclei, green: microtubule, red: mitochondria, and magenta: Annexin V apoptosis marker). **C** General cell viability of U2OS cells after 24h compound treatment classified by healthy, pyknotic or fragmented cells at the two tested concentrations 1 μM (left) and 10 μM (right). **D** Brightfield confocal image of stained U2OS cells after 24h of compound MU1210 at 1 μM and cytotoxic compound GW779439X at the same concentration (blue: DNA/nuclei, green: microtubule, red: mitochondria, and magenta: Annexin V apoptosis marker). Figure was made by Amelie Tjaden.

The candidates *in vitro* on-target potency, was assessed using a Differential Scanning Fluorimetry (DSF) assay. A higher potency correlates with a higher thermal stabilization of the protein. We tested 11 of the 17 splicing kinases, with exception of HIPK1, HIPK3, HIPK4, CLK4, DYRK1B and DYRK4, because no in-house expression constructs were available. Overall, our collected thermal shift data showed only minor correlation with reported literature data of the compound's potency. Reasons for the poor correlation may be (a) the different assay formats that were used in this comparison, (b) insufficient data points in our correlations or (c) a variety in chemical scaffolds tested, as it has been shown that different

binding modes may result in different degrees of protein stabilization and hence a comparison would be rendered difficult. For example, on HIPK2, the compounds tested have reported affinities in a range from 10 μM to two-digit nM, but we measured thermal shifts with a maximum of 2.5 K. Hence, the HIPK2 DSF assay only shows an assay window of about 2.5-fold, with errors being typically around 0.1 K. Lorecivint has a reported IC_{50} of 16.8 nM¹³⁸ and resulted in a thermal shift on HIPK2 of 2.1 K. The correlation is better for kinases which show a large thermal stabilization upon compound binding, like CLKs or DYRKs with (20 K and 8 K for CLK1 and DYRK3, respectively). It is worth mentioning that, because 16 of the 29 literature compounds have one of the CLKs as their main target, the data coverage was better for the CLKs. An exception is CmpdA¹³⁹, the only reported PRP4 inhibitor, that showed no on-target affinity for PRP4 in our DSF assay. When we assessed the compound's mass and HPLC spectrum, we discovered it had been hydrolysed which was reproducible when preparing new DMSO stocks. Because of these stability issues we removed the compound from further consideration as a useful tool for the chemogenomic set. The broader *in vitro* selectivity of the candidates was assessed using a kinase panel consisting of 96 kinases using DSF (additional to the 11 members of the splicing kinases family tested) and the resulting heatmap of these interactions is shown in Figure 10A. The kinases are listed in SI Table 1 and depicted in SI Figure 1 as a kinome tree showing the distribution of the kinases of the tested DSF panel that covers a representative fraction of the kinome. Most compounds showed high thermal shifts against the tested CLK1, CLK2 and CLK3 with Lorecivint showing the highest shifts with 21 K, 19 K and 19 K, respectively. To better compare the selectivity of the compounds we calculated a selectivity score, which is shown in the column on the right side of Figure 10A. All but four compounds showed a $S_{(5\text{ K})}$ below 0.15, meaning they show higher than 5 K thermal stabilization on less than 15% of the 96 tested kinases. The reported DYRK inhibitors GSK 626616, GW779439X, GNF4877 and AZ191 show a $S_{(5\text{ K})}$ selectivity score of 0.28, 0.36, 0.25, 0.23, respectively, in comparison to the promiscuous control Staurosporine with a much higher selectivity score of 0.75. Because DSF cannot be used to determine an inhibitor IC_{50} s as a high protein concentration is necessary for a sufficient assay quality and in order to test the cellular selectivity of the set, we next assayed the compounds in the cellular target engagement method NanoBRET in a lysed assay format. To ensure that the results in intact cells and in lysed cells are comparable, we tested the inhibitor set against

CLK1 in two assay modi. The data obtained in lysed format and intact format correlate with $r = 0.93$ (Figure 10F), indicating that all compounds are cell permeable and show the same behaviour in lysed cells as in intact cells for CLK1. We previously reported ATP assay interference to be a main driver of differences between lysed format and intact cell format¹²⁴. All NanoBRET data were collected in the lysed modus for comparability reasons and are visualized in Figure 10B as a heatmap and will be further discussed for each subfamily individually in the next sections.

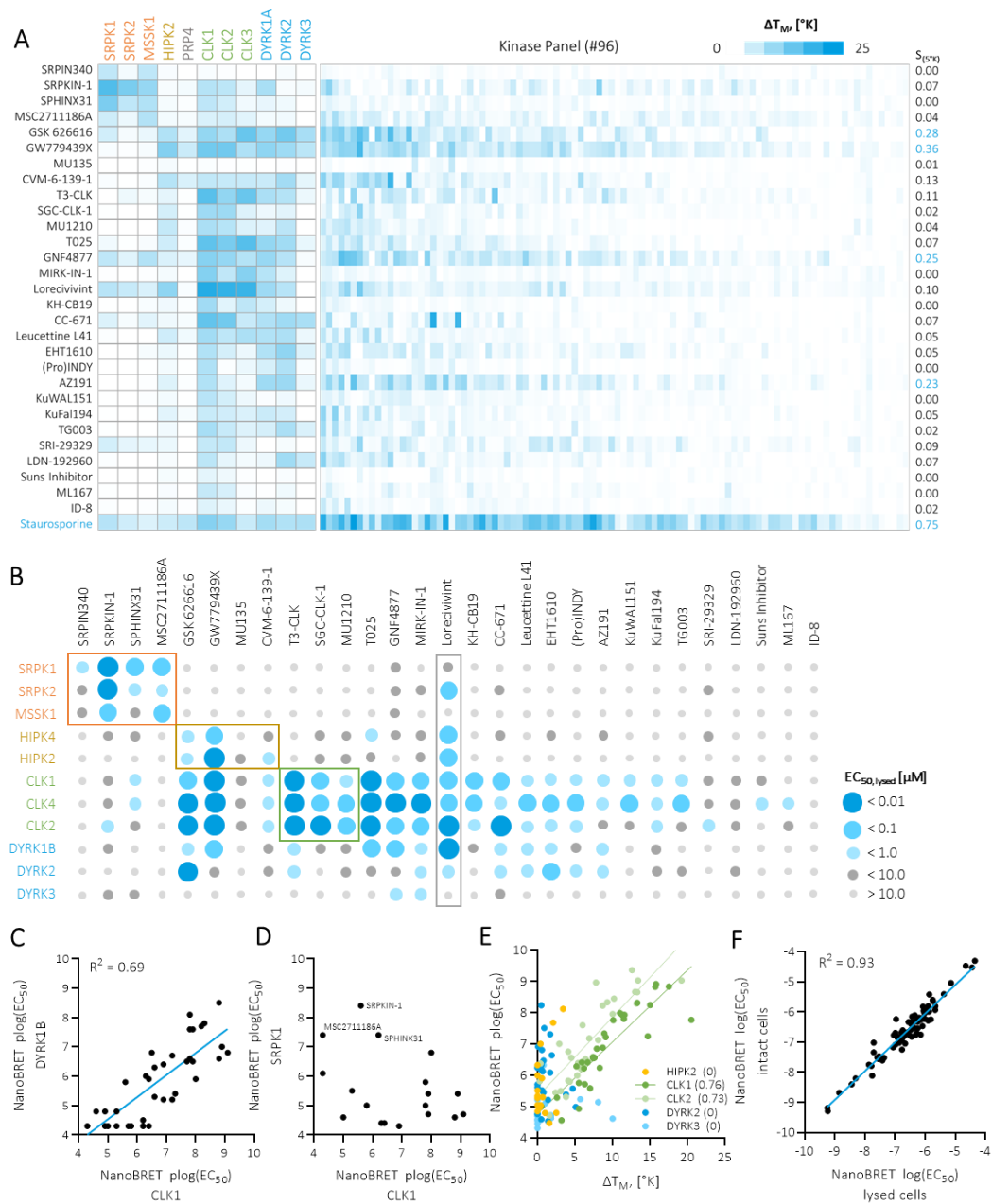


Figure 10 | Inhibitor profiling to access druggability of the splicing kinases. **A** DSF screening of 29 kinase inhibitors against available splicing kinases and 96 additional kinases sampled across the kinome. **B** NanoBRET EC_{50} (lysed mode) as a dot heat plot. Big dark blue spots correspond to high potency of below 10 nM against the target. Coloured squares indicate the best group of compounds to target certain families. orange = SRPK, yellow

5. Results and Discussion

= HIPKs, green = CLK and grey = pan-family compound. **C** Correlation of NanoBRET EC₅₀ of DYRK1B and CLK. Hits bigger than 50 μ M were set to 4.3 (plog (50 μ M)). All compounds targeting DYRK1B also target CLK1. **D** Correlation of NanoBRET EC₅₀ of SRPK1 and CLK1. Hits bigger than 50 μ M were set to 4.3 (plog(50 μ M)). Only three compounds from our set – SRPKIN-1, MSC271186A and SPHINX31, targeting SRPK1 are selective over CLK1. **E** Correlation of NanoBRET EC₅₀ and ΔT_M data. A good correlation was observed for CLK1 and CLK2 (R^2 values of 0.76 and 0.73), but no correlations were observed for HIPK2, DYRK2 and DYRK3 (R^2 values of 0). **F** Correlation of data collected in this study between intact cells and lysed cells in NanoBRET on CLK1 (R^2 of 0.93).

There are 16 small molecule inhibitors reported targeting the CLK kinase family characterized in this work, as demonstrated in Figure 8 for more detailed information. Because all reported DYRK inhibitors also target the CLK subfamily with similar potency we decided to evaluate them together. Lorecivint (Adavint, SM08502) is a first-in-class small molecule CLK2/DYRK1A dual kinase inhibitor developed by Biosplice for the treatment of osteoarthritis in the knee and is currently in Phase III clinical trials¹³⁸. Lorecivint demonstrated relatively good selectivity with 19 of 402 wild-type kinases (4.7%) for which the IC₅₀ was < 50 nM or within 25-fold of that of CLK2 in a DiscoverX commercial kinome panel. Next to CLK2 the compound is reported to also inhibit the whole CLK subfamily as well as the whole DYRK subfamily. In our cell-based NanoBRET assay, Lorecivint was binding to CLK2 most potently with an EC₅₀ of 1 nM and additionally binding to the CLK and DYRK subfamily and binding to HIPK2, HIPK4, SRPK2 with 20 nM, 27 nM and 80 nM, respectively, which makes Lorecivint a pan-splicing kinase inhibitor. Benzothiazole TG003 is reported as a CLK inhibitor^{140, 141} with reported potencies in the nM range for CLK1, CLK2 and CLK4 and also potent IC₅₀ for DYRK1A and DYRK1B (12 nM and 130 nM). In our cell-based assay TG003 showed moderate potencies on CLK1, CLK2 and CLK4, with EC₅₀s of 580 nM, 1 μ M and 60 nM, but no potency higher than 1 μ M toward the other tested targets. None of the reported literature DYRK compounds showed selectivity against another subfamily. Most compounds targeting DYRKs also target CLKs. Figure 10C shows a correlation of the NanoBRET data for DYRK1B and CLK1 with a good correlation with an $R^2 = 0.69$., indicating that most compounds showed a similar potency for CLK1 and for DYRK1B. It is challenging to develop compounds that are selective for DYRK without targeting CLK, due to a high sequence similarity between the two subfamilies. Nathanael Grays lab recently published a selective DYRK1A macrocyclic inhibitor JH-XVII-10¹⁴². The macrocyclic compound was screened in a KiNativ kinase assay in CAL57 cells and showed no significant targets other than DYRK1A. It shows an IC₅₀ of 13 nM against DYRK1A and 15 nM against DYRK1B (Select Screen Kinase Profiling by Thermo Fisher). This compound was not tested in this inhibitor set because it is currently not commercially

available and could not be obtained on time from the Gray lab in time of this thesis. As already discussed above, the four DYRK inhibitors GSK 626616, GW779439X, GNF4877 and AZ191 showed high selectivity scores for the tested kinases, making them unsuitable for the inclusion in chemogenomic compound libraries. GNF4877 together with dual probe MIRK-IN-1 were the only tested compounds also binding to DYRK3 with below 1 μM (480 and 590 nM, respectively). In comparison to the other tested compounds AZ191 showed a relatively low potency against all splicing kinases. Interestingly, GSK 626616 and GW779439X, together with Lorecivint were the only compounds that showed good binding to CLKs and DYRKs, but also the HIPK subfamily. The compound (Pro)INDY, a prodrug of INDY, showed good activity in ATP-competitive *in vitro* assays against DYRK1A¹⁴³. In the lysed NanoBRET it showed an EC_{50} of 6 μM against DYRK1B and 582 nM against DYRK2, but was much more potent for the tested CLKs (274, 425 and 37 nM). LDN-192960 is published as a potent and selective DYRK2 inhibitor¹⁴⁴, which was not reflected in our cellular assay system. DYRK2 showed a relatively low EC_{50} of 3.6 μM .

Within the 16 reported literature compounds for targeting the CLK family are three well characterized small molecule probes. SGC-CLK-1 is a chemical probe for CLK1, CLK2 and CLK4 (<https://www.thesgc.org/chemical-probes/SGC-CLK-1>) developed by the SGC in collaboration with Luceome Biotechnologies. In the lysed NanoBRET assay it had an EC_{50} of 60, 5 and 40 nM for the corresponding CLKs and a small shift of 3.2 K for CLK3 in the DSF assay were observed, which is negligible in comparison to a shift of CLK3 of 18 K for Lorecivint. A NanoBRET assay for CLK3 was not available because the tracer shows no binding to CLK3. The furo[3,2- β]pyridine MU1210, which was developed in collaboration with Kamil Paruch, Masaryk University in Brno, has been recommended as a quality chemical biology probe for pan-CLKs (CLK1/2/4)¹⁴⁵ and shows a binding of 140, 65 and 40 nM to the tested CLKs, which is in good correlation with the published data. Similar to SGC-CLK-1, MU1210 shows a small thermal shift of 3.3 K in CLK3, but we published data that shows no binding to CLK3 up to 3 μM (<https://www.thesgc.org/chemical-probes/MU1210>). Next to the two probe scaffolds that inhibit the subfamily of CLKs except CLK3, a chemical probe was developed by Takeda Pharmaceutical Company and further characterized by the SGC Frankfurt (<https://www.sgc-ffm.uni-frankfurt.de/chemProbes#!specificprobeoverview/T3-CLK>). T3-CLK is 10- times more potent than the other two chemical probes and additionally

inhibits CLK3. T3-CLK shows minor off-target *in vitro* activity tested at 100 nM against DYRK1A/B (32/67 nM), DYRK2 (274 nM), SIK2 (125 nM), FLT1(D385W) (138 nM) and FLT3 (668 nM) as shown in Figure 10B, D. In our T_M-panel it showed a good selectivity score of 0.20 with high shifts for CLK1, CLK2 and CLK3 (16, 10 and 14 K). This is also reflected in the NanoBRET data. T3-CLK shows an EC₅₀ of 1.5, 3.5 and 1.4 nM towards CLK1, CLK2 and CLK4 with relatively good selectivity over DYRK1B and DYRK2 with 270 and 760 nM (7-fold and 21-fold to lowest bound CLK2). This makes T3-CLK the most potent probe for CLKs in this set. The binding mode of T3-CLK to CLK3 is shown in Figure 10C. It binds as a type I kinase inhibitor with polar interactions to K241 and L239 from the hinge region and K186 from β3. The backpocket is shielded by the large phenylalanine gatekeeper. The negative controls - small molecules with the same scaffold as the probe with only minor chemical changes rendering the compound inactive - for all three CLK probes were also included in the inhibitors set and tested against the splicing kinases. The information of MU140, SGC-CLK-1N and T3-CLKN are shown in SI Figure 2. All negative control compounds show only low thermal shifts against the tested kinases and close to no potency on any other tested splicing kinases in NanoBRET. To assess the CLKs biological functions, these three probes can be used, providing three different chemical scaffolds. However, there is no selectivity within the CLK-family which stays a task for future optimizations.

From the four HIPKs present in human, HIPK2 was tested in DSF and HIPK2 and HIPK4 were further tested in NanoBRET measurements in this work. The study that explored MU1210 as a potential chemical probe for targeting the CLKs also discussed a promising starting point for targeting HIPK2¹⁴⁶. MU135, a MU1210 scaffold with 4-tert-butyl-phenyl substituent at position 3, shows promising selectivity for the HIPKs with similar binding mode to MU1210 and CLK¹⁴⁶ (PDB ID: 7NCF). The potency of MU135 was previously described using the radiometric assay from Eurofins and showed an IC₅₀ of 248 nM, 119 nM and 476 nM for HIPK1, HIPK2 and HIPK3, respectively¹⁴⁶. The selectivity of MU135 was determined using the Eurofins kinase panel consisting of 373 kinases at a concentration of 10 μM. Despite this selectivity MU135 showed a thermal shift on HIPK2 of 1 K and a cellular EC₅₀ of 4.7 μM and 11 μM on HIPK2 and HIPK4, respectively. These *in cellulo* potencies fit the cell-based activity of close analogues of MU135 (21e) 12c and 12d of 30 μM and >100 μM in MCF-7, that was performed by Nemeč *et al*¹⁴⁶. Despite its low cellular potency against its main target HIPK2,

MU135 remains a valuable starting point for future HIPK probes, due to its exceptional family selectivity especially over the closely related DYRKs and their shared mechanism of activation by tyrosine autophosphorylation¹⁴⁷. The more potent compound CVM-6-139-1 (HY-U00439A) (reported HIPK2 IC₅₀ = 74 nM) has a moderate selectivity profile across the kinome (determined via screening against 353 kinases at 10 μM concentration¹⁴⁸ that was reflected in our internal T_M-panel with a selectivity score at 5 K of 0.20. CVM-6-139-1 shows good binding for HIPK2 of 478 nM with also targeting all tested CLK variants CLK1, CLK2 and CLK4 (358 nM, 409 nM and 286 nM). HIPK4 showed a weaker potency of 1.1 μM in comparison the other HIPKs. GSK626616¹⁴⁹ a reported DYRK3 inhibitor shows next to CLK4, CLK2 and DYRK2 a relatively good potency for HIPK2 and HIPK4. GW779439X¹³⁶, a published STK1 kinase inhibitor shows a similar profile as GSK626616 with good potencies for HIPK2 and HIPK4 and for all CLKs and DYRKs, but also generally insufficient kinome selectivity with a selectivity score (5 K) of 0.28 and 0.36, respectively. In combination with the CLK probes presented in the paper both compounds could be used nonetheless as chemogenomics compounds for targeting HIPKs – although a possible strong CLK phenotype could overshadow the effects caused by inhibiting the HIPKs. Because of the general lack of a potent and selective small molecule inhibitor for the HIPK subfamily we decided to further screen a representative - HIPK4 - against a large set of compounds to find new starting points or potential chemogenomic candidates. This data will be discussed in the SGC Initial Screening library section below.

The family of SRPKs consists of three proteins (SRPK1-3). Compared to the ubiquitously expressed SRPK1, the expressions of SRPK2 and SRPK3 are mainly limited to the nervous system and muscles, respectively^{150, 151}. The constitutively active SRPK1 is one of the best studied splicing kinases. SRPK1 knockout mice are embryonically lethal¹⁵². SRPK1 interacts with and influences functioning of CLK1 kinase¹⁵³. There is a strong need for chemical probes to study the function of SPRK3, because its function is unknown. Our inhibitor set contains four compounds reported to be selective towards the SRPK family. SRPIN340 gets covalently attached to the tyrosine phenol group in the SRPK2-ATP binding pocket, thereby behaving as a competitive inhibitor¹⁵⁴. With a cellular EC₅₀ of 0.77, 4.2 and 2.1 μM against SRPK1, SRPK2 and SRPK3 it was the least potent out of the four tested SRPK literature compounds. SPHINX compounds (SPHINX, SPHINX-7, SPHINX-31) have a similar structure and were able

to target SRPK1 kinase, which can affect the VEGF phenotype. In this study we tested SPHINX31. SPHINX31 shows decent EC_{50} for SRPK1 and 2 with 40 and 258 nM, but low affinity against SRPK3 with 2.36 μ M. Inside the splicing kinase family the CLK subfamily is also inhibited with 336 to 1,620 nM. The SPHINX compounds are currently in preclinical studies for the treatment of different cancer types, including prostate cancer¹⁵⁴. SRPKIN-1 is, similarly to SRPIN340, an irreversible covalent inhibitor that binds to Y227 inside the ATP-binding side of SRPK1 and 2. In our cellular assay it showed high potency for all SRPKs with 4.3, 3.2 and 20 nM for SRPK1, SRPK2 and SRPK3 and also affinity for CLK2 with around 200 nM. MSC2711186 is an accepted chemical probe developed by Merck¹⁵⁵. MSC2711186 shows a shift of 5 and 7 K on SRPK1 and SRPK3 (MSSK1), and a relatively small shift on SRPK2 with 2 K. This translates well to the cellular NanoBRET data with 42 nM and 172 nM on SRPK1 and 2 and 45 nM on MSSK1. In comparison to the other SRPK compounds, SRPKIN-1 and SPHINX31, MSC2711186 shows no activity on the other tested splicing kinases, which makes it selective for the SRPK family. Similar to the proposed HIPK chemogenomics compounds identified from this set we propose to use the SRPK compounds SRPKIN-1 and SPHINX31 in combination with the accepted CLK probes to create a set of SRPK selective compounds together with MSC2711186. Although the strong CLK phenotype may be overshadowing¹⁵⁶.

5.2.2.2 SGC initial screening library to identify chemical starting points for targeting understudied splicing kinases

Due to the lack of sufficiently potent and selective compounds for PRP4 and part of the HIPKs, DYRKs and SRPKs we assembled an initial screening library consisting of 2064 compounds to find new chemical starting points for these proteins. It consists of the LOPAC library, published kinase inhibitors, clinical kinase inhibitors and diverse and representative compounds from our kinase inhibitor development projects that used macrocyclization, covalent inhibition and SARs as strategies for gaining selectivity over several different kinase families. Notably, our selected screening library consists of a large number of compounds, but it is biased and shows limited chemical diversity. The data analysis was supported by clustering the compounds into similar scaffolds using the build-in function of DataWarrior V5.5.0 (<https://openmolecules.org/datawarrior/download.html>) called "Cluster Compounds or Reactions" with a threshold of 0.6 (highest similarity falls below). A total of 736 different

clusters were identified. PRP4 was not available as a NanoBRET assay because no tracer could be identified and hence we decided to test the library in DSF only. The results are shown in Figure 11A-B. All compounds were tested at a concentration of 10 μM . A potent c-Met inhibitor BMS 794833 showed the highest shift with 7.1 K. The multi kinase inhibitor staurosporine showed a shift of 5.3 K and has a reported K_D for PRP4 of 220 nM¹⁵⁷ making BMS 794833 a potentially very potent PRP4 inhibitor. HIPK4 is a difficult protein to express so we decided to screen the initial screening library in the lysed format NanoBRET assays. The results are shown in Figure 11C-D. All compounds were tested at a concentration of 10 μM . The best hits were further evaluated in full EC_{50} measurements (SI Table 5). Surprisingly, LDN-192960, a known Haspin and DRYK2 inhibitor, which was also tested in our set, was binding to HIPK4 with 52 ± 5 nM.

5. Results and Discussion

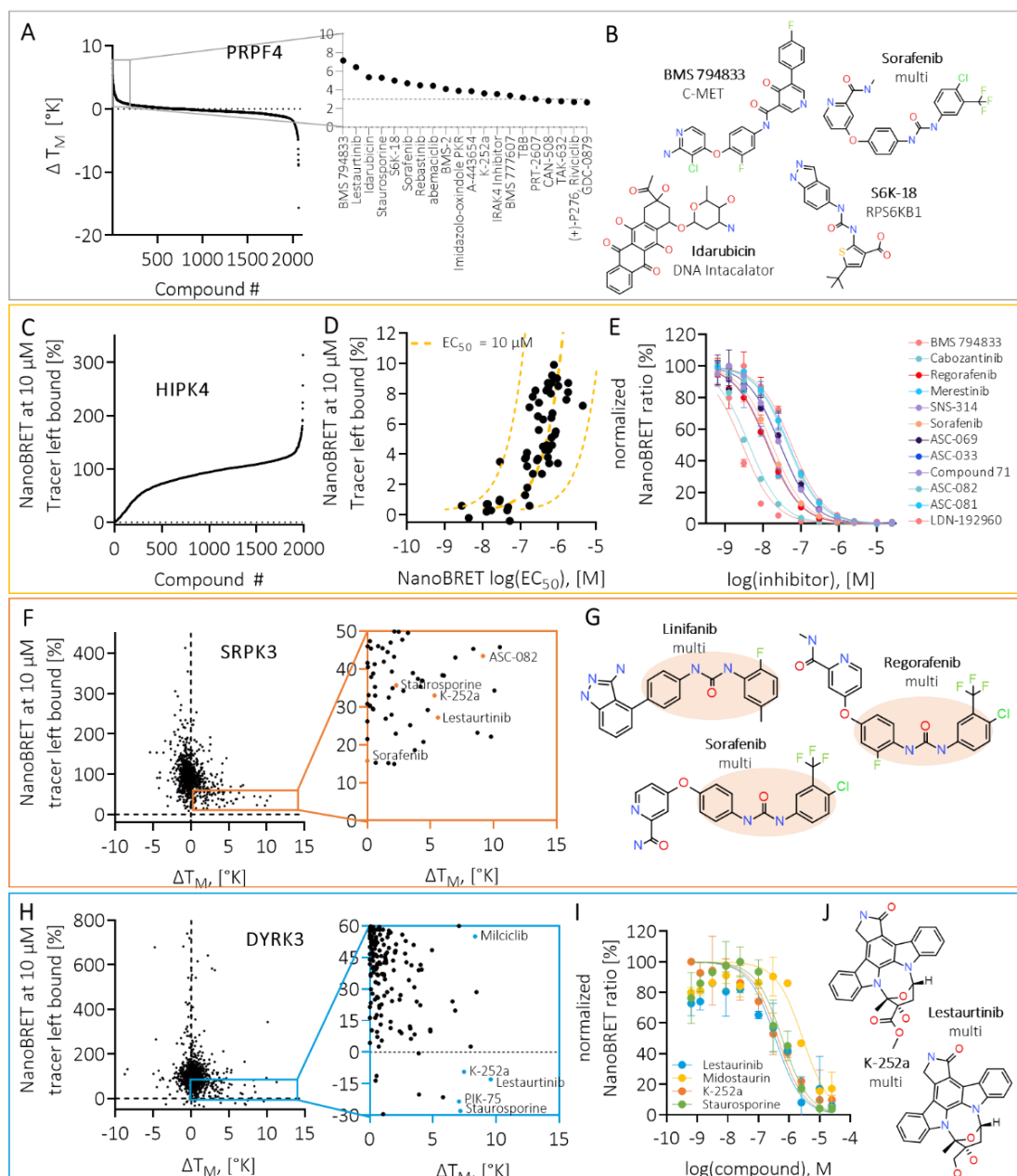


Figure 11 | Hits of an “Initial Screen” against understudied kinases PRP4, HIPK4, SRPK3 and DYRK3. **A** DSF results for PRP4 screened at 10 μM against an initial screening library and zoomed in to a cut-out of the 20 highest shifts. Compound name can be found on the x-axis (right side). **B** Chemical structure of compounds with highest shifts against PRP4. **C** NanoBRET 1-shot results at 10 μM for HIPK4 using tracer molecule K10. **D** Correlation between 1-shot at 10 μM and $\log(\text{EC}_{50})$ both measured in NanoBRET. For correlation comparison, the yellow dashed lines indicate a perfect modelled fit for 1, 10 and 100 μM , respectively. The fitted line for $\text{EC}_{50} = 10 \mu\text{M}$ describes the data best. **E** EC_{50} curves for the 12 best hits with EC_{50} s below 100 nM. The data was measured in technical duplicates ($n=2$). **F** Correlation of 1-shot NanoBRET data and DSF for SRPK3 with focus on positive DSF shifts and NanoBRET tracer remaining % to 100% on the right side. **G** Diarylurea compounds are the compound scaffold which had the highest affinity against SRPK3 in our tested set, including type-II inhibitors Linifanib, Sorafenib and Regorafenib with 1-shot NanoBRET tracer remaining of 22, 16 and 23%, respectively. Similarity in scaffold is marked with light red circles. **H** Correlation of 1-shot NanoBRET data and DSF hits for DYRK3 with focus on the right side on positive DSF shifts and NanoBRET tracer remaining below 100%. **I** Follow-up EC_{50} data for 5 hits, including the indolocarbazole multi kinase inhibitors Lestauritinib and K-252a, with chemical structures shown in **J**. NanoBRET curves of identified cluster of indolocarbazole that showed strongest binding to DYRK3. ($n=2$, technical duplicates).

Additionally, we tested this initial library against CLK1, SRPK3 and DYRK3 both in DSF as well as in NanoBRET. For hits that showed up in both orthogonal assay systems with a threshold in NanoBRET of 25% (corresponding to 1 μ M with 11% and including a (large) margin of error) and for DSF of 5 K, a full EC₅₀ curve was measured in NanoBRET. CLK1 as a target is already well covered with the probes we discussed previously, but we decided to test CLK1 as a control to compare the *in vitro* and *in cellulo* data to more easily access the hits on the more interesting targets SRPK3 and DYRK3. The DSF and NanoBRET hits correlate well and show that both assays are suitable for this large screening effort. Figure 11 shows the hits from the initial screening library against SRPK3 (Figure 11F-G) and DYRK3 (Figure 11H-J). After assessing the more than 2000 compounds in both screening assays DSF and 1-shot NanoBRET, both screened at 10 μ M concentrations, the best hits were identified and further assessed in full EC₅₀ curves, screened using NanoBRET. The best hit for SRPK3 with an affinity of 79 ± 1 nM was identified as ASC-082, a promiscuous kinase inhibitor. This compound is a member of a cluster consisting of 5 members, namely ASC-033, ASC-069, ASC-081 and ASC-086. Interestingly, ASC-082 was the only compound from this cluster which showed a % tracer bound value from the NanoBRET 1-shot experiment of below 50%, with all other members varying from 54-106%. Notably this scaffold was among the most potent hits for all tested kinases, including HIPK4, CLK1, DYRK3 and SRPK3. The next cluster which was a frequent hit in the screening were the diarylurea molecules Sorafenib, Linafanib and regorafenib with 1-shot values of 16, 22 and 23%, respectively. Part of the same cluster are NS5806, NF023 and Suramin with 1-shot values of 78, 77 and 101%. All three compounds are multi-target inhibitors of RTKs, specifically the VEGFR and PDGFR family^{158, 159}. G-749 showed an EC₅₀ of 655 ± 432 nM against SRPK3, which is interesting because it showed a tracer remaining 1-shot value of 127% in the same assay system. It was included in the follow-up screening due to its relatively high DSF shift of 4.23 K. Probably it showed a high tracer signal at the tested 10 μ M due to autofluorescence, which is a phenomenon we often observe in NanoBRET. This autofluorescence mimics the tracer signal and results in a false negative result. This issue can be addressed by measuring a full 11-step curve. G-749 is a pico-molar FLT3 inhibitor, which shows lower potency against other tyrosine kinases¹⁶⁰. It is part of a cluster including other compounds like TAK-901 a promiscuous kinase inhibitor and R54, a selective CDK inhibitor. None of the other compounds in the cluster showed a 1-

shot NanoBRET of < 50%, or a similarly high thermal shift. In summary, SRPK3 was bound by six small molecules below a cellular EC₅₀ of 1 μM, all of which are more or less promiscuous tyrosine kinase inhibitors. The best hit for DYRK3 with an affinity of 192 ± 214 nM was the ATP-competitive CDK inhibitor milciclib¹⁶¹ (Figure 11H). The related cluster consists of four compounds in total of which NMS-1286937 (PLK1 inhibitor in Phase 1 clinical trials¹⁶¹) shows a thermal shift of 3.5 K and Dovitinib (multi-target RTK inhibitor¹⁶²) a 1-shot NanoBRET value of 43% (Figure 11I). The second most affine hit in the set with an EC₅₀ of 214 ± 2 nM was PIK-75, a reversible DNA-PK inhibitor, which is known to induce apoptosis¹⁶³. PIK-75 was clustered together with 3 other compounds, namely Compound4, IP9 and IP12, but none of these showed binding for DYRK3. The scaffold that was most represented in the hits of DYRK3 was a common scaffold known for kinase inhibitors, indolocarbazole, including its most famous representative multi-kinase inhibitor staurosporine. Some representatives from this cluster (Figure 11J) showed - next to high thermal stabilization - corresponding low 1-shot NanoBRET values. This was validated by the follow up EC₅₀ determination and resulted in affinities for Lestaurtinib, K-252a and Staurosporine of 387 ± 149, 391 ± 36 and 565 ± 106 nM, respectively (Figure 11I). This cluster was identified as one of the biggest in the screening set with 30 members of which only 4 hit DYRK3 with a 1-shot NanoBRET value of below 50% (3 mentioned above and midostaurin). Other clusters showed up with a coverage of 100%, but could not be validated by the follow-up EC₅₀. The promiscuous kinase inhibitor ASC-082, which was mentioned above as the best hit for SRPK3 and its cluster, including ASC-033, ASC-069, ASC-081 and ASC-086 with relatively low 1-shot NanoBRET values of -20.2 to 47% and high thermal shifts of 0.2 - 4.8 K. These findings could not be confirmed by the follow-up EC₅₀, which showed only two-digit micro-molar binding ranging from 2105 ± 409 nM for ASC-082 to > 50 μM for ASC-086 and ASC-069. Two other clusters were conspicuous, despite low 1-shot NanoBRET values, these hits could not be confirmed, neither by DSF nor by the follow-up NanoBRET experiments. In summary DYRK3, similarly to SRPK3 was bound by only five more or less promiscuous kinase inhibitors. Nonetheless it would be useful to confirm these hits in an orthogonal assay method and validate them by creating a 3D-bound structure with SRPK3 or DYRK3 respectively, to obtain an idea of the binding mode of the compounds and find

potential new starting points for a structure-based drug design, to create selective and potent compounds for these yet only unselectively targeted kinases.

We identified the best in class kinase inhibitors to be included in a set of chemogenomic compounds to study the individual protein functions of a selected subfamily of the CMGC branch using chemical biology. We thus covered the landscape of the CLK and SRPK subfamily with quality chemical probe molecules but found insufficient coverage for the DYRKs and HIPKs. To address this lack of chemical biology tool compounds for these subfamilies we performed an initial screening of more than 2000 compounds and identified several promising chemical starting points for future structure-based drug design studies.

In particular, the inhibitors identified here often displayed identical or similar potency against CLKs and DYRKs. DYRK1A, as an example, is highly homologous in sequence to e.g. CLK1 and inhibition of DYRK1A has been shown to pose a potential toxicological risk¹⁶⁴. CLK1 is a particularly critical target, because it is one of the key enzymes in the alternative splicing machinery, which has a huge impact in almost all aspects of tumour biology including, angiogenesis, apoptosis and cell cycle control and therefore could overshadow any other protein inhibition¹⁵⁶. It is therefore crucial to not only identify selective probes that target a subfamily of the splicing kinases, but to identify compounds that show family selectivity.

5.2.3 Cellular selectivity assessment as quality control step for chemogenomics libraries

Although all these literature compounds screened for the splicing kinase project were described as potent and selective compounds, many failed the strict criteria the Structural Genomics Consortium has published for a chemical probe and even a chemogenomic compound. Surprisingly, also the cellular potency was often below the required threshold, although the *in vitro* data showed sufficient potencies below 100 nM. For the first described, a subfamily selective compound was developed that targets the TAIRE family of the CDKs. Screening the family for on-target and off-target effects was crucial for this project and would have been laborious using purified proteins. Using the NanoBRET technique made protein production and activation with the required co-constructs much easier and allowed the expression of activated proteins with their respective cyclin. The second project was more focused on characterizing current inhibitors than designing and developing new chemical compounds and using NanoBRET enabled us to verify or diversify literature data and provide

a screening platform that made the cellular potency and family selectivity data more comparable, because the same assay system was used. We validated chemical probes and identified starting points for new development projects for uncovered splicing kinases.

5.3 Assessing the human kinome using the NanoBRET technology

The NanoBRET cellular target engagement technology is a powerful approach to study small molecule ATP-competitive kinase inhibitors under close-to-physiological conditions. It is a quantitative binding assay that measures the displacement of a tracer molecule upon small molecule binding and enables the user to assess the cellular potency (as discussed in introduction chapter 3.4). Currently, eight different disclosed tracer molecules are commercially available that enable to measure the target engagement of about 340 kinases including clinically relevant mutants (<https://www.promega.de/products/cell-signaling/kinase-target-engagement/>). The next chapter will provide an overview over the kinase assays with the best assay quality and will present how the selectivity of clinical and FDA-approved kinase inhibitors changes compared to *in vitro* reported affinities.

5.3.1 Large-scale analysis of *in cellulo* selectivity against 234 kinases using NanoBRET

(Parts of the next chapter are part from the publication (Kinome-wide *in cellulo* selectivity assessment of kinase inhibitors and probe molecules), where the manuscript is currently in preparation).

Despite a great progress in the field of developing clinical protein kinase inhibitors for the treatment of various diseases, the cellular targets of the small molecules used in the clinics remain largely unknown. In this project we used the NanoBRET cellular target engagement assay to create an *in cellulo* protein kinase selectivity panel consisting of 234 kinase assays spanning various kinase families and determined the affinity for a large set of 165 small molecule FDA approved and clinical kinase inhibitors *in cellulo*. The data that we collected was validated against published potency data using conventional *in vitro* enzyme or binding assays. The next chapter will report progress on cellular profiling of clinical kinase inhibitors and mechanisms explaining differences of inhibition data measured outside and in cellular environments.

To test the kinase selectivity of a large number of small molecule kinase inhibitors we conducted low volume high-throughput kinase assays using a panel of 234 transiently expressed full-length human protein kinases (Figure 12A)

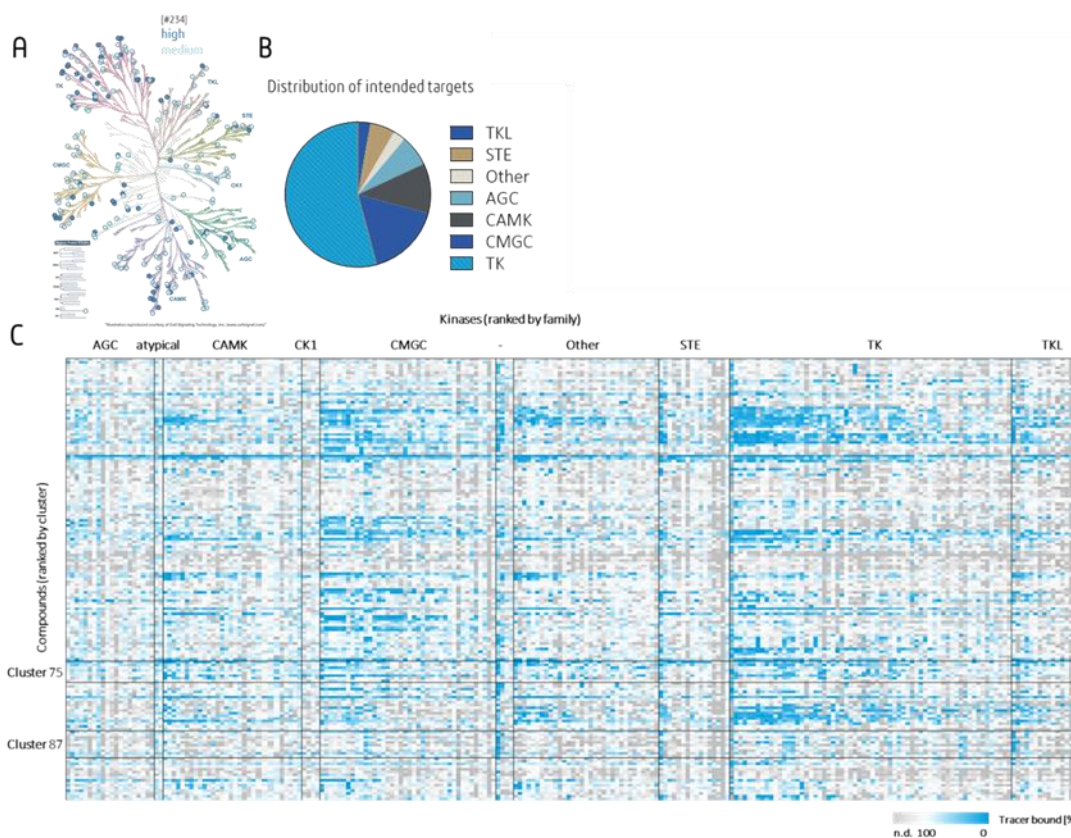


Figure 12 | Large-scale kinase- inhibitor interaction map. **A** Panel of 234 screened NanoBRET kinases depicted as a kinome tree. Each kinase represented in the assay panel is marked with a light blue circle. The kinase dendrogram was adapted from Science and Cell Signaling Technology (cellsignaling.com). **B** Distribution of intended targets of the tested kinase inhibitor library, by kinase sub-family. **C** Hierarchical cluster analysis of kinase targets against clinical and approved kinase drugs. Darker blue colours correspond to more affine interaction. 165 kinase inhibitors were profiled against 234 kinases.

We used the NanoBRET cellular engagement assay, a bioluminescence competitive tracer displacement assay, which measures the binding of a small molecule in competition to a fluorescently labelled tracer molecule. The small molecule kinase inhibitor library comprised 189 compounds known to bind to kinases from all major protein kinase subfamilies rather selectively or unselectively. Unfortunately, we had to exclude compounds (SI Table 7), that showed high autofluorescence often accompanied with a bright yellow colour that interfered with the fluorescent readout of the assay. Testing these compounds in a 1-shot experiment led to values much higher than 100% (tracer control) due to the occurrence of the same wavelength as the tracer molecule, which led to false negative data. Inhibitors that exhibit selectivity for a very limited number of kinases targets are most valuable as research tools for probing kinases function as discussed in previous chapters. The collection of kinase inhibitors included FDA-approved drugs, compounds in clinical testing, and compounds primarily used as research tools. The library comprised 165 small molecules known to inhibit kinases from

all major protein kinase subfamilies as shown in Figure 12B. To obtain a general idea of the kinome-wide selectivity of the compounds, they were screened at a single concentration of 10 μM and the results are shown as a heatmap in Figure 12C.

After collecting information about the cellular potency and selectivity data of our kinase test set the first step was to compare it with reported data originating from another method. The 1-shot data was compared with an established method for testing kinase selectivity, the DSF assay. The resulting correlation broken down by kinase inhibitor binding type is shown in Figure 13A and B.

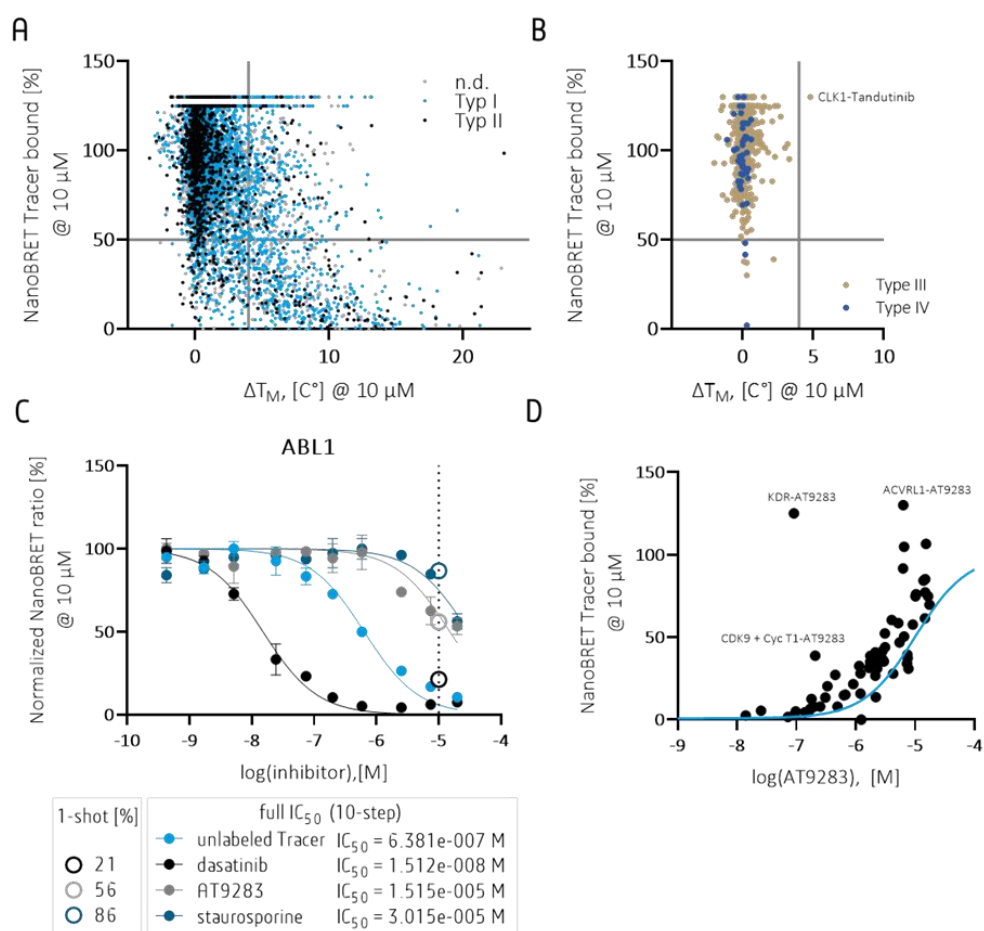


Figure 13 | Comparison of data across multiple assay platforms. **A** Cellular target engagement is plotted against the change in T_M shift, caused by compound binding for 64 of 189 kinase-inhibitor pairs. The grey horizontal line highlights the 50% threshold of cellular binding, and the vertical line denotes the threshold of >4 K that was also used in Fedorov *et al*¹⁰⁴. A hit in NanoBRET was considered $< 50\%$ and in DSF >4 K which varies for each individual kinase. **B** Correlation of 1-shot NanoBRET at 10 μ M with in house measured T_M shifts at 10 μ M for type 3 and type 4 allosteric kinase inhibitors. The grey horizontal line highlights the 50% threshold of cellular binding and the vertical line denotes the threshold of >4 K that was also used in Fedorov *et al*¹⁰⁴. A hit in NanoBRET was considered $< 50\%$ and in DSF >4 K which varies for each individual kinase. **C** ABL1 example data for a full EC_{50} data in comparison to 1-shot data at 10 μ M. **D** 1-shot NanoBRET data correlation of AT9283 with the kinases tested. Blue curve shows the perfect fit for compound at EC_{50} of 10 μ M.

The correlation between the NanoBRET and DSF data cannot be interpreted unambiguously, since it compares displacement in a cellular system, which is displayed as a percentage, with stabilization of the melting temperature in an *in vitro* system. Overall, however, the trend of a correlation can still be observed, especially looking at the ATP-competitive type I and type II inhibitors (Figure 13A). Compound-kinase pairs that show a strong displacement of the tracer molecule in the NanoBRET, *i.e.* show a low percentage value, usually also show a high shift in the melting temperature of the corresponding kinase. The compound-kinase pairs can be divided into different quadrants when a line is drawn at specific thresholds. The upper left

quadrant shows compound-kinase pairs with a NanoBRET value >50% and DSF shifts < 4 K. The compounds located in this region did not show binding/ stabilization in both assay systems. The lower right quadrant on the other hand shows the top hits in both assay systems with tracer displacement in NanoBRET of <50% and thermal shifts > 4 K. The two others quadrants show the data point that are in no correlation to each other with either good tracer displacement and low thermal shifts or high thermal shifts and no tracer displacement. Type III and type IV inhibitors (Figure 13B) on the other hand often show only a small thermal stabilization of the proteins, most likely because no significant structural conformational changes are induced to stabilize the protein. Figure 13B shows the correlation of 1-shot NanoBRET data with the DSF data and visualized that although the inhibitors tested in the NanoBRET show displacement of the tracer molecule at 10 μM of up to below 50% no significant thermal shift is observed. To confirm the correctness of our 1-shot NanoBRET data and to verify that the nonexistent correlation of the two assay systems for some compound-kinase pairs is not due to limitations in one assay system, we chose three highly unselective inhibitors to be tested in a full dose-response and compared the data with the 1-shot data. Figure 13C shows the overlay of the single concentration data (circle, 10 μM or $\log(-5)$) with the full response curve of the three inhibitors dasatinib, staurosporine and AT2983 and Figure 13D depicts the correlation of 1-shot data at 10 μM with full EC_{50} of each compound-kinase pair for compound AT2983. The light blue line shows the perfect fit of an inhibitor at EC_{50} of 10 μM and 1-shot data screened at that concentration should overlay with this curve. Except for a few kinases (KDR, ACVRL1 and CDK9) both data points, 1-shot and full EC_{50} , correlates very well, validating that the single-shot data correlates well with the dose-response data.

In the next step we took a closer look at the kinase inhibitor selectivity (Figure 14A) and the kinase durability (Figure 14B).

Kinase inhibitor selectivity. We ranked the compounds according to the number of kinases that were bound with more than 75% (or 25% tracer remained bound) at the tested concentration of 10 μM . The left side shows the small molecule that were able to target a lot of kinases, like known promiscuous kinase inhibitors staurosporine and AT2983. Very promiscuous cell-penetrant inhibitors are valuable to be used as tools for proteomic pull-

downs of target proteins or as a scaffold for tracer development. The right side shows small molecules that exhibit selectivity for a very limited number of kinases targets are most valuable as research tools for probing kinases function.

Kinase durability. We ranked the kinases with respect to a selectivity score (S (25%)), the fraction of all compounds tested that bound to the kinase by >25% (75% tracer displaced). Despite the 11 kinases (left insert), including NIM1K, PAK6 and MAP3K14 in the set that were not inhibited by any compound in the test set, except for the internal control of the unlabelled tracer molecule (CC1), we overall observed a good coverage of the kinome by this set of inhibitors (Figure 14B). These untargeted kinases show a set of targets that are highly unlikely to be bound by ATP-like compound scaffolds, that are already FDA approved or are currently used in clinical studies based on the intended targets of the inhibitor set. A subset of targets (FLT1, NTRK2, TIE2, RIPK2, FER, ADK and STK10) was broadly inhibited by a large number of compounds (right insert), representing kinases that are prone to chemical inhibition. These results have a potential impact on the selection of kinases that could be grouped into a smaller representative screening panel and the sensitivity of these kinases should be taken into consideration for focused selectivity panels. We cannot exclude that these selectivity results will be impacted by hidden biases in our compound set. Very promiscuous cell-penetrant inhibitors are valuable to be used as tools for proteomic pull-downs of target proteins or as a scaffold for tracer development. Based on the assumption that off-target interaction is more likely to be found with kinases with closely related by amino acid sequence, the selectivity of novel kinase inhibitors is frequently assessed by testing against a limited panel of closely related kinases.

5. Results and Discussion

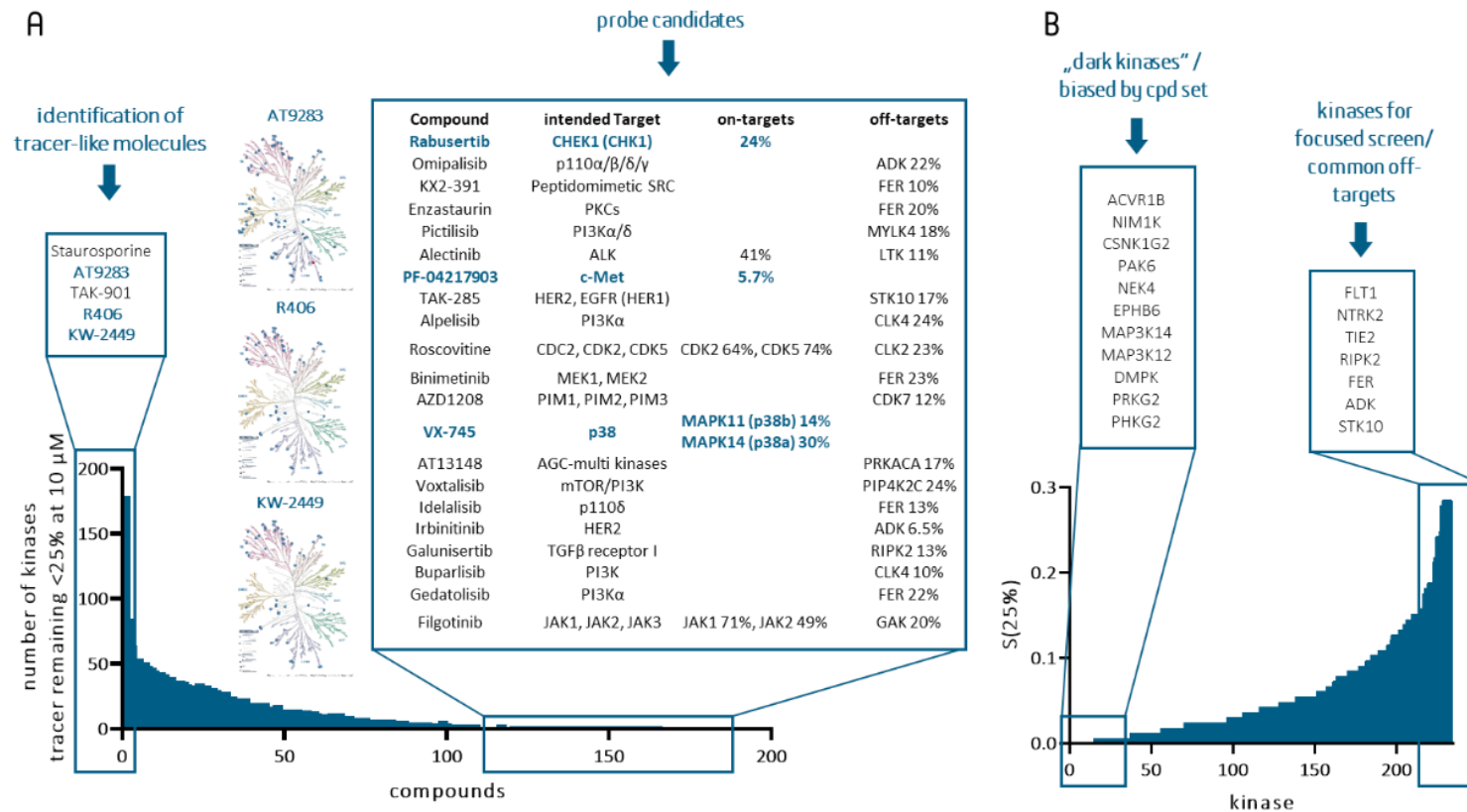


Figure 14 | Selectivity of kinase inhibitors. **A** Rank plot of kinase inhibitors according to hits below 25% showing staurosporine, AT9283 and TAK-901 as highly unselective inhibitors (left side) and rabusertib, PF-04217903 and VX-745 as highly selective “probe-like” inhibitors (right side). The corresponding kinome coverage of highly unselective compounds AT9283, R406 and KW-2449 is depicted in a kinome dendrogram was adapted and is reproduced, courtesy of Cell Signaling Technologies (cellsignaling.com). **B** Ranked bar chart of selectivity score (25%) of tested kinases at 10 μ M testing concentration, identification of dark kinases and common off-targets of the inhibitor set. This score corresponds to the fractions of all tested inhibitors that displace the tracer molecule by >75% at 10 μ M (and hence correspondingly 25% tracer remains bound). Each bar represents the selectivity score of an individual kinase, left inset identifies 11 kinases that were not bound by any of the tested compounds. Right panel shows the seven most frequently inhibited kinases.

5.3.2 Comparison of data between published *in vitro* and *in cellulo* assay formats

For comparison with already published datasets, we standardized protein kinases names using the UniProt identifier and compound names using InCHI identifier in both datasets for a direct comparison. Moreover, studies have shown that assessment of compound selectivity using cellular or enzymatic assays may provide different results¹⁰⁹.

5.3.3 Influence of ATP concentration on potency

Most inhibitors target the ATP binding site either directly or allosterically. As a consequence, cellular ATP directly competes with inhibitor binding and the K_M for the substrate and therefore influences the inhibitor potency. The concentration of ATP in cells is estimated to be in the range of 1 to 3 mM and typical K_M s are in the micromolar range, hence very potent inhibitors are needed for a full inhibition of the target in competition with ATP. Vasta and colleagues¹⁰⁹ showed that kinases which have a higher K_M did not shift to lower potencies as much as kinases showing a low K_M for ATP in cells. Furthermore, they showed that the K_M for ATP for individual kinases is dependent on kinase activation states and interaction partners. We compared our data with different assay formats, that utilize different concentrations of ATP. The *in vitro* methods that were used to assess kinome-wide selectivity of a large amount of inhibitors tested here, use ATP at the individual kinases K_M or at low concentrations and are either enzymatic activity assays (radioactivity-based by Reaction Biology) or binding assays (KINOMEScan by DiscoverX). The Kinobeads assay uses endogenous full-length protein but lyses their cells which leads to a large dilution of ATP. NanoBRET uses full-length overexpressed proteins and cellular concentrations of ATP. Comparing the data (Figure 15), we observe an about 10-fold shift between the Kinobeads data and NanoBRET with NanoBRET showing lower potency.

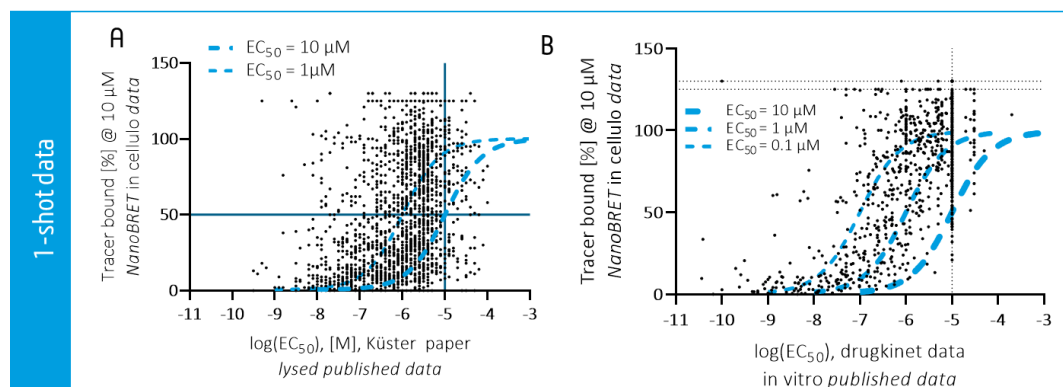


Figure 15 | Comparison of data between *in vitro* and *in cellulo* assay formats. **A** Correlation of NanoBRET 1-shot data at 10 μM with published IC_{50} data calculated using the Kinobeads assay¹⁶⁵. Displayed are 127 of 156 (19812) kinase-inhibitor pairs. The blue fitted curve shows the perfect distribution of data points. The black horizontal line highlights 50% threshold for binding of the tested compounds and the vertical line denotes the screening concentration in the NanoBRET assay. **B** Correlation of in-house NanoBRET 1-shot data at 10 μM and published *in vitro* data extracted from drugkinet.ca.

When comparing NanoBRET to the *in vitro* data, we observe a shift of 10 to 100-fold. This shows that a part of cellular data being less potent may be attributed to the cellular high concentration of ATP, but another part may be attributed to full-length proteins being used in the NanoBRET assay and Kinobeads assay opposed to classical *in vitro* assays that use the catalytic domains only.

5.3.4 Deviations in selectivity profiles of published kinase inhibitors

As discussed already in the introduction of this work the publication from Vasta *et al* in 2018¹⁰⁹ investigated that FDA-approved kinase inhibitors dasatinib and crizotinib showed a narrowed selectivity profile in cells than compared to *in vitro* assays. This discovery could be confirmed on a larger kinase inhibitor set in this project.

It is worth mentioning that the 234 kinases selected for this project only consist of the assay with high assay quality in a 384-well plate format. It is possible to test more kinases and their mutants in other format with higher assay volumes or in the lysed assay mode (as used in chapter 5.2.2), where the cell walls are lysed by addition of a detergent and an overall better assay quality is observed.

Although strong kinase selectivity may not be essential for efficacy of therapeutic agents it is critical for tool compounds used in cells to elucidate kinase biology. The assay platform generated here may be used for future studies and has been made commercially available.

5.4 Beyond kinases – targeting dysregulated proteins

In the previous chapters 5.1 to 5.3 it was discussed how the cellular target engagement method NanoBRET influenced many different protein kinase projects from development of chemical probes to a kinome-wide cellular selectivity panel. However, NanoBRET as an assay method is a versatile displacement technique that enables to not only study a single protein family like kinases but also enables the investigation of other proteins. The small luciferase NLuc can also be fused to different proteins and with a suitable tracer molecule, a displacement can be measured and a cellular affinity of small molecules can be determined. In the next chapter, two non-kinase projects will be presented in which the NanoBRET method was used as an additional screening method to determine the on-target potency in cells as well as the cell permeability of test compounds.

5.4.1 WD-Repeat-Containing Protein 5 (WDR5) Degraders to target transcription factor MYC (In the following subchapter, parts of the publication “Design, Synthesis, and Evaluation of WD-Repeat-Containing Protein 5 (WDR5) Degraders” are included¹⁶⁶).

Dysregulated transcription is often associated with cellular growth and proliferation and might ultimately induce the development of cancer¹⁶⁷. The transcription process is highly regulated by transcription factors, such as the MYC proteins and their expression is frequently enhanced and dysregulated in human tumours¹⁶⁸. Transcription factors, like many other proteins, rely on the help of other proteins to obtain the correct protein tertiary structure, so called scaffolding proteins. For example, the WD-repeat-containing protein 5 (WDR5) binds directly to the MYC oncoprotein family¹⁶⁹. WDR5's propeller-shaped WD interaction domain interacts with a large diversity of proteins as well as some long noncoding RNAs. Both surfaces of the doughnut-shaped WD domain protein present docking sites, which are called WIN (WDR5-interacting site) and WBM (WDR5-binding motif) sites¹⁷⁰. MYC binds to the WBM site of WDR5 with an evolutionary conserved N-terminal region, which is called Myc-box IIIb¹⁷¹. The transcription factor MYC is an attractive drug target, however, attempts to develop small molecules that modulate MYC functions have not been developed yet as MYC was deemed undruggable. In this project presented in the next chapter, we aimed to use the PROTAC approach to degrade the MYC scaffold protein WDR5 and thereby modulate the oncogenic function of MYC. A PROTAC molecule consists of two linked moieties that act as

binders for the target of interest on one hand and an E3 ubiquitin ligase on the other hand. When binding both proteins, the PROTAC creates proximity between the two proteins, leading to a polyubiquitination of the target by the E3 ligase and subsequent proteasomal degradation. The PROTAC emerges unchanged by this reaction and can enter a new cycle to degrade the target of interest. We designed two compound series targeting WDR5, based on two published inhibitors OICR-9429¹⁷² and a modified pyrroloimidazole-based inhibitor^{173, 174} that were combined with known E3 ligase ligands targeting cereblon, VHL and MDM2. The rational compound design is shown in Figure 16.

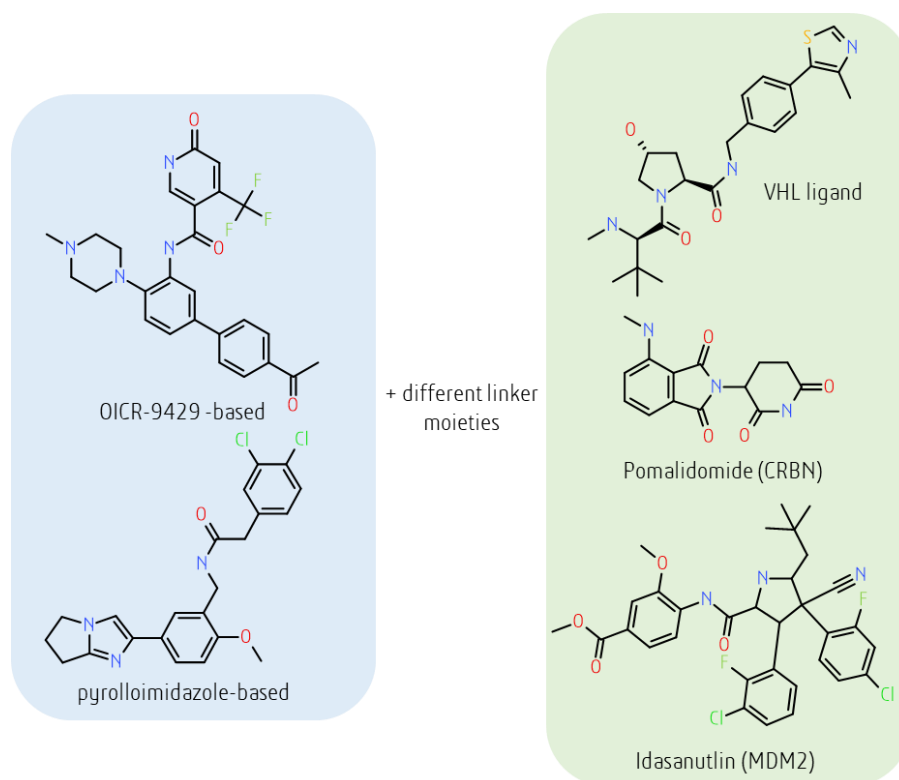


Figure 16 | Synthesis design of WDR5 degraders based on two different literature WDR5 binders. The molecules contain either the OICR-derivate or the pyrroloimidazole derivate as WDR5 ligands (ligand for target protein, blue) that are connected with different linker molecules (PEG linker, aliphatic linker or aromatic linker) with a different E3 ligase ligand (VHL, CRBN or MDM2, green). CRBN = cereblon. Figure adapted from Dölle *et al.*¹⁶⁶.

WDR5 shows two binding pockets. Both literature compounds target WDR5 at its WIN pocket, in order for the WBN pocket of WDR5 to remain free for MYC to bind and be degraded alongside its scaffold protein WDR5. As a first indication of binding of the molecules a DSF assay was performed. OICR-9429 was used as a reference compound in all assays. Unfortunately, some compounds that contained aliphatic linkers showed weaker thermal stabilization due to the limiting solubility. Heterobifunctional molecules that contained shorter PEG linkers showed the highest melting temperature shifts, regardless of the E3

ligase ligand used. The unmodified E3 ligase ligand did not show any temperature shift on WDR5. As a next step the *in vitro* K_D s of the CRBN-based degrader 7a and the VHL based degrader 8a were determined using the ITC assay. Both molecules exhibited relatively high thermal shifts that could not be confirmed by the ITC data. For both PROTACs that we selected, large negative binding enthalpies were observed ranging from -10 to -4.9 kcal/mol. 8a showed large negative binding enthalpies of -10 kcal/mol with close-to-zero entropy changes (-0.2 to 1.1 kcal/mol), whereas compounds with large positive entropy changes showed small binding enthalpies (e.g., 8e: $\Delta H = -6.3$ kcal/mol, $T\Delta S = +4.5$ kcal/mol). Taken the solubility issues of some tested compounds as well as unexpected behaviour of the attached linker into account, ITC is not necessarily a suitable method to measure binding of PROTACs. As a next method to test the binding affinity of the molecules and have an orthogonal method to DSF that verifies the binding of our molecules against WDR5, a NanoBRET assay was performed. Additionally, to the binding, also the cell permeability can be measured, which is most likely a limiting factor, due to the large molecular weight of the heterobifunctional molecules. For the NanoBRET assay the construct of the protein of interest was fused with a Nano Luciferase. This C-terminal and N-terminal constructs were kindly provided by our collaborating site in the SGC Toronto. Furthermore, we needed to design a tracer molecule, which later could be used in the assay as the displacement molecule. The C-terminally tagged WDR5 showed the best assay parameters, including the assay window and overall luciferase signal and was selected as best NanoLuc construct for the NanoBRET assays (Figure 17A).

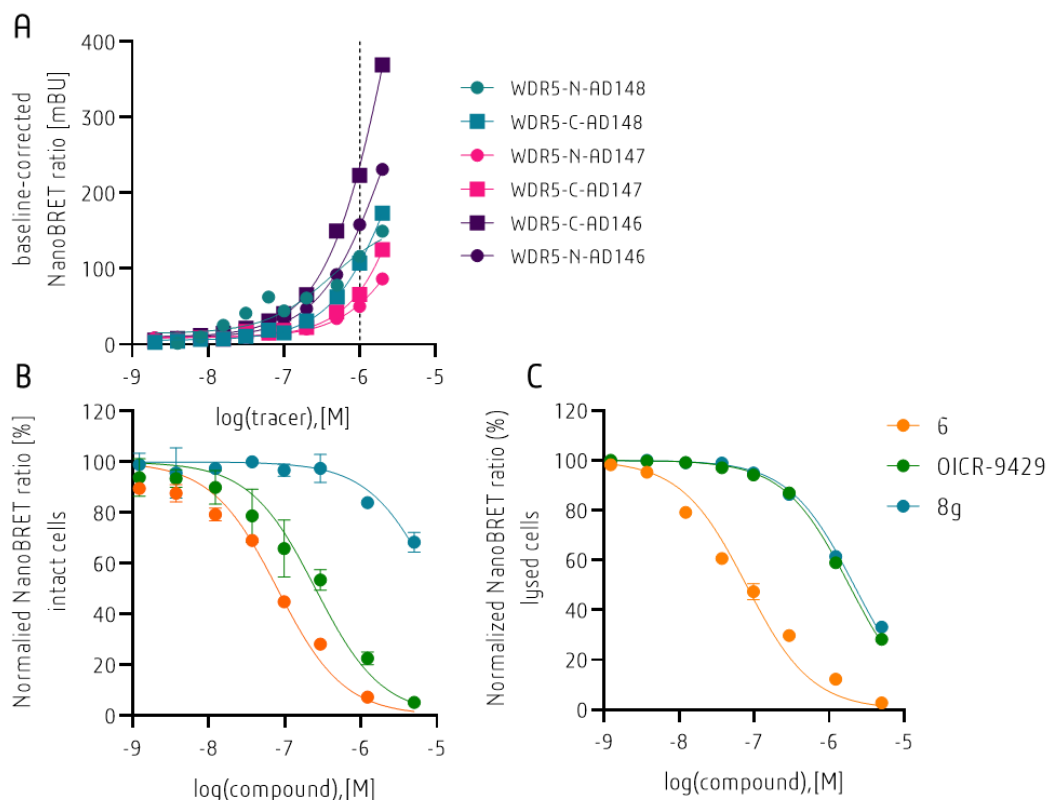


Figure 17 | Cellular permeability and target engagement on WDR5. **A** Tracer titration of all three newly synthesised tracer molecules based on the OICR-9429 scaffold on either C-terminal or N-terminal NanoLuc-tagged WDR5. NanoBRET dose-response curves for degrader molecule 6 and 8g, and parental compound OICR-9429 in intact cells (**B**) and in lysed cells (**C**).

The lead compound for compound 7a and 8a showed a cellular potency of 139 nM and the addition of a linker molecule as well as the E3 ligase handle led to a significant decrease in the compound affinity towards WDR5. Furthermore, both assay modes measured in NanoBRET, intact and lysed format showed only low micromolar affinity for WDR5. The only aliphatic linker containing degrader 8g showed a two-digit micromolar affinity in the intact cellular experiment. MDM2 targeting degraders showed weak *in vitro* affinity in the DSF assay, the BRET measurements confirmed this weak activity of these molecules to WDR5. Taken together with the DSF results, the MDM2 targeting degraders were excluded from further experiments. Several degrader molecules were identified as cell-permeable and able to bind to WDR5 in cells and cell-lysates, demonstrating their potential to degrade WDR5 in *in vivo* experiments.

Before testing the degradation of WDR5 in a cellular context we confirmed the formation of a PRTOAC-bound complex between WDR5 and the respective E3 ligase using the split-luciferase based HiBiT system. In this assay the open reading frame of WDR5 is fused to a

small 11 amino acid luciferase peptide (called HiBiT) and stably transduced into the AML cell line MV4-11 (MV4-11WDR5-HiBiT). The final cells are then treated with various concentration of degrader molecules for 24 h and a depletion of WDR5-HiBiT is measured by observing a decrease in the luciferase activity that occurred after addition of the LgBiT part of the split luciferase and a luciferase substrate. Unfortunately, none of the cereblon-based PROTAC molecules showed depletion of the luciferase signal, while many different VHL-PROTACs showed good cellular degradation. The most effective degrader was identified as 8g, which showed a maximum WDR5-HiBiT depletion of 58% and a calculated DC_{50} value of 53 ± 10 nM. Strikingly, degrader 8a, a degrader resembling 8g, but containing a [PEG]₁ moiety instead of an aliphatic chain, did not induce degradation of WDR5. The best degrader from the pyrroloimidazole-based series was 17b, which contained a [PEG]₂ linker, although the degradation was smaller than compared to 8g. To verify the degradation effect in the HiBiT-assay system, two negative control compounds resembling 17b and 8g, but with an inactive E3 ligase ligand, were synthesized and tested. None of the tested control compounds showed degradation of WDR5. To confirm that the degrader molecules did not alter the WDR5 transcription, but only reduce the protein level of WDR5, the MV4-11 cells were treated with both ligands and the mRNA level was quantified using quantitative qPCR. As expected, all molecules only reduce the protein level of WDR5 by degradation. The next step was to analyse the cellular protein levels by quantitative proteomics to measure if the molecule induced degradation is specific to WDR5 or rather unspecific. Among the 5805 proteins that were detected in the treated MV4-11 cells compared to the untreated control only WDR was significantly and substantially depleted.

In this project, we were able to develop a selective WDR5 PROTAC that was able to degrade WDR5 in cells. This PROTAC was accepted by the SGC with new criteria for PROTAC molecules¹⁷⁵ under the name Homer (<https://www.thesgc.org/chemical-probes/homer>) as a chemical tool compounds to study WDR5 function in cells. We established a variety of assay systems such as a BRET-based target engagement assay and a stable HiBiT cell line, which will allow further testing of future second-generation WDR5 degrader molecules with improved potency. Moreover, the molecules presented here are versatile tools that will allow comprehensive evaluation of WDR5 degraders in diverse cancer types and the potential of this strategy for drug discovery. Unfortunately, we did not further test the degradation of

transcription factor MYC, respectively the interaction between the MYC binding protein WDR5 and MYC itself, but helped to develop a tool compound that could be used to investigate this interaction in the future.

5.4.2 Cellular family-wide selectivity platform for BIRC proteins

(In the following subchapter, parts of the publication “A Toolbox for the Generation of Chemical Probes for Baculovirus IAP Repeat Containing Proteins” are included¹⁷⁶.

E3 ligases form a large and diverse family of proteins that play a central role in the proteasomal degradation machinery and are of special interest as hijacking the E3 function has become a proven method to degrade dysregulated proteins and thereby stopping the function of a protein of interest. The small molecule PROTACs recruit protein targets to the ubiquitin system and form a new class of pharmacologically active drugs. Recent efforts have focused on identifying new E3 ligases and the structurally conserved interaction domain RING domain was discovered. In this project 16 BIR domains, that contain the RING E3 ligase domain, have been investigated. Although there are known small molecule ligands for these Inhibitors of Apoptosis (IAP) family, the family selectivity and overall characterization of these molecules is lacking. In this project we developed assays that allowed the determination of the inhibitor potency *in vitro* and *in cellulo*, as well as to gain insight into the family selectivity of the BIRC inhibitor landscape.

The first objective was to cluster the 8 different BIRC proteins that contain 16 BIR domains based on their BIR-domain sequence homology to identify constructs needed for a comprehensive selectivity platform. The resulting homology tree is shown in Figure 18 and clusters the BIRC domains according to the presence of the 3 individual identified BIR domains (BIR1-3).

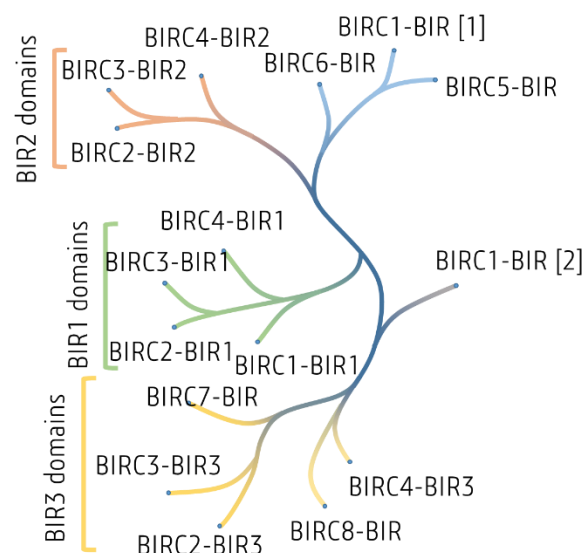


Figure 18 | Phylogenetic tree of BIRC family. Analysis of the BIR domains from all 8 BIRC proteins showing the clustering of BIR1 (green), BIR2 (orange) and BIR3 (yellow), as well as ungrouped BIR domains (blue). The figure was made by Martin P. Schwalm and is adapted from Schwalm and Berger *et al*¹⁷⁶.

5.4.2.1 *In vitro* affinity assessment of literature BIRC compounds

We chose to test the BIRC2-BIR3 domain as representative domain for all *in vitro* assay since the published data was often based on this domain. The *in vitro* selectivity platform consisted of three orthogonal assay methods including fluorescence polarization (FP) assay, differential scanning fluorimetry (DSF) and isothermal titration calorimetry (ITC). 10 diverse and commercially available inhibitors were identified from literature reports as candidate compounds, including monovalent as well as bivalent molecules that bind two BIR-domains simultaneously. All selected inhibitors showed literature potencies from 300 μ M for SM-164³⁹ to 169 nM for BV-6 towards different BIR domains¹⁷⁷. The FP assay was based on the displacement of a fluorescent tracer molecule, in this case a SMAC mimetic, from the binding site and was established first, since it was reported in most references as a BIRC *in vitro* binding assay. Nearly all tested compounds showed potent IC₅₀ values in the range of 1.8 nM for SM-164 to 8.4 nM for BV-6, which are in good correlation with the published data and no difference in the potencies between monovalent and bivalent molecules could be observed. UC-112 did not bind the BIRC2-BIR3 construct. As a second assay we chose the DSF assay. Although BIRC2-BIR3 shows a relatively high native melting temperature of 74 K it was possible to stabilize it even further with thermal shifts of up to 18 K (AZD5582). Overall, 7 of the 10 compounds displayed good thermal shifts and a good correlation to the FP assay, demonstrating that higher shifts correlate to higher affinities in the FP binding assay.

Addition of UC-112 did not lead to an increase of the thermal stability of BIRC2-BIR3, which is in good agreement with the FP data. As last biophysical method ITC measurements were performed. Overall, the data generated from ITC correlate well with the other two assay methods and showed dissociation constants between 20 and 60 nM. AZD5582, which showed a high stabilization of BIRC2-BIR3 did show lower affinities than compared to other molecules which showed less thermal stabilization, which could mean that the DSF assay is influenced by another characteristic, like the compound composition.

5.4.2.2 BIRC family *in cellulo* selectivity characterization platform

To assess the cellular affinity and establish a family-wide selectivity platform we established NanoBRET assays for full-length BIRC proteins as well as individual BIR domains. All constructs were cloned using an N-terminal NanoLuc placement. Constructs for BIRC1 and BIRC6 could not be obtained, due to accumulations of mutations in the construct or the large size of the protein and a lack of cDNA, respectively. A pan-BIRC tracer was synthesized that was believed to be able to target all BIRC protein, using the pan-BIRC inhibitor LCL161¹⁷⁸. To test the newly synthesized tracer which we obtained from Promega, we performed tracer titrations for all constructs, including full-length BIRCs and single BIR domains. All five full-length BIRC proteins (BIRC2, 3, 4, 7 and 8) bound to the tracer with high affinities of below 250 nM with overall good assay quality (Figure 19A-B). The single BIR domains often bound to the tracer molecule in much lower affinity of higher than 1 μ M up to 4 μ M which is due to solubility problems of the fluorophore the highest possible tracer concentration. However, BIRC2-BIR3, BIRC3-BIR3 and BIRC7-BIR3 showed higher affinities with $K_{D, app}$ values of below 1 μ M. In general, all BIR3 single domain constructs showed good assay quality, which was unfortunately not the case for the BIR1 and BIR2 domains. The tracer molecule was based on the LCL161, which was also included in the test set. The cellular potency of the BIRC2-BIR3 construct was 20 nM, which is slightly higher than the biophysical data we generated using ITC with 50 nM. The cellular environment could be a possible explanation for this increase in cellular affinity of the tracer molecule.

After establishment of all possible full-length and single domain assays all 10 literature compounds were tested. As with the *in vitro* data, UC-112 did not show any binding in the cellular assay format. All other compounds showed potent binding to all BIR proteins. BV-6

and birinapant were the least potent molecules with an affinity of higher than 1 μ M. In addition, these compounds showed a significant loss of affinity in our cellular assay compared to the measured *in vitro* efficacy. Since the bivalent molecules SM-164 and AZD5582 did not exhibit such a drastic loss of efficacy, the high molecular weight and size of the bivalent compounds cannot be the factor influencing the lower cellular activity. None of the tested compounds showed any selectivity towards a specific BIRC protein. CUDC-427 was the most selective inhibitor with a cellular affinity of 38.8 ± 2.5 nM for BIRC7 but a much weaker affinity towards the remaining measured BIRC proteins ranging from 190–720 nM. The same behaviour was observed for AZD5582 (Table 2), suggesting that family selectivity for BIRC7 could be achieved. Next to the full-length E3 ligases, the test set was measured against the single domain proteins and their cellular potency was determined. The results of the selectivity screening were visualized on the established phylogenetic tree (Figure 19C). Large difference in binding affinity were observed between individual BIR domains. For example, BV-6 showed no binding to BIRC2-BIR2 but bound strongly to other closely related BIR2 domains. Some molecules, such as the bivalent inhibitor AZD5582, bound with almost equal affinity to BIR2 and BIR3 domains, whereas others, such as CUDC-427 or LCL161, bound almost exclusively to the BIR3 domains.

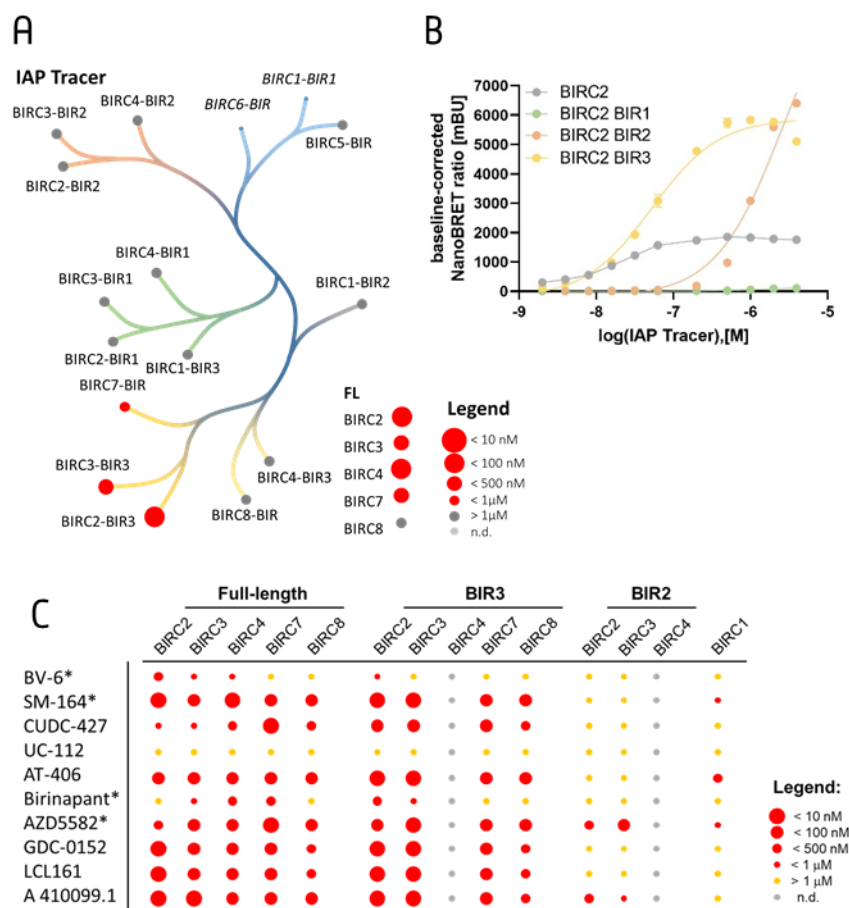


Figure 19 | NanoBRET Tracer Titration and full-length screening data of compound set. **A** Tracer potency across the BIRC family. Here, BIRC6 was not tested and the BIRC1-BIR1 domain did not show a significant luciferase signal and therefore, both constructs were excluded (*italic*). **B** Tracer Titration curves for BIRC2 full-length protein and its corresponding BIR domains (n=4). **C** Heatmap for 10 literature compound potencies towards the corresponding protein constructs. Bivalent compounds are marked with (*). Figure is adapted from Schwalm and Berger *et al*¹⁷⁶.

In this project, we established a cellular family-wide screening panel for BIR domain proteins and assessed the commercially available inhibitor landscape for BIRC proteins towards their BIRC selectivity. Unfortunately, most of the tested compounds did not show any selectivity within in the small family, including clinical candidates. BIRC proteins are involved in a diversity of pathways, and hence a pan-BIRC inhibitor could induce unwanted side effects. However, cellular potency and cell membrane penetrance was observed which makes the ten BIRC inhibitors suitable PROTAC handles. The established *in vitro* platforms as well as the cellular selectivity panel will prove helpful for the development of more selective BIRC inhibitors.

5.4.3 NanoBRET target engagement beyond kinases – challenges and new applications

The last two projects presented in the last chapter have shown that NanoBRET can be used as a highly effective assay method in non-kinase projects. Using a suitable tracer molecule, NanoBRET can be used as a simple assay method to test multiple proteins simultaneously due to the rapid and efficient overnight transfection of the protein of interest. It enables an assay method to target many proteins at the same time and is a good medium-high throughput screening method compared to conventional biophysical methods that require purified protein, as presented in the BIRC family toolbox project. The last aim of this thesis was to investigate another protein family, the BIRC proteins and develop tools to design better PROTACS and examine the current coverage of literature compounds in prospect of their potency and family selectivity.

6. General Discussion and Outlook

6.1 The future of cellular target engagement assays

Throughout this thesis it was the aim to understand the selectivity and affinity of small molecule inhibitors in living cells. As a general technique, NanoBRET was used for that purpose. NanoBRET is a displacement assay where the compounds ability is measured to bind the target of interest. The technique does not measure the influence of the compound on the kinase activity and hence gives no insight about the inhibitory effect of the compound. Here, binding does not necessarily indicate an influence of the compound on the activity or inhibiting the protein function. However, in the case of protein kinases any inhibitor binding to the ATP binding pocket and hence being characterized as a type I or type II binder, will automatically also be a competitive inhibitor. For other types binding as allosteric inhibitor this may not be the case.

There are different methods reported in the literature that measure cellular target engagement as a binding assay. For example, the cellular thermal shift assay (CETSA) measures thermal stabilization of a protein upon compound binding, similar to the DSF assay used throughout the projects in this thesis. CETSA has the advantage to measure large amounts of proteins simultaneously on an endogenous level without any labels if coupled with a mass spectrometry-based readout. This is beneficial as the cellular model may be chosen that is most applicable for the scientific question. However, many proteins are not detectable in mass spectrometric assays. In NanoBRET, there is a need for labeling with the NLuc and the cell used, HEK293T, is only used as a mammalian expression system. A different technique measuring endogenous cellular activity used for decades' is Western Blotting. Here, cells are treated, lysed and analyzed using an SDS gel electrophoresis, subsequent blotting to a membrane and readout using a primary antibody usually directed towards the phosphorylated substrate and secondary antibody for detection are employed. This way, the activity of proteins may be monitored. However, the throughput is low compared to CETSA or NanoBRET and not always are specific antibodies available.

The biggest limitation of the NanoBRET method is that it requires the use of a suitable tracer molecule. According to Cheng-Prusoff, the binding of a tracer molecule may influence the resulting inhibitor potency. In this thesis a comprehensive selectivity platform was developed

to compare a large panel of different protein kinases. To make them comparable, the effect of the tracer on the resulting inhibitor potency needed to be similar. To achieve that, for each kinase-tracer pair a tracer titration was performed and the $K_{D, app}$ determined was used as the tracer concentration in subsequent compound EC_{50} determinations. This way, the resulting EC_{50} differed no more than 2-fold, making all assays comparable within this threshold.

6.2 Chemical tool compounds are valuable resources, if they are well characterized

The first aim of this thesis was to support medicinal chemistry SAR projects using the cellular target engagement method NanoBRET and determine both the on-target affinity as well as off-target profiles for different chemical probes and chemogenomics library compounds. Chemical probes are highly characterized molecules that are intended to be used as mechanistic tool for target identification and validation. Using a chemical probe with a distinct selectivity profile it is able to investigate the phenotypical responses of their targets. Many researchers use poorly characterized inhibitors as selective tool compounds which prevents the field from correctly identifying the protein kinase causing the phenotypic effect. In several probe development projects NanoBRET was able to provide cellular characterization that led to approval by an independent committee. It is crucial to determine the selectivity of protein kinase inhibitors in cells, as the resulting chemical probes are intended for cellular use.

Correctly characterized and applied chemical probes are valuable tools for both drug discovery as well as academic research and help to understand cellular function of a protein that later could become a drug target. There is still a need for chemical tool compounds for understudied kinases as well as other proteins, because their function is yet unknown but could have the potential to become drug targets. Using medicinal chemistry efforts and understanding protein targets using a chemical SAR, we developed chemical tool compounds for the understudied kinase DRAK1 and for the known drug target SIK2.

Another approach to identify tool compounds is a literature review and a subsequent comprehensive cellular characterization of the candidates for their suitability as chemical probes or chemogenomic candidates. Hence, the second aim for this thesis was to examine the current status and coverage with literature compounds in prospect of their potency and family selectivity and subsequent use as chemical tool compounds of two specific

understudied subfamilies of the human kinome, the splicing kinase family and the CDK family. In this thesis we characterized novel compounds and enabled development of a highly selective inhibitor for the PCTAIRE family and identified the best reported inhibitors to be used to study the function of the splicing kinase family.

Within the known set of clinical and approved kinase inhibitors some dark kinases that may be assayed with NanoBRET may be hidden. To identify promising starting points or find chemogenomic candidates, the third aim of this thesis was to elucidate the target space of a large library of published FDA approved and clinical small molecule kinase inhibitors using an optimized target engagement method in cells, in order to find new highly selective chemical probes and novel compounds for so far untargeted kinases to better understand their modes of action. Using this set as a starting point there was an inherent bias for known drug targets. However, using this set we were able to better understand differences in inhibitor selectivity profiles comparing in vitro methods such as binding and activity assays with cellular target engagement. We identified a subset of kinases that were showing differences and that may better be analysed using cellular methods. The FDA approved kinase inhibitors only target a small section of the kinome and this explains why they exhibit a similar selectivity profile.

Another yet underdeveloped strategy for cellular selectivity is the so-called kinetic selectivity that was not investigated in this thesis. Here, selectivity may not be assessed on the criteria of equilibrium affinity alone, but on the cells as an open system. After a wash-out of treated compounds only compounds binding longer to the target may lead to a phenotypic response. In the open system of in vivo the pharmacology may have an influence on the selectivity of protein kinase inhibitors.

6.3 Cellular target engagement method as versatile tool to study proteins

Using NanoBRET to study the cellular selectivity of protein kinase inhibitors may not be enough for future projects. Within the Structural Genomics Consortium, the next large effort is to identify a chemogenomic tool compound for each of the about 5000 druggable proteins in the proteome. With the large NanoBRET platform for protein kinases, this thesis provided a subset available for testing. Additionally, we identified and developed constructs and tracers for non-kinase proteins to study new methods to target proteins. Therefore, the last aim of this thesis was to investigate another protein family, namely the BIRC proteins and

develop tools to design better PROTACS and examine the current coverage of literature compounds in prospect of their potency and family selectivity. We provided tools to be used for future mechanistic studies and for more development programs for family-selective inhibitors. These tools may be used to answer whether BIRCs may be used as E3 ligases in PROTAC approaches or whether binding of a PROTAC to the BIR domains of the BIRCs is sufficient to reach the RING domain acting as an E3. Using NanoBRET as a technique to study the proteins of the proteome, many more landscape characterizations of known and yet unknown chemical matter may lead to exciting insights into these proteins' functions. The project described in this thesis was a first step towards this goal.

7. List of Abbreviations

Proteins and gene names are based on UniProt and HUGO nomenclature.

ADP	adenosine diphosphate
AR	androgen receptor
ATP	adenosine triphosphate
AVPI	N-terminal tetrapeptide
BRET	bioluminescence resonance energy transfer
C-lobe	C-terminal lobe
C-loop	catalytic loop
C-spine	catalytic spine
CETSA	cellular thermal shift assay
CRBN	cereblon (E3 ligase)
DFG	aspartate-phenylalanine-glycine motif
DMEM	Dulbecco's modified eagles' medium
DMSO	dimethyl sulfoxide
DSF	differential scanning fluorimetry
EC ₅₀	concentration at half maximal effect
ER	oestrogen receptor
FBS	fetal bovine serum
FDA	Food and Drug Administration (US)
FP	Fluorescence Polarisation
GBM	glioblastoma multiform
RING	Really Interesting New Gene finger domain
HEK293	human embryonic kidney cells
HeLa	adenocarcinoma/ cervical carcinoma cells
HRD	Histidine-arginine-aspartate motif
IAP	inhibitors of apoptosis
IBM	IAP binding motif
IC ₅₀	Concentration at half maximal inhibitory effect
ITC	isothermal titration calorimetry
K _D	dissociation constant
K _{D, app}	apparent dissociation constant
MV4-11	biphenotypic B myelomonocytic leukemia cells

7. List of Abbreviations

MRC-9	fibroblasts
N-lobe	N-terminal lobe
Nluc	Nanoluciferase
NSCLC	non-small cell lung cancer
PANC1	epithelioid carcinoma cells
PCR/ qPCR	Polymerase Chain Reaction/ quantitative Polymerase Chain Reaction
PEG	polyethylene glycol linkers
POI	Protein of interest
PRTOAC	Proteolysis targeting chimeras
PTM	Posttranslational modifications
RBPs	RNA binding proteins
RRM	RNA-recognition motif
RS	serine-proline dipeptides
R-spine	Regulatory spine
SAR	Structural Affinity Relationship
SGC	Structural Genomics Consortium
SMAC	Second Mitochondria-derived Activator of Caspases
SR	arginine-rich splicing factor proteins
THP-1	acute monocytic leukemia cells
T _M	Thermal shift (DSF assay)
U-2OS	osteosarcoma cells

8. References

- 1 Kennelly, P. J. Protein kinases and protein phosphatases in prokaryotes: a genomic perspective. *FEMS microbiology letters* **206**, 1-8 (2002).
- 2 Park, S. J., Itoh, T. & Takenawa, T. Phosphatidylinositol 4-phosphate 5-kinase type I is regulated through phosphorylation response by extracellular stimuli. *Journal of Biological Chemistry* **276**, 4781-4787 (2001).
- 3 Krebs, E. G. An accidental biochemist. *Annual review of biochemistry* **67**, R12 (1998).
- 4 Santarius, T., Shipley, J., Brewer, D., Stratton, M. R. & Cooper, C. S. A census of amplified and overexpressed human cancer genes. *Nature Reviews Cancer* **10**, 59-64 (2010).
- 5 Zhong, M., Lee, G. M., Sijbesma, E., Ottmann, C. & Arkin, M. R. Modulating protein-protein interaction networks in protein homeostasis. *Current opinion in chemical biology* **50**, 55-65 (2019).
- 6 Manning, G., Whyte, D. B., Martinez, R., Hunter, T. & Sudarsanam, S. The protein kinase complement of the human genome. *Science* **298**, 1912-1934 (2002).
- 7 Kannan, N. & Taylor, S. S. Rethinking pseudokinases. *Cell* **133**, 204-205 (2008).
- 8 Sheetz, J. B. & Lemmon, M. A. Looking lively: emerging principles of pseudokinase signaling. *Trends in Biochemical Sciences* (2022).
- 9 Liosi, M.-E. *et al.* Insights on JAK2 Modulation by Potent, Selective, and Cell-Permeable Pseudokinase-Domain Ligands. *Journal of Medicinal Chemistry* (2022).
- 10 Ardito, F., Giuliani, M., Perrone, D., Troiano, G. & Lo Muzio, L. The crucial role of protein phosphorylation in cell signaling and its use as targeted therapy. *International journal of molecular medicine* **40**, 271-280 (2017).
- 11 Wee, P. & Wang, Z. Epidermal growth factor receptor cell proliferation signaling pathways. *Cancers* **9**, 52 (2017).
- 12 Chappell, W. H. *et al.* Ras/Raf/MEK/ERK and PI3K/PTEN/Akt/mTOR inhibitors: rationale and importance to inhibiting these pathways in human health. *Oncotarget* **2**, 135 (2011).
- 13 Choi, S., Kim, W. & Chung, J. Drosophila salt-inducible kinase (SIK) regulates starvation resistance through cAMP-response element-binding protein (CREB)-regulated transcription coactivator (CRTC). *Journal of Biological Chemistry* **286**, 2658-2664 (2011).
- 14 Conkright, M. D. *et al.* TORCs: transducers of regulated CREB activity. *Molecular cell* **12**, 413-423 (2003).
- 15 Sun, Z., Jiang, Q., Li, J. & Guo, J. The potent roles of salt-inducible kinases (SIKs) in metabolic homeostasis and tumorigenesis. *Signal transduction and targeted therapy* **5**, 1-15 (2020).
- 16 Chen, F., Chen, L., Qin, Q. & Sun, X. Salt-inducible kinase 2: an oncogenic signal transmitter and potential target for cancer therapy. *Frontiers in oncology* **9**, 18 (2019).
- 17 Cheng, H. *et al.* SIK1 couples LKB1 to p53-dependent anoikis and suppresses metastasis. *Science signaling* **2**, ra35-ra35 (2009).
- 18 Amara, S. *et al.* Critical role of SIK3 in mediating high salt and IL-17 synergy leading to breast cancer cell proliferation. *PloS one* **12**, e0180097 (2017).

8. References

- 19 Modi, V. & Dunbrack Jr, R. L. Defining a new nomenclature for the structures of active and inactive kinases. *Proceedings of the National Academy of Sciences* **116**, 6818-6827 (2019).
- 20 Taylor, S. S. & Kornev, A. P. Protein kinases: evolution of dynamic regulatory proteins. *Trends in biochemical sciences* **36**, 65-77 (2011).
- 21 Arter, C., Trask, L., Ward, S., Yeoh, S. & Bayliss, R. Structural features of the protein kinase domain and targeted binding by small-molecule inhibitors. *Journal of Biological Chemistry* **298** (2022).
- 22 Sridhar, J., Akula, N. & Pattabiraman, N. Selectivity and potency of cyclin-dependent kinase inhibitors. *The AAPS journal* **8**, E204-E221 (2006).
- 23 Wood, D. J. & Endicott, J. A. Structural insights into the functional diversity of the CDK–cyclin family. *Open biology* **8**, 180112 (2018).
- 24 Hanahan, D. & Weinberg, R. A. Hallmarks of cancer: the next generation. *cell* **144**, 646-674 (2011).
- 25 Hanahan, D. Hallmarks of cancer: new dimensions. *Cancer discovery* **12**, 31-46 (2022).
- 26 Kelemen, O. *et al.* Function of alternative splicing. *Gene* **514**, 1-30 (2013).
- 27 Kim, H. K., Pham, M. H. C., Ko, K. S., Rhee, B. D. & Han, J. Alternative splicing isoforms in health and disease. *Pflügers Archiv-European Journal of Physiology* **470**, 995-1016 (2018).
- 28 Danan-Gotthold, M. *et al.* Identification of recurrent regulated alternative splicing events across human solid tumors. *Nucleic acids research* **43**, 5130-5144 (2015).
- 29 Bonomi, S. *et al.* Oncogenic alternative splicing switches: role in cancer progression and prospects for therapy. *International journal of cell biology* **2013** (2013).
- 30 Agrawal, A. A., Yu, L., Smith, P. G. & Buonamici, S. Targeting splicing abnormalities in cancer. *Current opinion in genetics & development* **48**, 67-74 (2018).
- 31 Hentze, M. W., Castello, A., Schwarzl, T. & Preiss, T. A brave new world of RNA-binding proteins. *Nature reviews Molecular cell biology* **19**, 327-341 (2018).
- 32 Pastor, F., Shkreta, L., Chabot, B., Durantel, D. & Salvetti, A. Interplay Between CMGC Kinases Targeting SR Proteins and Viral Replication: Splicing and Beyond. *Frontiers in Microbiology* **12**, 658721 (2021).
- 33 Long, J. C. & Caceres, J. F. The SR protein family of splicing factors: master regulators of gene expression. *Biochemical Journal* **417**, 15-27 (2009).
- 34 Howard, J. M. & Sanford, J. R. The RNAissance family: SR proteins as multifaceted regulators of gene expression. *Wiley Interdisciplinary Reviews: RNA* **6**, 93-110 (2015).
- 35 Varjosalo, M. *et al.* The protein interaction landscape of the human CMGC kinase group. *Cell reports* **3**, 1306-1320 (2013).
- 36 Wang, H.-Y. *et al.* SRPK2: a differentially expressed SR protein-specific kinase involved in mediating the interaction and localization of pre-mRNA splicing factors in mammalian cells. *The Journal of cell biology* **140**, 737-750 (1998).
- 37 Duncan, P. I., Stojdl, D. F., Marius, R. M., Scheit, K. H. & Bell, J. C. The Clk2 and Clk3 dual-specificity protein kinases regulate the intranuclear distribution of SR proteins and influence pre-mRNA splicing. *Experimental cell research* **241**, 300-308 (1998).

- 38 Álvarez, M., Estivill, X. & de la Luna, S. DYRK1A accumulates in splicing speckles through a novel targeting signal and induces speckle disassembly. *Journal of cell science* **116**, 3099-3107 (2003).
- 39 Lu, J. *et al.* SM-164: a novel, bivalent Smac mimetic that induces apoptosis and tumor regression by concurrent removal of the blockade of cIAP-1/2 and XIAP. *Cancer research* **68**, 9384-9393 (2008).
- 40 Alahari, S. K., Schmidt, H. & Kaufer, N. F. The fission yeast *prp4+* gene involved in pre-mRNA splicing codes for a predicted serine/threonine kinase and is essential for growth. *Nucleic acids research* **21**, 4079-4083 (1993).
- 41 Kojima, T., Zama, T., Wada, K., Onogi, H. & Hagiwara, M. Cloning of human PRP4 reveals interaction with Clk1. *Journal of Biological Chemistry* **276**, 32247-32256 (2001).
- 42 Gui, J.-F., Lane, W. S. & Fu, X.-D. A serine kinase regulates intracellular localization of splicing factors in the cell cycle. *Nature* **369**, 678-682 (1994).
- 43 Colwill, K. *et al.* SRPK1 and Clk/Sty protein kinases show distinct substrate specificities for serine/arginine-rich splicing factors. *Journal of Biological Chemistry* **271**, 24569-24575 (1996).
- 44 Schröder, M. *et al.* DFG-1 residue controls inhibitor binding mode and affinity, providing a basis for rational design of kinase inhibitor selectivity. *Journal of Medicinal Chemistry* **63**, 10224-10234 (2020).
- 45 Nayler, O., Stamm, S. & Ullrich, A. Characterization and comparison of four serine- and arginine-rich (SR) protein kinases. *Biochemical Journal* **326**, 693-700 (1997).
- 46 Menegay, H. J., Myers, M. P., Moeslein, F. M. & Landreth, G. E. Biochemical characterization and localization of the dual specificity kinase CLK1. *Journal of cell science* **113**, 3241-3253 (2000).
- 47 Menegay, H., Moeslein, F. & Landreth, G. The dual specificity protein kinase CLK3 is abundantly expressed in mature mouse spermatozoa. *Experimental cell research* **253**, 463-473 (1999).
- 48 Aranda, S., Laguna, A. & Luna, S. d. I. DYRK family of protein kinases: evolutionary relationships, biochemical properties, and functional roles. *The FASEB Journal* **25**, 449-462 (2011).
- 49 Guimerá, J. *et al.* A human homologue of *Drosophila* minibrain (MNB) is expressed in the neuronal regions affected in Down syndrome and maps to the critical region. *Human molecular genetics* **5**, 1305-1310 (1996).
- 50 Laham, A. J., Saber-Ayad, M. & El-Awady, R. DYRK1A: A down syndrome-related dual protein kinase with a versatile role in tumorigenesis. *Cellular and Molecular Life Sciences* **78**, 603-619 (2021).
- 51 Becker, W. & Sippl, W. Activation, regulation, and inhibition of DYRK1A. *The FEBS journal* **278**, 246-256 (2011).
- 52 Banroques, J. & Abelson, J. N. PRP4: a protein of the yeast U4/U6 small nuclear ribonucleoprotein particle. *Molecular and Cellular Biology* **9**, 3710-3719 (1989).
- 53 Dellaire, G. *et al.* Mammalian PRP4 kinase copurifies and interacts with components of both the U5 snRNP and the N-CoR deacetylase complexes. *Molecular and cellular biology* **22**, 5141-5156 (2002).

- 54 Schneider, M. *et al.* Human PRP4 kinase is required for stable tri-snRNP association during spliceosomal B complex formation. *Nature structural & molecular biology* **17**, 216-221 (2010).
- 55 Fauvel, B. & Yasri, A. in *MAbs*. 838-851 (Taylor & Francis).
- 56 Hojjat-Farsangi, M. Small-molecule inhibitors of the receptor tyrosine kinases: promising tools for targeted cancer therapies. *International journal of molecular sciences* **15**, 13768-13801 (2014).
- 57 Dupont, C. A., Riegel, K., Pombaiah, M., Juhl, H. & Rajalingam, K. Druggable genome and precision medicine in cancer: current challenges. *The FEBS Journal* **288**, 6142-6158 (2021).
- 58 Lee, P. Y., Yeoh, Y. & Low, T. Y. A recent update on small-molecule kinase inhibitors for targeted cancer therapy and their therapeutic insights from mass spectrometry-based proteomic analysis. *The FEBS Journal* (2022).
- 59 Roskoski Jr, R. Classification of small molecule protein kinase inhibitors based upon the structures of their drug-enzyme complexes. *Pharmacological research* **103**, 26-48 (2016).
- 60 Meharena, H. S. *et al.* Deciphering the structural basis of eukaryotic protein kinase regulation. *PLoS biology* **11**, e1001680 (2013).
- 61 Kufareva, I. & Abagyan, R. Type-II kinase inhibitor docking, screening, and profiling using modified structures of active kinase states. *Journal of medicinal chemistry* **51**, 7921-7932 (2008).
- 62 Namboodiri, H. V. *et al.* Analysis of imatinib and sorafenib binding to p38 α compared with c-Abl and b-Raf provides structural insights for understanding the selectivity of inhibitors targeting the DFG-out form of protein kinases. *Biochemistry* **49**, 3611-3618 (2010).
- 63 Hanke, T. *et al.* Development and Characterization of Type I, Type II, and Type III LIM-Kinase Chemical Probes. *Journal of medicinal chemistry* **65**, 13264-13287 (2022).
- 64 Jones, J. K. & Thompson, E. M. Allosteric Inhibition of ABL Kinases: Therapeutic Potential in Cancer Allosteric Inhibition of ABL1 and ABL2. *Molecular cancer therapeutics* **19**, 1763-1769 (2020).
- 65 Gharwan, H. & Groninger, H. Kinase inhibitors and monoclonal antibodies in oncology: clinical implications. *Nature reviews Clinical oncology* **13**, 209-227 (2016).
- 66 Voice, A. T., Tresadern, G., Twidale, R. M., Van Vlijmen, H. & Mulholland, A. J. Mechanism of covalent binding of ibrutinib to Bruton's tyrosine kinase revealed by QM/MM calculations. *Chemical science* **12**, 5511-5516 (2021).
- 67 Roskoski Jr, R. Properties of FDA-approved Small Molecule Protein Kinase Inhibitors: A 2023 Update. *Pharmacological research*, 106552 (2022).
- 68 Amrhein, J. A., Knapp, S. & Hanke, T. Synthetic opportunities and challenges for macrocyclic kinase inhibitors. *Journal of Medicinal Chemistry* **64**, 7991-8009 (2021).
- 69 Zou, H. Y. *et al.* PF-06463922, an ALK/ROS1 inhibitor, overcomes resistance to first and second generation ALK inhibitors in preclinical models. *Cancer cell* **28**, 70-81 (2015).
- 70 Wang, B. *et al.* An overview of kinase downregulators and recent advances in discovery approaches. *Signal Transduction and Targeted Therapy* **6**, 1-19 (2021).

- 71 Chartier, M., Morency, L.-P., Zylber, M. I. & Najmanovich, R. J. Large-scale detection of drug off-targets: hypotheses for drug repurposing and understanding side-effects. *BMC Pharmacology and Toxicology* **18**, 1-16 (2017).
- 72 Berger, S. I. & Iyengar, R. Role of systems pharmacology in understanding drug adverse events. *Wiley interdisciplinary reviews: systems biology and medicine* **3**, 129-135 (2011).
- 73 Fedorov, O., Müller, S. & Knapp, S. The (un) targeted cancer kinome. *Nature chemical biology* **6**, 166-169 (2010).
- 74 Edwards, A. M. *et al.* Too many roads not taken. *Nature* **470**, 163-165 (2011).
- 75 Singh, P., Ravanan, P. & Talwar, P. Death associated protein kinase 1 (DAPK1): a regulator of apoptosis and autophagy. *Frontiers in molecular neuroscience* **9**, 46 (2016).
- 76 Mao, P. *et al.* Serine/threonine kinase 17A is a novel p53 target gene and modulator of cisplatin toxicity and reactive oxygen species in testicular cancer cells. *Journal of Biological Chemistry* **286**, 19381-19391 (2011).
- 77 Manivannan, P., Reddy, V., Mukherjee, S., Clark, K. N. & Malathi, K. RNase L induces expression of a novel serine/threonine protein kinase, DRAK1, to promote apoptosis. *International journal of molecular sciences* **20**, 3535 (2019).
- 78 Sun, J. *et al.* PDRG1 promotes the proliferation and migration of GBM cells by the MEK/ERK/CD44 pathway. *Cancer science* **113**, 500 (2022).
- 79 Wells, C. I. *et al.* The Kinase Chemogenomic Set (KCGS): An open science resource for kinase vulnerability identification. *International journal of molecular sciences* **22**, 566 (2021).
- 80 Kim, J. H. & Scialli, A. R. Thalidomide: the tragedy of birth defects and the effective treatment of disease. *Toxicological sciences* **122**, 1-6 (2011).
- 81 Rehman, W., Arfons, L. M. & Lazarus, H. M. The rise, fall and subsequent triumph of thalidomide: lessons learned in drug development. *Therapeutic advances in hematology* **2**, 291-308 (2011).
- 82 Sasso, J. M. *et al.* Molecular glues: The adhesive connecting targeted protein degradation to the clinic. *Biochemistry* (2022).
- 83 Békés, M., Langley, D. R. & Crews, C. M. PROTAC targeted protein degraders: the past is prologue. *Nature Reviews Drug Discovery* **21**, 181-200 (2022).
- 84 Qin, L., Dai, H. & Wang, J. Key considerations in targeted protein degradation drug discovery and development. *Frontiers in Chemistry* **10** (2022).
- 85 Mullard, A. Targeted protein degraders crowd into the clinic. *Nature reviews. Drug discovery* (2021).
- 86 Schapira, M., Calabrese, M. F., Bullock, A. N. & Crews, C. M. Targeted protein degradation: expanding the toolbox. *Nature reviews Drug discovery* **18**, 949-963 (2019).
- 87 Shirasaki, R. *et al.* Functional genomics identify distinct and overlapping genes mediating resistance to different classes of heterobifunctional degraders of oncoproteins. *Cell reports* **34**, 108532 (2021).
- 88 Williams, F. P., Haubrich, K., Perez-Borrajero, C. & Hennig, J. Emerging RNA-binding roles in the TRIM family of ubiquitin ligases. *Biological Chemistry* **400**, 1443-1464 (2019).

- 89 Kannt, A. & Đikić, I. Expanding the arsenal of E3 ubiquitin ligases for proximity-induced protein degradation. *Cell chemical biology* **28**, 1014-1031 (2021).
- 90 Sherpa, D. *et al.* GID E3 ligase supramolecular chelate assembly configures multipronged ubiquitin targeting of an oligomeric metabolic enzyme. *Molecular cell* **81**, 2445-2459. e2413 (2021).
- 91 Dove, K. K. & Klevit, R. E. RING-between-RING E3 ligases: emerging themes amid the variations. *Journal of molecular biology* **429**, 3363-3375 (2017).
- 92 Lee, J. *et al.* Discovery of E3 ligase ligands for target protein degradation. *Molecules* **27**, 6515 (2022).
- 93 Deshaies, R. J. & Joazeiro, C. A. RING domain E3 ubiquitin ligases. *Annual review of biochemistry* **78** (2009).
- 94 Wu, H., Tschopp, J. & Lin, S.-C. Smac mimetics and TNF α : a dangerous liaison? *Cell* **131**, 655-658 (2007).
- 95 Mudde, A. C., Booth, C. & Marsh, R. A. Evolution of our understanding of XIAP deficiency. *Frontiers in Pediatrics*, 557 (2021).
- 96 Dubrez-Daloz, L., Dupoux, A. & Cartier, J. IAPs: more than just inhibitors of apoptosis proteins. *Cell cycle* **7**, 1036-1046 (2008).
- 97 Salvesen, G. S. & Duckett, C. S. IAP proteins: blocking the road to death's door. *Nature reviews Molecular cell biology* **3**, 401-410 (2002).
- 98 Dubrez, L., Berthelet, J. & Glorian, V. IAP proteins as targets for drug development in oncology. *OncoTargets and therapy*, 1285-1304 (2013).
- 99 Eckelman, W. C. & Mathis, C. A. Molecular targets. *Nuclear Medicine and Biology* **1**, 1 (2006).
- 100 Wang, Y. & Ma, H. Protein kinase profiling assays: a technology review. *Drug Discovery Today: Technologies* **18**, 1-8 (2015).
- 101 Lemeer, S., Zörgiebel, C., Ruprecht, B., Kohl, K. & Kuster, B. Comparing immobilized kinase inhibitors and covalent ATP probes for proteomic profiling of kinase expression and drug selectivity. *Journal of proteome research* **12**, 1723-1731 (2013).
- 102 Klaeger, S. *et al.* Chemical proteomics reveals ferroxidase as a common off-target of kinase inhibitors. *ACS chemical biology* **11**, 1245-1254 (2016).
- 103 Robers, M. B. *et al.* Target engagement and drug residence time can be observed in living cells with BRET. *Nature communications* **6**, 1-10 (2015).
- 104 Fedorov, O., Niesen, F. H. & Knapp, S. in *Kinase Inhibitors* 109-118 (Springer, 2012).
- 105 Wiseman, T., Williston, S., Brandts, J. F. & Lin, L.-N. Rapid measurement of binding constants and heats of binding using a new titration calorimeter. *Analytical biochemistry* **179**, 131-137 (1989).
- 106 Hafner, M., Niepel, M., Chung, M. & Sorger, P. K. Growth rate inhibition metrics correct for confounders in measuring sensitivity to cancer drugs. *Nature methods* **13**, 521-527 (2016).
- 107 Tjaden, A., Giessmann, R. T., Knapp, S., Schröder, M. & Müller, S. High-content live-cell multiplex screen for chemogenomic compound annotation based on nuclear morphology. *STAR protocols* **3**, 101791 (2022).
- 108 Dale, N. C., Johnstone, E. K., White, C. W. & Pflieger, K. D. NanoBRET: the bright future of proximity-based assays. *Frontiers in Bioengineering and Biotechnology* **7**, 56 (2019).

- 109 Vasta, J. D. *et al.* Quantitative, wide-spectrum kinase profiling in live cells for assessing the effect of cellular ATP on target engagement. *Cell chemical biology* **25**, 206-214. e211 (2018).
- 110 Yung-Chi, C. & Prusoff, W. H. Relationship between the inhibition constant (KI) and the concentration of inhibitor which causes 50 per cent inhibition (I50) of an enzymatic reaction. *Biochemical pharmacology* **22**, 3099-3108 (1973).
- 111 Kurz, C. G. *et al.* Illuminating the Dark: Highly Selective Inhibition of Serine/Threonine Kinase 17A with Pyrazolo [1, 5-a] pyrimidine-Based Macrocycles. *Journal of Medicinal Chemistry* (2022).
- 112 Howard, S. *et al.* Fragment-based discovery of the pyrazol-4-yl urea (AT9283), a multitargeted kinase inhibitor with potent aurora kinase activity. *Journal of medicinal chemistry* **52**, 379-388 (2009).
- 113 Reich, S. H. *et al.* Structure-based design of pyridone-aminal eFT508 targeting dysregulated translation by selective mitogen-activated protein kinase interacting kinases 1 and 2 (MNK1/2) inhibition. *Journal of medicinal chemistry* **61**, 3516-3540 (2018).
- 114 Picado, A. *et al.* A chemical probe for dark kinase STK17B derives its potency and high selectivity through a unique P-loop conformation. *Journal of medicinal chemistry* **63**, 14626-14646 (2020).
- 115 Gregg, B. T., Tymoshenko, D. O., Razzano, D. A. & Johnson, M. R. Pyrazolo [1, 5-a] pyrimidines. Identification of the privileged structure and combinatorial synthesis of 3-(hetero) arylpyrazolo [1, 5-a] pyrimidine-6-carboxamides. *Journal of Combinatorial Chemistry* **9**, 507-512 (2007).
- 116 Pike, A. C. *et al.* Activation segment dimerization: a mechanism for kinase autophosphorylation of non-consensus sites. *The EMBO journal* **27**, 704-714 (2008).
- 117 Mao, P. *et al.* Serine/threonine kinase 17A is a novel candidate for therapeutic targeting in glioblastoma. *PLoS One* **8**, e81803 (2013).
- 118 Tesch, R. *et al.* Structure-based design of selective salt-inducible kinase inhibitors. *Journal of Medicinal Chemistry* **64**, 8142-8160 (2021).
- 119 Ndubaku, C. O. *et al.* Design of selective PAK1 inhibitor G-5555: improving properties by employing an unorthodox low-p K a polar moiety. *ACS medicinal chemistry letters* **6**, 1241-1246 (2015).
- 120 Karpov, A. S. *et al.* Optimization of a dibenzodiazepine hit to a potent and selective allosteric PAK1 inhibitor. *ACS medicinal chemistry letters* **6**, 776-781 (2015).
- 121 Zhou, J. *et al.* A Novel Compound ARN-3236 Inhibits Salt-Inducible Kinase 2 and Sensitizes Ovarian Cancer Cell Lines and Xenografts to Paclitaxel. *Clinical Cancer Research* **23**, 1945-1954 (2017).
- 122 Amrhein, J. A. *et al.* Discovery of 3-Amino-1 H-pyrazole-Based Kinase Inhibitors to Illuminate the Understudied PCTAIRE Family. *International Journal of Molecular Sciences* **23**, 14834 (2022).
- 123 Adon, T., Shanmugarajan, D. & Kumar, H. Y. CDK4/6 inhibitors: a brief overview and prospective research directions. *RSC advances* **11**, 29227-29246 (2021).
- 124 Wells, C. I. *et al.* Quantifying CDK inhibitor selectivity in live cells. *Nature communications* **11**, 1-11 (2020).
- 125 Dixon-Clarke, S. E. *et al.* Structure and inhibitor specificity of the PCTAIRE-family kinase CDK16. *Biochemical Journal* **474**, 699-713 (2017).

- 126 Statsuk, A. V. *et al.* Tuning a three-component reaction for trapping kinase substrate complexes. *Journal of the American Chemical Society* **130**, 17568-17574 (2008).
- 127 Karaman, M. W. *et al.* A quantitative analysis of kinase inhibitor selectivity. *Nature biotechnology* **26**, 127-132 (2008).
- 128 Zhang, S. *et al.* Effects of Itraconazole and Rifampin on the Pharmacokinetics of Mobocertinib (TAK-788), an Oral Epidermal Growth Factor Receptor Inhibitor, in Healthy Volunteers. *Clinical Pharmacology in Drug Development* **10**, 1044-1053 (2021).
- 129 Li, F. *et al.* Metabolism of JQ1, an inhibitor of bromodomain and extra terminal bromodomain proteins, in human and mouse liver microsomes. *Biology of reproduction* **103**, 427-436 (2020).
- 130 Charrasse, S., Carena, I., Hagmann, J., Woods-Cook, K. & Ferrari, S. PCTAIRE-1: characterization, subcellular distribution, and cell cycle-dependent kinase activity. (1999).
- 131 Mikolcevic, P., Rainer, J. & Geley, S. Orphan kinases turn eccentric: a new class of cyclin Y-activated, membrane-targeted CDKs. *Cell Cycle* **11**, 3758-3768 (2012).
- 132 Zielke, N. & Edgar, B. FUCCI sensors: powerful new tools for analysis of cell proliferation. *Wiley Interdisciplinary Reviews: Developmental Biology* **4**, 469-487 (2015).
- 133 Brasca, M. G. *et al.* Identification of N, 1, 4, 4-Tetramethyl-8-[[4-(4-methylpiperazin-1-yl) phenyl] amino]-4, 5-dihydro-1 H-pyrazolo [4, 3-h] quinazoline-3-carboxamide (PHA-848125), a Potent, Orally Available Cyclin Dependent Kinase Inhibitor. *Journal of medicinal chemistry* **52**, 5152-5163 (2009).
- 134 Whittaker, S. R., Mallinger, A., Workman, P. & Clarke, P. A. Inhibitors of cyclin-dependent kinases as cancer therapeutics. *Pharmacology & therapeutics* **173**, 83-105 (2017).
- 135 Tjaden, A. *et al.* Image-Based Annotation of Chemogenomic Libraries for Phenotypic Screening. *Molecules* **27**, 1439 (2022).
- 136 Schaefer, A. J. *et al.* GW779439X and its pyrazolopyridazine derivatives inhibit the serine/threonine kinase Stk1 and act as antibiotic adjuvants against β -lactam-resistant *Staphylococcus aureus*. *ACS infectious diseases* **4**, 1508-1518 (2018).
- 137 Boni, J., Rubio-Perez, C., López-Bigas, N., Fillat, C. & de la Luna, S. The DYRK family of kinases in cancer: molecular functions and therapeutic opportunities. *Cancers* **12**, 2106 (2020).
- 138 Deshmukh, V. *et al.* Modulation of the Wnt pathway through inhibition of CLK2 and DYRK1A by lorecivint as a novel, potentially disease-modifying approach for knee osteoarthritis treatment. *Osteoarthritis and cartilage* **27**, 1347-1360 (2019).
- 139 Gao, Q. *et al.* Evaluation of cancer dependence and druggability of PRP4 kinase using cellular, biochemical, and structural approaches. *Journal of Biological Chemistry* **288**, 30125-30138 (2013).
- 140 Mott, B. T. *et al.* Evaluation of substituted 6-arylquinazolin-4-amines as potent and selective inhibitors of cdc2-like kinases (Clk). *Bioorganic & medicinal chemistry letters* **19**, 6700-6705 (2009).
- 141 Muraki, M. *et al.* Manipulation of alternative splicing by a newly developed inhibitor of Clks. *Journal of Biological Chemistry* **279**, 24246-24254 (2004).

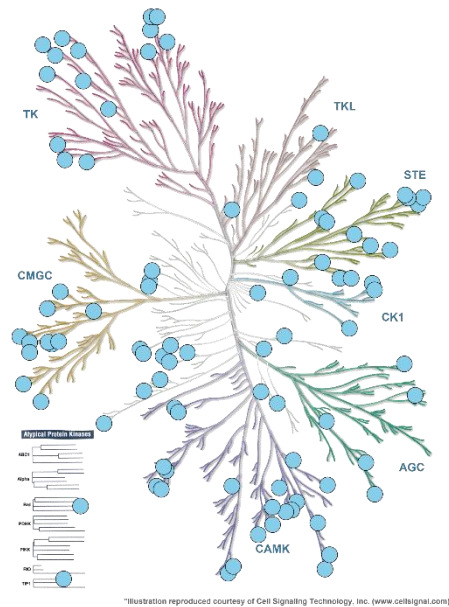
- 142 Powell, C. E. *et al.* Selective Macrocyclic Inhibitors of DYRK1A/B. *ACS Medicinal Chemistry Letters* **13**, 577-585 (2022).
- 143 Ogawa, Y. *et al.* Development of a novel selective inhibitor of the Down syndrome-related kinase Dyrk1A. *Nature communications* **1**, 1-9 (2010).
- 144 Banerjee, S. *et al.* Inhibition of dual-specificity tyrosine phosphorylation-regulated kinase 2 perturbs 26S proteasome-addicted neoplastic progression. *Proceedings of the National Academy of Sciences* **116**, 24881-24891 (2019).
- 145 Martín Moyano, P., Němec, V. & Paruch, K. Cdc-like kinases (CLKs): biology, chemical probes, and therapeutic potential. *International Journal of Molecular Sciences* **21**, 7549 (2020).
- 146 Němec, V. *et al.* Highly selective inhibitors of protein kinases CLK and HIPK with the furo [3, 2-b] pyridine core. *European Journal of Medicinal Chemistry* **215**, 113299 (2021).
- 147 van der Laden, J., Soppa, U. & Becker, W. Effect of tyrosine autophosphorylation on catalytic activity and subcellular localisation of homeodomain-interacting protein kinases (HIPK). *Cell Communication and Signaling* **13**, 1-11 (2015).
- 148 Miduturu, C. V. *et al.* High-throughput kinase profiling: a more efficient approach toward the discovery of new kinase inhibitors. *Chemistry & biology* **18**, 868-879 (2011).
- 149 Wippich, F. *et al.* Dual specificity kinase DYRK3 couples stress granule condensation/dissolution to mTORC1 signaling. *Cell* **152**, 791-805 (2013).
- 150 Kuroyanagi, N., Onogi, H., Wakabayashi, T. & Hagiwara, M. Novel SR-protein-specific kinase, SRPK2, disassembles nuclear speckles. *Biochemical and biophysical research communications* **242**, 357-364 (1998).
- 151 Nakagawa, O. *et al.* Centronuclear myopathy in mice lacking a novel muscle-specific protein kinase transcriptionally regulated by MEF2. *Genes & development* **19**, 2066-2077 (2005).
- 152 Wang, P. *et al.* Both decreased and increased SRPK1 levels promote cancer by interfering with PHLPP-mediated dephosphorylation of Akt. *Molecular cell* **54**, 378-391 (2014).
- 153 Czuby, A. & Piekietko-Witkowska, A. Protein kinases that phosphorylate splicing factors: Roles in cancer development, progression and possible therapeutic options. *The international journal of biochemistry & cell biology* **91**, 102-115 (2017).
- 154 Tang, J. *et al.* A critical update on the strategies towards small molecule inhibitors targeting Serine/arginine-rich (SR) proteins and Serine/arginine-rich proteins related kinases in alternative splicing. *Bioorganic & Medicinal Chemistry*, 116921 (2022).
- 155 Schröder, M. *et al.* MSC-1186, a Highly Selective Pan-SRPK Inhibitor Based on an Exceptionally Decorated Benzimidazole-Pyrimidine Core. *Journal of Medicinal Chemistry* (2022).
- 156 Corkery, D. P., Holly, A. C., Lahsae, S. & Dellaire, G. Connecting the speckles: Splicing kinases and their role in tumorigenesis and treatment response. *Nucleus* **6**, 279-288 (2015).
- 157 Davis, M. I. *et al.* Comprehensive analysis of kinase inhibitor selectivity. *Nature biotechnology* **29**, 1046-1051 (2011).
- 158 Chiu, C.-Y. & Tsaur, M.-L. NS5806 inhibits ERK activation to attenuate pain induced by peripheral nerve injury. *Neuroscience Letters* **790**, 136890 (2022).

- 159 Berg, A. & Berg, T. A small-molecule screen identifies the antitrypanosomal agent suramin and analogues NF023 and NF449 as inhibitors of STAT5a/b. *Bioorganic & Medicinal Chemistry Letters* **27**, 3349-3352 (2017).
- 160 Lee, H. K. *et al.* G-749, a novel FLT3 kinase inhibitor, can overcome drug resistance for the treatment of acute myeloid leukemia. *Blood, The Journal of the American Society of Hematology* **123**, 2209-2219 (2014).
- 161 Besse, B. *et al.* (American Society of Clinical Oncology, 2018).
- 162 Hasinoff, B. B., Wu, X., Nitiss, J. L., Kanagasabai, R. & Yalowich, J. C. The anticancer multi-kinase inhibitor dovitinib also targets topoisomerase I and topoisomerase II. *Biochemical pharmacology* **84**, 1617-1626 (2012).
- 163 Duong, H.-Q. *et al.* Inhibition of NRF2 by PIK-75 augments sensitivity of pancreatic cancer cells to gemcitabine. *International Journal of Oncology* **44**, 959-969 (2014).
- 164 Fernandez-Martinez, P., Zahonero, C. & Sanchez-Gomez, P. DYRK1A: the double-edged kinase as a protagonist in cell growth and tumorigenesis. *Molecular & cellular oncology* **2**, e970048 (2015).
- 165 Klaeger, S. *et al.* The target landscape of clinical kinase drugs. *Science* **358**, eaan4368 (2017).
- 166 Dölle, A. *et al.* Design, synthesis, and evaluation of WD-repeat-containing protein 5 (WDR5) degraders. *Journal of Medicinal Chemistry* **64**, 10682-10710 (2021).
- 167 Bradner, J. E., Hnisz, D. & Young, R. A. Transcriptional addiction in cancer. *Cell* **168**, 629-643 (2017).
- 168 Dang, C. V. MYC on the path to cancer. *Cell* **149**, 22-35 (2012).
- 169 Thomas, L. R. *et al.* Interaction of the oncoprotein transcription factor MYC with its chromatin cofactor WDR5 is essential for tumor maintenance. *Proceedings of the National Academy of Sciences* **116**, 25260-25268 (2019).
- 170 Dharmarajan, V., Lee, J.-H., Patel, A., Skalnik, D. G. & Cosgrove, M. S. Structural basis for WDR5 interaction (Win) motif recognition in human SET1 family histone methyltransferases. *Journal of Biological Chemistry* **287**, 27275-27289 (2012).
- 171 Thomas, L. R. *et al.* Interaction with WDR5 promotes target gene recognition and tumorigenesis by MYC. *Molecular cell* **58**, 440-452 (2015).
- 172 Getlik, M. u. *et al.* Structure-based optimization of a small molecule antagonist of the interaction between WD repeat-containing protein 5 (WDR5) and mixed-lineage leukemia 1 (MLL1). *Journal of medicinal chemistry* **59**, 2478-2496 (2016).
- 173 Grebien, F. *et al.* Pharmacological targeting of the Wdr5-MLL interaction in C/EBP α N-terminal leukemia. *Nature chemical biology* **11**, 571-578 (2015).
- 174 Wang, F. *et al.* Discovery of potent 2-Aryl-6, 7-dihydro-5 H-pyrrolo [1, 2-a] imidazoles as WDR5-WIN-site inhibitors using fragment-based methods and structure-based design. *Journal of medicinal chemistry* **61**, 5623-5642 (2018).
- 175 Němec, V., Schwalm, M. P., Müller, S. & Knapp, S. PROTAC degraders as chemical probes for studying target biology and target validation. *Chemical Society Reviews* (2022).
- 176 Schwalm, M. P. *et al.* A Toolbox for the Generation of Chemical Probes for Baculovirus IAP Repeat Containing Proteins. *Frontiers in Cell and Developmental Biology* **10** (2022).
- 177 Varfolomeev, E. *et al.* IAP antagonists induce autoubiquitination of c-IAPs, NF- κ B activation, and TNF α -dependent apoptosis. *Cell* **131**, 669-681 (2007).

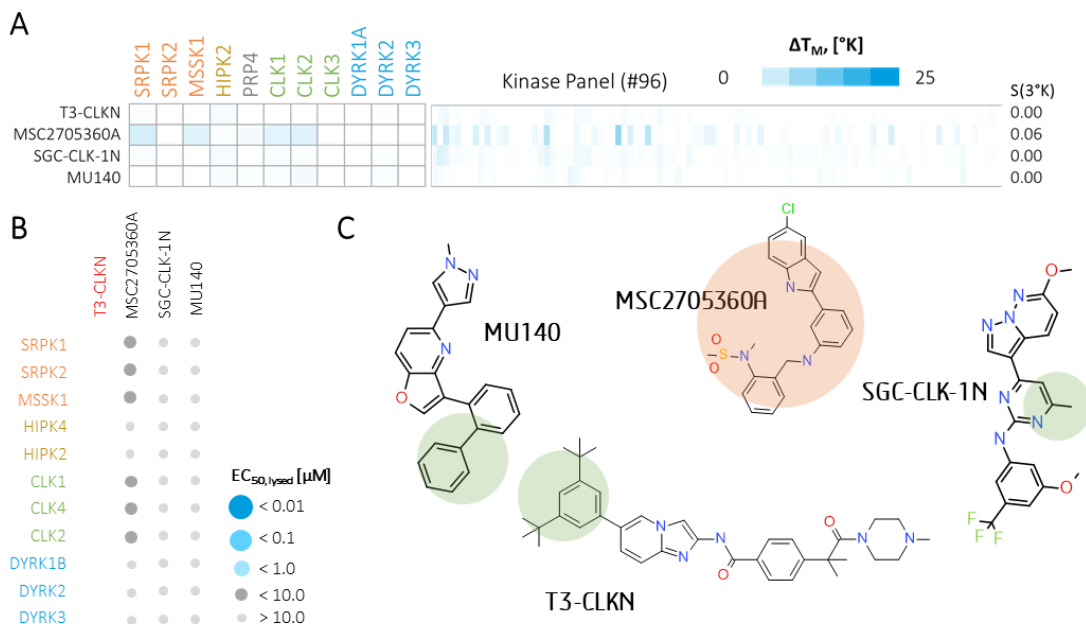
- 178 Baggio, C. *et al.* Aryl-fluorosulfate-based lysine covalent pan-Inhibitors of apoptosis protein (IAP) antagonists with cellular efficacy. *Journal of medicinal chemistry* **62**, 9188-9200 (2019).

9. Appendix

9.1 Supplementary Figures



SI Figure 1 | Kinome coverage of the DSF assay panel. Each kinase represented in the assay panel is marked with a light blue circle. The kinase dendrogram was adapted from Science and Cell Signaling Technology (cellsignaling.com).



SI Figure 2 | Data for negative control compounds for CLK and SRPK probe. **A** DSF screening of 29 kinase inhibitors against available splicing kinases and 96 additional kinases sampled across the kinome. **B** NanoBRET EC_{50} (lysed mode) as a dot heat plot. Big dark blue spots correspond to high potency of below 10 nM against the target. NanoBRET data for T3-CLK-NC missing. **C** Chemical structures of with circles indicating the changes from the probe molecule.

9.1 Supplementary Tables

SI Table 1 | Kinases used in the DSF panel.

HUGO name	SGC construct name	Group	AA start	AA end	vector	cutting site	Tag	Mutations
AAK1	AAK1A-c046	Other	T27	A365	pNIC-CTH0	TEV protease	C-terminal His-Tag	
ABL1	ABL1A-c006	TK	S229	K512	pNIC28-Bsa4	TEV protease	N-terminal His-Tag	
AKT3	AKT3A-c005	AGC	S120	E479	pNIC28-Bsa4	TEV protease	N-terminal His-Tag	
AURKB	AURKBA-c004	Other	Q55	A344	pNIC28-Bsa4	TEV protease	N-terminal His-Tag	
BMP2K	BMP2KA-c502	Other	S38	E345	pNIC-ZB	TEV protease	Basic solubility-enhancing Tag	
BMPR2	BMPR2A-c019	TKL	M189	T517	pNIC-CH	none	C-terminal His Tag	
BMX	BMXA-c031	TK	K264	H675	pNIC-CH	none	C-terminal His Tag	
BRAF	BRAFA-c039	TKL	R444	P705	pNIC28-Bsa4	TEV protease	N-terminal His-Tag	V600E
BRD4	BRD4A-c002	Atypical	N44	E168	pNIC28-Bsa4	TEV protease	N-terminal His-Tag	
BRPF1	BRPF1A-c001	Bromodomain	M626	G746	pNIC28-Bsa4	TEV protease	N-terminal His-Tag	
CAMK1D	CAMK1DA-c022	CAMK	S10	D329	pNIC28-Bsa4	TEV protease	N-terminal His-Tag	
CAMK1G	CAMK1GA-c034	CAMK	Q15	H316	pNIC28-Bsa4	TEV protease	N-terminal His-Tag	
CAMK2B	CAMK2BA-c013	CAMK	T11	A303	pNIC28-Bsa4	TEV protease	N-terminal His-Tag	
CAMK2D	CAMK2DA-c028	CAMK	T11	N335	pNIC28-Bsa4	TEV protease	N-terminal His-Tag	
CAMK4	CAMK4A-c007	CAMK	S15	G340	pNIC28-Bsa4	TEV protease	N-terminal His-Tag	
CAMKK2	CAMKK2B-c014	Other	H149	H449	pNIC28-Bsa4	TEV protease	N-terminal His-Tag	
CASK	CASKA-cf001	CAMK	M1	S337	pNIC28-Bsa4	TEV protease	N-terminal His-Tag	
CDC42BPA	CDC42BPAA-c004	AGC	M1	S424	pNIC-CTH0	TEV protease	C-terminal His-Tag	D254G
CDK2	CDK2A-c002	CMGC	M1	L298	pNIC28-Bsa4	TEV protease	N-terminal His-Tag	
CDKL1	CDKL1A-c024	CMGC	M1	H301	pNIC-CTHF	TEV protease	C-terminal His-Tag	
CHEK2	CHEK2A-c023	CAMK	T205	L543	pNIC28-Bsa4	TEV protease	N-terminal His-Tag	

9. Appendix

CLK1	CLK1A-c012	CMGC	H148	I484	pNIC28-Bsa4	TEV protease	N-terminal His-Tag	
CLK3	CLK3A-c005	CMGC	R134	T484	pNIC28-Bsa4	TEV protease	N-terminal His-Tag	
CSNK1D	CSNK1DA-c010	CK1	M1	K294	pNIC28-Bsa4	TEV protease	N-terminal His-Tag	
CSNK2A1	CSNK2A1A-c001	CK2	M1	S337	pNIC28-Bsa4	TEV protease	N-terminal His-Tag	
CSNK2A2	CSNK2A2A-c002	CK2	M1	P335	pNIC28-Bsa4	TEV protease	N-terminal His-Tag	
DAPK1	DAPK1A-c006	CAMK	M1	D334	pNIC28-Bsa4	TEV protease	N-terminal His-Tag	
DAPK3	DAPK3A-c010	CAMK	V9	G289	pNIC28-Bsa4	TEV protease	N-terminal His-Tag	
DCLK1	DCAMKL1A-c032	CAMK	S358	A680	pNIC-CTH0	TEV protease	C-terminal His-Tag	
DMPK	DMPK1A-c026	AGC	A64	P430	pNIC28-Bsa4	TEV protease	N-terminal His-Tag	
DYRK1A	DYRK1AA-c004	CMGC	S127	E485	pNIC28-Bsa4	TEV protease	N-terminal His-Tag	
DYRK2	DYRK2A-c022	CMGC	M73	R479	pNIC28-Bsa4	TEV protease	N-terminal His-Tag	
EPHA2	EPHA2A-c001	TK	D596	G900	pET28a	Thrombin	N-terminal His Tag and C-terminal His Tag	
EPHA5	EPHA5A-cf001	TK	P653	P939	pNIC-CH	none	C-terminal His Tag	
EPHA7	EPHA7A-cf001	TK	Q590	S899	pNIC-CH	none	C-terminal His Tag	
EPHB3	EPHB3A-cf001	TK	D616	S910	pLIC-SGC1	TEV protease	N-terminal His Tag	
FES	FESA-c001	TK	I448	R822	pNIC28-Bsa4	TEV protease	N-terminal His-Tag	
FGFR1	FGFR1B-cf003	TK	S461	E765	pLIC-SGC1	TEV protease	N-terminal His Tag	
FGFR2	FGFR2A-cf002	TK	T457	E768	pLIC-SGC1	TEV protease	N-terminal His Tag	
FGFR3	FGFR3A-cf003	TK	P449	E759	pLIC-SGC1	TEV protease	N-terminal His Tag	C582S and K650E
FLOT1	FLT1A-c002	TK	P801	L1158	pNIC28-Bsa4	TEV protease	N-terminal His-Tag	
GAK	GAKA-c028	Other	P14	V351	pNIC-H102	TEV protease	N-terminal His10	
GRK5	GPRK5A-c034	AGC	M1	E544	pNIC28-Bsa4	TEV protease	N-terminal His-Tag	
GSG2	GSG2A-c009	Other	G465	K798	pNIC28-Bsa4	TEV protease	N-terminal His-Tag	
GSK3B	GSK3BB-c026	CMGC	M26	R383	pNIC-CH	none	C-terminal His Tag	
MAP2K1	MAP2K1A-c007	STE	E62	V393	pNIC-CTHF	TEV protease	C-terminal His-Tag	
MAP2K4	MAP2K4A-c052	STE	S80	D399	pNIC-CH	none	C-terminal His Tag	

MAP2K6	MAP2K6A-c025	STE	E47	D334	pNIC28-Bsa4	TEV protease	N-terminal His-Tag	
MAP3K5	MAP3K5A-c005	STE	R659	L951	pNIC28-Bsa4	TEV protease	N-terminal His-Tag	
MAPK10	MAPK10A-c008	CMGC	M39	E402	pNIC28-Bsa4	TEV protease	N-terminal His-Tag	
MAPK13	MAPK13A-c011	CMGC	N15	R359	pNIC28-Bsa4	TEV protease	N-terminal His-Tag	
MAPK14	MAPK14A-c001	CMGC	M1	S360	pET-Duet-1	TEV protease	N-terminal His-Tag	Mouse
MAPK1	MAPK1A-c001	CMGC	M1	S360	pNIC28-Bsa4	TEV protease	N-terminal His-Tag	
MAPK8	MAPK8B-c007	CMGC	M1	L363	pNIC28-Bsa4	TEV protease	N-terminal His-Tag	
MAPK9	MAPK9A-c008	CMGC	M1	A380	pNIC28-Bsa4	TEV protease	N-terminal His-Tag	
MARK3	MARK3A-cf003	CAMK	D48	R366	pNIC-CT10HF	TEV protease	C-terminal His10+flag	
MARK4	MARK4A-c031	CAMK	H18	T397	pNIC28-Bsa4	TEV protease	N-terminal His-Tag	
MELK	MELKA-c060	CAMK	M1	T348	pNIC-ZB	TEV protease	Basic solubility-enhancing Tag	
MERTK	MERTKA-c002	TK	E571	V864	pNIC28-Bsa4	TEV protease	N-terminal His-Tag	
STK26	MST4A-c202	STE	M1	S300	pLIC-SGC1	TEV protease	N-terminal His Tag	
NEK1	NEK1A-c011	Other	M1	K328	pNIC28-Bsa4	TEV protease	N-terminal His-Tag	
NEK2	NEK2A-c112	Other	M1	I271	pET22b	none	C-terminal His-Tag	T175A
NEK7	NEK7A-c022	Other	N29	S302	pNIC-CH	terminal-His	C-terminal His Tag	
OXR1	OSR1A-c001	STE	M1	P322	pNIC28-Bsa4	TEV protease	N-terminal His-Tag	
PAK1	PAK1A-c027	STE	M248	H545	pNIC28-Bsa4	TEV protease	N-terminal His-Tag	
PAK4	PAK4A-c010	STE	S291	R591	pGEX-6P-2-Nde-Xho	PreScission protease	N terminal GST-Tag	
CDK16	PCTK1A-c031	CMGC	E163	S478	pNIC-CH	none	C-terminal His Tag	
PHKG2	PHKG2A-c020	CAMK	G6	R293	pNIC-ZB	TEV protease	Basic solubility-enhancing Tag	
PIM1	PIM1A-c001	CAMK	M1	S312	pLIC-SGC1	TEV protease	N-terminal His Tag	R250G
PIM3	PIM3A-c030	CAMK	M1	L326	pNIC28-Bsa4	TEV protease	N-terminal His-Tag	
PKMYT1	PKMYT1A-c004	Other	H75	P362	pNIC28-Bsa4	TEV protease	N-terminal His-Tag	
PLK4	PLK4A-c115	other	M1	M265	pNIC-CTHF	TEV protease	C-terminal His-Tag	
RIOK1	RIOK1A-cf001	Atypical	E143	T494	pNIC28-Bsa4	TEV protease	N-terminal His-Tag	

9. Appendix

RPS6KA1	RPS6KA1A-c036	CAMK	V413	L735	pNIC28-Bsa4	TEV protease	N-terminal His-Tag	
RPS6KA5	RPS6KA5A-c049	CAMK	S417	N696	pNIC28-Bsa4	TEV protease	N-terminal His-Tag	
SLK	SLKA-c004	STE	R26	E320	pNIC28-Bsa4	TEV protease	N-terminal His-Tag	
SRC	SRCA-c004	TK	A262	L536	pNIC28-Bsa4	TEV protease	N-terminal His-Tag	
SRPK1	SRPK1A-c002	CMGC	D58	S655	pNIC28-Bsa4	TEV protease	N-terminal His-Tag	
STK10	STK10A-c013	STE	R18	E317	pNIC28-Bsa4	TEV protease	N-terminal His-Tag	
STK17A	STK17AA-c029	CAMK	A39	E369	pNIC-H102	TEV protease	N-terminal His10	
STK17B	STK17BA-c014	CAMK	M25	S329	pNIC28-Bsa4	TEV protease	N-terminal His-Tag	
STK24	STK24A-c019	STE	R4	D301	pNIC-CH	none	C-terminal His Tag	
STK38L	STK38LA-c006	AGC	E76	N410	pNIC28-Bsa4	TEV protease	N-terminal His-Tag	
STK39	STK39A-c006	STE	A53	P357	pLIC-SGC1	TEV protease	N-terminal His Tag	
STK3	STK3A-c013	STE	S18	H302	pNIC28-Bsa4	TEV protease	N-terminal His-Tag	D47V
STK4	STK4A-cf001	STE	M1	E311	pNIC28-Bsa4	TEV protease	N-terminal His-Tag	
AURKA	STK6A-c001	Other	E122	S403	pETM-11	TEV protease	N-terminal His-Tag	
TAF1	TAF1A-c005	Bromodomain	D1522	D1656	pNIC28-Bsa4	TEV protease	N-terminal His-Tag	
PBK	TOPKA-c066	other	S32	N302	pNIC28-Bsa4	TEV protease	N-terminal His-Tag	
TTK	TTKA-c013	Other	S519	E808	pNIC28-Bsa4	TEV protease	N-terminal His-Tag	
ULK1	ULK1A-c900	Other	M1	S283	pET47b	SUMO	N-terminal His-tag	
ULK3	ULK3A-c900	Other	A2	Y204	pET28a	Thrombin	N-terminal His Tag and C-terminal His Tag	
VRK1	VRK1A-c025	CK1	R3	G347	pNIC-H102	TEV protease	N-terminal His10	
WNK1	WNK1A-c003	other	Q194	E488	pNIC28-Bsa4	TEV protease	N-terminal His-Tag	
PDK4	PDK4A-c017	atypical	G16	E401	pNIC28-Bsa4	TEV protease	N-terminal His-Tag	
MAPK15	MAPK15HSD-cf009	CMGC	V5	N414	pNIC28-Bsa4	TEV protease	N-terminal His-Tag	
TLK1	TLK1A-c010	other	D448	N746	pNIC28-Bsa4	TEV protease	N-terminal His-Tag	
MAPKAPK2	MAPKAPK2A-cf002	CAMK	H47	K353	pNIC28-Bsa4	TEV protease	N-terminal His-Tag	

SI Table 2 | List of all cellular target engagement NanoBRET assays.

Kinase	Reported Assay Quality	Family	NanoLuc Fusion Catalog #	Preferred Nluc Orientation	Recommended TE Tracer ADH Format	Recommended [Tracer] ADH Format
AAK1	High	Other	NV1001	N	K10	0.063
ABL1	Medium	TK	NV1011	N	K4	0.13
ABL1(E255K)	Medium	TK	NV2251	N	K4	0.25
ABL1(F317I)	Medium	TK	NV2261	N	K4	0.25
ABL1(F317L)	Medium	TK	NV2271	N	K4	0.13
ABL1(H396P)	High	TK	NV2281	N	K4	0.063
ABL1(M351T)	High	TK	NV2291	N	K4	0.13
ABL1(Q252H)	High	TK	NV2301	N	K4	0.13
ABL1(Y253F)	High	TK	NV2311	N	K4	0.13
ABL2	High	TK	NV2331	N	K4	0.016
ACVR1	High	RTKL	NV2341	C	K11	0.078
ACVR1(G328V)	High	RTKL	NV2351	C	K11	0.16
ACVR1(G356D)	High	RTKL	NV2361	C	K11	0.31
ACVR1(Q207D)	High	RTKL	NV2371	C	K11	0.16
ACVR1(R206H)	High	RTKL	NV2381	C	K11	0.16
ACVR2A	Medium	RTKL		C	lead discovered	1
ACVR2B	Medium	RTKL		C	lead discovered	1
ACVRL1	High	RTKL	NV2391	C	K11	0.31
ADK	Medium		NV2401	C	K8	0.5
AKT1	Medium	AGC	NV2411	C	K10	1
AKT1(E17K)	Medium	AGC	NV2421	C	K10	0.5
AKT2	Medium	AGC	NV1031	C	K10	0.5
AKT2(E17K)	Medium	AGC	NV2431	C	K10	0.25
ALK	Medium	RTK		C	K15	0.13
ALK(C1156Y)	Medium	RTK		C	K15	0.13
ALK(L1196M)	Medium	RTK		C	K15	0.13
AURKA	High	Other	NV1041	C	K10	0.0078

AURKB	High	Other	NV1051	C	K10	0.0078
AURKC	High	Other	NV1061	C	K10	0.016
AXL	High	RTK	NV1071	C	K10	0.25
AXL(R492C)	Medium	RTK		C	K10	0.25
BLK	High	TK	NV2461	N	K4	0.13
BMPR1A	Medium	RTKL	NV2471	C	K11	0.63
BMPR2	Low/Medium	RTKL		C	lead discovered	0.5
BMX	High	TK	NV1101	C	K4	0.13
BRAF	Low	TKL		C	K10	1
BRAF + KRAS(G12C)	Medium	TKL		C	K10	0.063
BRAF(V600E)	High	TKL	NV2481	C	K10	0.13
BRSK1	High		NV2491	N	K10	0.25
BRSK2	High	CAMK	NV1111	N	K10	0.5
BTK	High	TK	NV2501	C	K10	0.5
BTK(C481S)	Medium	TK	NV2501	C	K10	1
BTK(E41K)	High	TK	NV2511	C	K10	0.13
BTK(L528W)	High	TK		C	K10	0.13
BTK(M437R)	High	TK		C	K4	0.13
BTK(P190K)	High	TK	NV2521	C	K10	0.13
BTK(T474I)	Medium	TK		C	K10	0.25
BTK(V416L)	High	TK		C	K4	0.016
CAMK1	High	CAMK	NV2531	N	K9	0.66
CAMK1D	Medium	CAMK	NV2541	N	K9	0.33
CAMK1G	High		NV2551	N	K9	0.66
CAMK2A	High	CAMK	NV2561	N	K10	0.5
CAMK2B	High			N	K16	0.25
CAMK2D	High	CAMK	NV2571	N	K10	0.5
CAMK2G	Medium	CAMK	NV2581	C	K10	0.13
CASK	Low	CAMK		N	K10	1
CDC7	Medium			N	lead discovered	0.5
CDK1/Cyclin A2	Medium	CMGC	NV2701	C	K12	0.5

CDK1/Cyclin B1	Medium	CMGC	NV2701	C	K9	0.66
CDK1/Cyclin E1	High	CMGC	NV2701	C	K9	0.66
CDK14/Cyclin Y	Medium		NV2721	C	K10	0.5
CDK15/Cyclin Y	Medium		NV2731	N	K10	0.25
CDK16/Cyclin Y	High		NV2741	C	K10	0.5
CDK17/Cyclin Y	High		NV2751	C	K10	0.5
CDK19/Cyclin C	Medium	CMGC	NV2771	N	K8	0.13
CDK2/Cyclin A2	High	CMGC	NV2781	C	K10	0.5
CDK2/Cyclin B1	High	CMGC	NV2781	C	K10	0.5
CDK2/Cyclin D1	High	CMGC	NV2781	C	K10	0.5
CDK2/Cyclin E1	High	CMGC	NV2781	C	K10	0.5
CDK20/Cyclin H	High	CMGC	NV2791	N	K10	0.5
CDK3/Cyclin E1	High	CMGC	NV2801	C	K10	0.5
CDK3/Cyclin E2	Medium	CMGC	NV2801	C	K12	0.25
CDK4/Cyclin D1	High	CMGC	NV2811	N	K10	0.25
CDK4/Cyclin D3	High	CMGC	NV2811	N	K10	0.25
CDK5/CDK5R1	High	CMGC	NV1121	C	K10	0.5
CDK5/CDK5R2	High	CMGC	NV1121	C	K10	0.5
CDK6/Cyclin D1	Medium	CMGC	NV2841	N	K10	0.5
CDK6/Cyclin D3	Medium	CMGC	NV2841	N	K7	0.13
CDK7	High	CMGC	NV2851	N	K10	0.5
CDK8/Cyclin C	Medium	CMGC	NV2861	N	K8	0.13
CDK9/Cyclin T1	High	CMGC	NV2871	N	K8	0.063
CDKL2	High	CMGC	NV2891	N	K11	0.63
CDKL3	High	CMGC	NV2901	N	K11	0.16
CDKL5	High	CMGC	NV2911	N	K11	0.31
CHEK1	Medium	CAMKL	NV2921	N	K9	0.33
CHEK2	Medium		NV2931	C	K10	1
CIT	Low			N	K9	1
CLK1	High	CMGC	NV1131	N	K10	0.25
CLK2	High	CMGC	NV1141	C	K9	0.33

CLK4	High	CMCG	NV1151	C	K9	0.17
COQ8A	Medium			N	lead discovered	1
COQ8B	High		NV2941	N	K10	0.5
CRAF	Low	TKL			K4	1
CRAF + KRAS(G12C)	Medium	TKL			K4	1
CSF1R	Medium	RTK	NV1161	C	K4	0.13
CSK	High	TK	NV1171	C	K4	0.25
CSNK1A1L	Medium	CK1	NV2951	N	K10	0.5
CSNK1D	High	CK1	NV2961	N	K8	0.13
CSNK1E	Medium	CK1	NV2971	N	K8	0.5
CSNK1G2	Medium	CK1	NV1181	N	K10	0.5
CSNK2A1	Medium	CMGC	NV2981	C	K10	0.5
CSNK2A2	High	CMGC	NV1191	C	K10	0.25
DAPK2	Medium	CAMK	NV2991	N	K10	0.5
DCLK1	High	CAMK		C	K15	0.5
DCLK1 isoform 2	High	CAMK		C	K15	0.5
DCLK3	Medium	CAMK	NV3001	C	K10	1
DDR1	High	RTK	N2451	C	K4	0.031
DDR2	High	RTK	NV1201	C	K4	0.063
DDR2(N456S)	High	RTK	NV3011	C	K4	0.063
DYRK1A	Medium	CMGC	NV3031	N	K10	0.5
DYRK1B	Medium	CMGC	NV1211	N	K10	0.5
DYRK2	Medium	CMGC	NV3041	C	K10	1
DYRK3	Low			C	K10, lead discovered	1
EGFR	medium	RTK		C	lead discovered	0.5
EGFR(D770,N771 insSVD)	low	RTK		C	lead discovered	0.5
EGFR(V769,D770 insASV)	low	RTK		C	lead discovered	0.5
EIF2AK4(Dom.2)	High	Other	NV3051	N	K10	0.5
EML4-ALK	Medium			C	K15	0.13
EPHA1	High	RTK	NV1221	C	K4	0.13
EPHA10	High	RTK		C	K4	0.063

EPHA2	High	RTK	NV1231	C	K4	0.031
EPHA3	Medium	RTK	NV3061	C	K11	0.63
EPHA4	High	RTK	NV1241	C	K4	0.016
EPHA7	High	RTK	NV1271	C	K10	0.5
EPHA8	High	RTK	NV1281	C	K4	0.0063
EPHB1	High	RTK	NV3071	C	K9	0.66
EPHB2	High	RTK	NV1291	C	K4	0.013
EPHB3	High	RTK	NV1301	C	K4	0.13
EPHB4	High	RTK	NV1311	C	K4	0.0063
ERN1	Medium	Other	NV1321	C	K10	0.25
ERN2	High		NV3081	C	K10	0.25
FER	Medium	TK	NV1331	C	K10	0.5
FES	High	TK	NV3091	C	K9	0.66
FGFR1	High	RTK	NV1341	C	K10	0.25
FGFR2	Medium	RTK	NV1351	C	K10	0.13
FGFR2(K659M)	High	RTK		C	K10	0.25
FGFR2(L617F)	Medium	RTK		C	K10	0.25
FGFR2(L617V)	High	RTK		C	K10	0.25
FGFR2(M537I)	High	RTK		C	K10	0.13
FGFR2(N549H)	High	RTK		C	K10	0.25
FGFR2(N549K)	Medium	RTK		C	K10	0.25
FGFR2(V564F)	High	RTK		C	K10	0.13
FGFR4	Medium	RTK	NV1371	C	K10	0.5
FGR	High	TK	NV1381	N	K4	0.25
FLT1	Medium	RTK	NV3111	C	K9	0.33
FLT3	Medium	RTK	NV1391	C	K10	0.13
FLT3(D835H)	Medium	RTK	NV3121	C	K10	0.016
FLT3(D835V)	High	RTK	NV3131	C	K10	0.016
FLT3(D835Y)	High	RTK	NV3141	C	K10	0.016
FLT3(K663Q)	High	RTK	NV3151	C	K9	0.041
FLT3(N841I)	High	RTK	NV3161	C	K10	0.063

9. Appendix

FLT3(R834Q)	Medium	RTK	NV3171	C	K10	0.063
FRK	Medium	TK	NV1401	C	K4	0.13
FYN	High	TK	NV1411	C	K4	0.13
FYN(Y531F)	High	TK	NV3181	C	K4	0.016
GAK	High	Other	NV1421	N	K10	0.031
GRK1	Medium	AGC		N	K16	0.5
GRK7	Medium	AGC		N	K16	0.13
GSK3A	High	CMGC	NV3191	N	K8	0.13
GSK3B	High	CMGC	NV3201	N	K8	0.063
HCK	Medium	TK	NV3211	C	K4	0.25
HIPK2	Medium	CMGC	NV3221	N	K10	1
HIPK3	Medium	CMGC	NV3231	N	K10	1
HIPK4	High		NV3241	N	K10	0.25
HUNK	Low	CAMK		N	K10	1
ICK	High	CMGC	NV3251	N	K8	0.25
IGF1R	High	RTK	NV3261	C	K9	0.33
IKBKE	High	Other	NV1431	N	K10	0.25
INSR	High	RTK	NV3271	C	K9	0.33
IRAK1	Medium		NV3281	N	K9	0.66
IRAK3	High	TKL	NV1441	N	K10	0.032
IRAK4	High	TKL	NV1451	C	K10	0.13
ITK	High	TK	NV1461	N	K10	0.25
JAK1	Low	TK		C	K10	0.25
JAK1_JH1 Domain	High	TK		N	K10	0.25
JAK2	Medium	TK	NV3291	C	K10	1
JAK2(JH1 Domain)	Medium	TK	NV3311	N	K10	0.25
JAK2(V617F)	High	TK	NV3301	C	K10	0.25
JAK3	Medium	TK	NV1471	C	K10	0.25
JNK3	Medium	CMGC	NV1481	C	K10	0.25
KDR	Low	RTK		C	K9	0.5
Kit	Medium	RTK	NV1491	C	K4	0.063

KIT(A829P)	Medium	RTK	NV3321	C	K4	0.25
KIT(D816H)	Medium	RTK	NV3331	C	K4	0.5
KIT(D816V)	High	RTK	NV3341	C	K9	0.33
KIT(L576P)	High	RTK	NV3351	C	K4	0.13
KIT(V559D)	High	RTK	NV3361	C	K4	0.031
KIT(V559D,T670I)	Medium	RTK	NV3371	C	K8	0.13
KIT(V559D,V654A)	Medium	RTK	NV3381	C	K4	0.5
LATS1	High	AGC	NV1501	C	K10	0.13
LATS2	High	AGC	NV1511	C	K10	0.016
LCK	High	TK	NV1521	C	K4	0.031
LIMK1	High	TKL	NV3391	C	K10	0.5
LIMK2	High	TKL	NV1531	C	K10	0.5
LRRK2	High	TKL	NV3401	C	K9	0.0083
LRRK2(G2019S)	Medium	TKL	NV3421	C	K9	0.0083
LRRK2(I2020T)	High	TKL	NV3411	C	K9	0.031
LRRK2(R1441C)	Medium	TKL	NV3431	C	K9	0.0039
LTK	High	RTK	NV1541	C	K9	0.33
LYN	High	TK	NV1551	C	K4	0.031
MAP2K1 + KRAS(G12C)	Low	STE		C	K10	0.5
MAP2K2 + KRAS(G12C)	Low	STE		C	K10	0.5
MAP2K5	Low/Medium	STE		C	K10	0.5
MAP2K6	Medium	STE	NV3441	C	K11	0.63
MAP3K10	High	TKL	NV1561	N	K10	0.5
MAP3K11	High	TKL	NV1571	N	K10	0.25
MAP3K12	High	TKL	NV1581	N	K9	0.66
MAP3K13	Medium	TKL	NV3451	N	K9	0.17
MAP3K19	Medium	STE	NV3461	C	K10	0.13
MAP3K2	Medium	STE	NV3471	C	K10	0.5
MAP3K21	Medium		NV3481	N	K10	0.5
MAP3K3	Medium	STE	NV3491	C	K10	0.5
MAP3K4	High	STE	NV1591	C	K10	0.5

MAP3K5	High	STE		C	lead discovered	0.5
MAP3K9	Medium	TKL	NV1601	N	K10	0.25
MAP4K1	High	STE	NV1611	N	K10	0.5
MAP4K2	High	STE	NV1621	N	K10	0.063
MAP4K3	High	STE	NV1631	N	K10	0.5
MAP4K5	Medium	STE	NV3501	C	K10	1
MAPK1	Low	CMGC	NV1641	N	K10	1
MAPK1 + KRAS(G12C)	High	CMGC	NV1641	N	K10	0.5
MAPK11	High	CMGC	NV1651	N	K4	0.13
MAPK13	Medium	CMGC		C	lead discovered	0.5
MAPK14	High	CMGC	NV1661	C	K4	0.031
MAPK14(T106M)	High	CMGC	NV3511	C	K10	0.25
MAPK15	High	CMGC		N	K10	0.0078
MAPK3 + KRAS(G12C)	Medium	CMGC	NV1671	N	K10	0.5
MAPK4	High	CMGC	NV1681	N	K10	0.031
MAPK6	High	CMGC	NV1691	N	K10	0.0078
MAPK7(1-713)	High	CMGC		N	K10	0.5
MAPK8	High	CMGC	NV1701	N	K10	0.13
MAPK9	High	CMGC	NV1711	N	K10	0.13
MARK2	High	CAMK	NV1721	N	K9	0.33
MARK3	Medium	CAMK	NV3521	N	K9	0.33
MARK4	High	CAMK	NV1731	N	K10	0.13
MAST3	Medium	AGC	NV3531	N	K10	1
MELK	High	CAMK	NV1741	N	K9	0.66
MELK(T460M)	High	CAMK	NV3551	N	K9	0.5
MERTK	Medium	RTK	NV3561	C	K9	0.17
MERTK(A708S)	Medium	RTK	NV3571	C	K9	0.25
MET	High	RTK	NV1751	C	K10	0.25
MET(D1228H)	High	RTK	NV3691	C	K10	0.25
MET(D1228N)	High	RTK	NV3681	C	K10	0.25
MET(F1200I)	High	RTK	NV3701	C	K10	0.25

MET(M1250T)	High	RTK	NV3581	C	K10	0.25
MET(P991S)	High	RTK	NV3601	C	K10	0.25
MET(T1173I)	High	RTK	NV3621	C	K10	0.25
MET(T992I)	High	RTK	NV3611	C	K10	0.25
MET(V1092I)	High	RTK	NV3631	C	K10	0.25
MET(Y1230A)	High	RTK	NV3641	C	K10	0.25
MET(Y1230C)	High	RTK	NV3651	C	K10	0.25
MET(Y1230D)	High	RTK	NV3661	C	K10	0.25
MET(Y1230H)	High	RTK	NV3671	C	K10	0.25
MET(Y1235D)	Medium	RTK	NV3591	C	K10	0.5
MKNK1	Medium	CAMK		N	lead discovered	
MKNK2	Medium		NV3711	N	K10	0.5
MLTK	Medium	TKL	NV3721	N	K10	0.25
MOK	High		NV3731	N	K10	0.5
MUSK	High	RTK	NV1761	C	K10	0.25
MYLK2	High	CAMK	NV1771	C	K10	0.13
MYLK3	High		NV3741	C	K10	0.5
MYLK4	High		NV3751	C	K10	0.13
NEK1	High	Other	NV3761	N	K10	0.5
NEK11	High	Other	NV3771	N	K10	0.5
NEK2	Medium	Other	NV1781	N	K10	0.5
NEK3	High	Other	NV1791	N	K10	0.25
NEK4	Medium		NV3781	N	K10	0.5
NEK5	High	Other	NV3791	N	K10	0.063
NEK6	High	Other	NV3801	C	K9	0.17
NEK9	High	Other	NV1801	N	K10	0.5
NIM1K	High	CAMK	NV3811	C	K10	0.5
NPM1-ALK	Medium			C	K15	0.063
NRK	Medium		NV3831	N	K11	0.32
NTRK1	High	RTK	NV1811	C	K10	0.13
NTRK1(G667C)	High	RTK	NV3841	C	K10	0.13

NTRK2	High	RTK	NV1821	C	K10	0.25
NUAK1	High	CAMK	NV1831	N	K10	0.063
NUAK2	Medium	CAMK	NV3851	C	K10	0.25
PAK4	High	STE	NV1841	C	K10	0.5
PAK6	High	STE	NV3861	C	K10	0.5
PDGFRA(V561D)	Medium	RTK	NV3871	C	K4	0.13
PDPK1	Medium	AGC		C	K16	0.25
PHKG1	High	CAMK	NV1861	N	K10	0.25
PHKG2	Medium	CAMK	NV3881	N	K10	0.5
PI4KA	High			C	K17	0.13
PI4KB	Medium			C	K17	0.13
PIK3C3	Medium		NV3891	C	K9	0.33
PIK3CA	High	Atypical	NV3901	N	K3	0.016
PIK3CA(C420R)	High	Atypical	NV3911	N	K3	0.031
PIK3CA(E542K)	Medium	Atypical	NV3921	N	K3	0.031
PIK3CA(E545A)	High	Atypical	NV3931	N	K3	0.031
PIK3CA(E545K)	High	Atypical	NV3941	N	K3	0.031
PIK3CA(H1047L)	High	Atypical	NV3951	N	K3	0.031
PIK3CA(H1047R)	High	Atypical	NV3961	N	K3	0.031
PIK3CA(H1047Y)	High	Atypical	NV3971	N	K3	0.031
PIK3CA(I800L)	High	Atypical	NV3981	N	K3	0.063
PIK3CA(M1043I)	High	Atypical	NV3991	N	K3	0.063
PIK3CA(Q546K)	High	Atypical	NV4001	N	K3	0.031
PIK3CB	High	Atypical	NV4011	N	K3	0.13
PIK3CD	High	Atypical	NV4021	N	K3	0.13
PIK3CG	Low/Medium	Atypical		C	K3	0.5
PIKFYVE	Medium		NV4041	C	K8	0.13
PIM3	Medium	CAMK	NV4051	N	K10	1
PIP4K2C	High		NV4061	C	K8	0.063
PIP5K1B	Medium		NV4071	N	K8	0.25
PKMYT1	Medium	Other	NV1871	C	K10	1

PKN1	Medium	AGC		C	K16	0.13
PKN2	Medium	AGC		C	K16	0.25
PLK1	Medium	Other		N	K18	0.25
PLK2	High	Other	NV4081	N	K9	0.17
PLK3	High	Other	NV4091	N	K9	0.33
PLK4	High	OTHER	NV1881	N	K10	0.25
PNCK	Low			C	K10	1
PRKAA1	High	CAMK	NV4101	N	K10	0.13
PRKAA2	High	CAMK	NV1891	N	K10	0.063
PRKACA	High	AGC	NV1901	C	K10	0.5
PRKACB	Medium	AGC	NV4111	C	K10	0.25
PRKCa + PMA stim	High	AGC		C	K10, lead discovered	0.5
PRKCB + PMA stim	High			C	K10, lead discovered	0.5
PRKCD + PMA stim	High	AGC		C	K10, lead discovered	0.5
PRKCE	Medium	AGC	NV4121	C	K10	0.5
PRKCE + PMA stim	High	AGC	NV4121	C	K10, lead discovered	0.5
PRKCG + PMA stim	High			C	K10, lead discovered	0.5
PRKCH + PMA stim	Low	AGC		C	K10, lead discovered	0.5
PRKCQ + PMA stim	High	AGC		C	K10, lead discovered	0.5
PRKG2	High	AGC	NV4131	C	K9	0.66
PRKX	High	AGC	NV1911	C	K10	0.25
PTK2	High	TK	NV1921	N	K10	0.25
PTK2B	Medium	TK	NV1931	C	K10	0.25
PTK6	High	TK	NV1941	C	K4	0.25
RET	High	RTK	NV1951	C	K10	0.13
RET(M918T)	High	RTK	NV4141	C	K10	0.25
RET(V804L)	High	RTK	NV4151	C	K10	0.13
RET(V804M)	High	RTK	NV4161	C	K10	0.13
RIOK2	High	Atypical	NV1961	N	K10	0.5
RIPK1	High	TKL	NV4171	N	K9	0.25
RIPK2	High	TKL	NV1971	N	K10	0.13

RIPK3	Medium	TKL		N	K19	1
ROCK1	High	AGC		N	K16	0.25
ROCK2	High	AGC		N	K16	0.25
RON	High	RTK	NV4181	C	K9	0.66
ROS1	Low			C	K9	1
ROS1(1883-2347)	High			N	K9	0.25
RPS6KA1	High	AGC	NV1981	N	K10	0.063
RPS6KA2	High	AGC	NV1991	N	K10	0.13
RPS6KA4	High	AGC	NV2011	N	K10	0.063
RPS6KA6	High	AGC	NV2021	N	K10	0.13
RPS6KB1	Medium	AGC		N	K10	0.25
RPS6KB1 + KRAS2B(G12C)	Medium	AGC		N	K10	0.25
SBK3	High		NV4211	N	K10	0.5
SGK1	High	AGC	NV4221	C	K10	0.5
SGK2	Medium	AGC	NV4231	C	K9	0.66
SGK3	Low/Medium	AGC		N	K10	1
SIK1	High	CAMK	NV2031	N	K10	0.063
SLK	Medium	STE	NV2051	N	K10	1
SNF1LK2	High	CAMK	NV2061	N	K10	0.063
SNRK	High	CAMK	NV4241	N	K10	0.5
SRC	High	TK	NV2071	C	K4	0.063
SRMS	Medium	TK	NV4251	N	K10	1
STK10	High	STE	NV4261	N	K10	0.5
STK11	High	CAMK	NV2081	N	K10	0.5
STK16	High	Other	NV2091	N	K10	0.063
STK17B	High	CAMK	NV4271	C	K9	0.66
STK24	High	STE	NV4281	C	K9	0.66
STK26	High		NV4291	C	K9	0.66
STK3	Medium	STE	NV4301	N	K10	0.25
STK32A	Medium	AGC	NV4311	N	K9	0.66
STK32B	High	AGC	NV2101	N	K9	0.66

STK33	Medium	CAMK	NV2111	N	K10	0.5
STK35	High		NV4321	C	K10	0.25
STK38	High	AGC	NV2121	C	K10	0.5
STK38L	High	AGC	NV4341	C	K10	0.5
STK4	High	STE	NV4351	N	K10	0.25
TBK1	High	Other	NV2131	N	K10	0.13
TEC	High	TK	NV2141	N	K4	0.5
TEK	High	RTK	NV2151	C	K10	0.13
TEK(A1124V)	High	RTK	NV4361	C	K10	0.25
TEK(P883A)	High	RTK	NV4371	C	K10	0.25
TEK(R849W)	High	RTK	NV4381	C	K10	0.25
TEK(Y1108F)	High	RTK	NV4391	C	K10	0.25
TEK(Y897C)	High	RTK	NV4401	C	K10	0.25
TEK(Y897S)	High	RTK	NV4411	C	K10	0.25
TESK1	Medium	TKL	NV2161	N	K4	0.5
TGFBR1	Medium	RTKL		C	K14	0.5
TGFBR2	High	RTKL	NV4421	C	K11	0.32
TIE1	High	RTK	NV2171	C	K10	0.25
TLK1	Medium	Other	NV4431	C	K10	0.5
TLK2	High	Other	NV4441	C	K10	0.5
TNIK	Low			N	K16	0.25
TNIK + KRAS2B(G12C)	Medium			N	K16	0.25
TNK1	High	TK	NV2181	N	K10	0.031
TNNI3K	High		NV4461	C	K10	0.5
TSSK1B	Medium	CAMK	NV4471	N	K9	0.66
TTK	High	Other	NV2191	C	K9	0.66
TXK	High	TK	NV2201	C	K4	0.13
TYK2(JH2 Domain)	High		NV4531	C	K10	0.5
TYRO3	Medium	RTK	NV4481	C	K10	0.5
UHMK1	Low			N	K10	1
ULK1	High	Other	NV2211	N	K10	0.13

ULK3v1	High	Other	NV4491	N	K10	0.25
WEE1	High	Other	NV2231	C	K10	0.13
WEE2	Medium	Other	NV4501	N	K10	0.5
YES1	Medium	TK	NV2241	C	K4	0.063

SI tables to chapter 5.2 Family selectivity of small molecule chemogenomics candidate for splicing kinase family

SI Table 3 | Chemogenomic candidates for splicing kinase family.

Compound	Intended Target	SMILES	CAS	Supplier
SRPIN340	SRPK1, MSSK1; SRPK2	<chem>O=C(Nc1cc(C(F)(F)F)ccc1N1CCCCC1)c1ccncc1</chem>	218156-96-8	Cayman Chemical, Cat. No. 16284
SRPKIN-1	SRPK1, SRPK2	<chem>CCc1cc2c(cc1-c1cccc(S(=O)(=O)F)c1)C(C)(C)1[nH]c3cc(C#N)ccc3c1C2=O</chem>	2089226-94-6	MedChemExpress, Cat. No. HY-116856
SPHINX31	SRPK1, MSSK1; SRPK2, CLK1, CLK2	<chem>O=C(Nc1cc(C(F)(F)F)ccc1N1CCN(Cc2cccn2)CC1)c1ccc(-c2ccncc2)o1</chem>	1818389-84-2	Cayman Chemical, Cat. No. 21582
MSC2711186A	SRPK1, SRPK2, SRPK3 (MSSK1)	<chem>CN(c1cccc1CNc1cccc(-c2nc3c(F)c(Cl)ccc3[nH]2)c1)S(C)(=O)=O</chem>		SGC Frankfurt, inhouse/ Merck
GSK 626616	DYRK1A, DYRK1B; DYRK3	<chem>O=C(N=C(NC1=C(Cl)C=CC=C1Cl)S/2)C2=C\C3=CC=C(N=CC=N4)C4=C3</chem>	1025821-33-3	Tocis, Cat. No. 6638
GW779439X	CLKs, DYRKs, HIPKs, others	<chem>CN1CCN(c2ccc(Nc3nccc(-c4cnn5ncccc45)n3)cc2C(F)(F)F)CC1</chem>	551919-98-3	MedChemExpress, Cat. No. HY-103645
MU135	HIPK2	<chem>CC(C)(C)c1ccc(-c2coc3ccc(-c4cn[nH]c4)nc23)cc1</chem>		
HY-U00439A/CVM-6-139-1	HIPK1, HIPK2	<chem>O=C(O)C(F)(F)F.O=C1NC(=O)/C(=C/c2c[nH]c(=O)c(-c3ccc(N4CCNCC4)nc3)c2)S1</chem>	2321337-71-5	MedChemExpress, Cat. No. HY-U00439A
T3-CLK	CLK1, CLK2, CLK3, CLK4	<chem>CN1CCN(C(=O)C(C)(C)c2ccc(C(=O)Nc3cn4cc(-c5cncnc5)ccc4n3)cc2)CC1</chem>		SGC Frankfurt, inhouse
SGC-CLK-1	CLK1, CLK2, CLK4	<chem>COc1cc(Nc2nccc(-c3cnn4nc(OC)ccc34)n2)cc(C(F)(F)F)c1</chem>		SGC Frankfurt, inhouse
MU1210	CLK1, CLK2, CLK4	<chem>Cn1cc(-c2ccc3occ(-c4cccc(-c5cncnc5)c4)c3n2)cn1</chem>		SGC Frankfurt, inhouse
T025	CLK1, CLK2, CLK3, CLK4, DYRK1A/B/2, HIPK1/2/3	<chem>CNc1nc(NCc2nccn2)c2c(-c3ccc4ncccc4c3)c[nH]c2n1</chem>	2407433-00-3	MedChemExpress, Cat. No. HY-112296
GNF4877	DYRK1A, DYRK1B, GSK3	<chem>CC(C)Oc1ccc(F)c(-c2cnc(N)c(C(=O)Nc3cncnc3N3CCC[C@@H](C(=O)O)C3)n2)c1</chem>	2041073-22-5	MedChemExpress, Cat. No. HY-129492

MIRK-IN-1	DYRK1A, DYRK1B	<chem>COc1ncc2cc(C(=O)Nc3cc(C(=O)Nc4cccc(Cl)c4)ccc3Cl)c(=O)[nH]c2n1</chem>	1386979-55-0	MedChemExpress, Cat. No. HY-12838
Lorecivivint (Adavivint, SM04690)	DYRK1A, DYRK1B, CLK2, CLK1, CLK3, HIPK1/3	<chem>CC(C)CC(=O)Nc1cncc(-c2ccc3[nH]nc(-c4nc5cncc(-c6cccc(F)c6)c5[nH]4)c3c2)c1</chem>	1467093-03-3	MedChemExpress, Cat. No. HY-109049
KH-CB19	CLK1, CLK2, CLK3, CLK4, DYRK1A, DYRK1B	<chem>CCOC(=O)c1c/C(C#N)=C\N)c2ccc(Cl)c(Cl)c2n1C</chem>	1354037-26-5	MedChemExpress, Cat. No. HY-12828
CC-671	CLK2 (+CLK4? unknown)	<chem>CNC(=O)c1ccc(Nc2nc(OC3CCCC3)c3c(-c4ccc5nc(C)oc5c4)c[nH]c3n2)c(OC)c1</chem>	1618658-88-0	Cayman Chemical, Cat. No. 26184
Leucettine L41	DYRK1A, DYRK1B, CLK1, CLK4, DYRK2	<chem>O=C1N=C(Nc2cccc2)N/C1=C\c1ccc2c(c1)OC2</chem>	1112978-84-3	Cayman Chemical, Cat. No. 29225
EHT1610	DYRK1A, DYRK1B	<chem>COC(=N)c1nc2ccc3ncnc(Nc4ccc(OC)cc4F)c3c2s1</chem>	1425945-60-3	MedChem Express, Cat. No. HY-111380
(Pro)INDY	CLK1, CLK2, CLK3, CLK4, DYRK1A, DYRK1B	<chem>CCN1/C(=C/C(C)=O)Sc2ccc(OC(C)=O)cc21</chem>	719277-30-2	Tocris, Cat. No. 4998
AZ191	DYRK1B	<chem>COc1cc(N2CCN(C)CC2)ccc1Nc1nccc(-c2cn(C)c3cnccc23)n1</chem>	1594092-37-1	Tocris, Cat. No. 5232
KuWAL151	CLK1, CLK2, CLK3, CLK4	<chem>O=C1NCc2ccc3c(-c4cccc(Cl)c4)c[nH]c3c21</chem>		Conrad Kunick, TU-Braunschweig
Compound 5j/KuFal194	DYRK1A, DYRK1B	<chem>O=C(O)c1nc2cccc2c2[nH]c3c(l)cccc3c12</chem>		Conrad Kunick, TU-Braunschweig
TG003	CLK1, CLK2, CLK3, CLK4, DYRK1A, DYRK1B	<chem>C(=CC(=C1N(C2=CC(=O)C)CC)S2)C(=C1)OC</chem>	300801-52-9	Cayman Chemical, Cat. No. 10398
SRI-29329	CLK1, CLK2, CLK4	<chem>CC(C)n1cnc2c(Nc3cccc(Cl)c3)nc(N[C@H]3CCCC[C@H]3N)nc21</chem>	2086809-58-5	MedChemExpress, Cat. No. HY-123600
LDN-192960	DYRK2, DYRK1A, DYRK1B, DYRK3, CLK1-4	<chem>COc1ccc2nc3ccc(OC)cc3c(SCCCN)c2c1.Cl</chem>	184582-62-5	MedChemExpress, Cat. No. HY-13455
Compound 25/Suns Inhibitor	DYRK1A, DYRK1B, CLK1, CLK4	<chem>C[C@H](c1ccc(F)cc1)n1nnc2cnc3ccc(-c4ccc5ocnc5c4)cc3c21</chem>		resynthesized by Jonathan Morris
ML167	CLK4	<chem>CC1=CC=C(O1)CNC2=NC=NC3=C2C=C(C=C3)C4=CC=C(O4)CO</chem>	1285702-20-6	Cayman Chemical, Cat. No. 18098
ID-8	DYRK1A, DYRK1B (maybe CLKs)	<chem>CC2=C([N+](O-))C1=CC=C(O)C=C1N2C3=CC=C(OC)C=C3</chem>	147591-46-6	Tocris, Cat. No. 3853
SGC-CLK-1N	NC	<chem>CCOc1ccc2c(-c3cc(C)nc(Nc4cc(OC)cc(C(F)F)c4)n3)cnn2n1</chem>		SGC Frankfurt, inhouse
MU140	NC	<chem>Cn1cc(-c2ccc3oc(-c4cccc4-c4cccc4)c3n2)cn1</chem>		SGC Frankfurt, inhouse
T3-CLKN	NC	<chem>CN1CCN(C(=O)C(C)C)c2ccc(C(=O)Nc3cn4cc(-c5cc(C(C)C)cc(C(C)C)c5)ccc4n3)cc2)CC1</chem>		SGC Frankfurt, inhouse
MSC2705360A	NC	<chem>CN(c1cccc1CNc1ccc(-c2cc3cc(Cl)ccc3[nH]2)c1)S(C(=O)=O)=O</chem>		SGC Frankfurt, inhouse

CVM-6-139-1		19/9*		62		74, 9.5*		S(10) 0.16					
SPRK	SRPIN340	>10000	>10000	>10000	>10000	>10000	>10000	>10000	>10000	83, 2358	1510, 2560	27, 393	0/141 (10 μ M, >90%)
	MSC2711186	>10000	>10000	>10000	>10000	>10000	>10000	>10000	>10000	3, 98	81, 149	1, 40	0
	SPHINX31	839	5700	>10000	266	1580	1840	>10000	>10000	17, 60	256, 648	166, 6149	0/58 (Tm, 10 μ M, > 2°)
	SRPKIN-1	422	920	>10000	159	225	293	5720	6780	2	3	5	0/>400 (5 μ M, > 90 %)

SI Table 5 | Screening of SGC library splicing kinase family. Follow up NanoBRET dose response EC₅₀ (M) of identified hit compounds. n.d. = not determined

	lysed	lysed	lysed	lysed	intact
	SRPK3	HIPK4	DYRK3	CLK1	CLK1
KF01145a	2.47E-05	n.d.	1.02E-05	5.86E-10	5.50E-10
KF01021a	6.72E-06	1.59E-07	3.98E-07	4.87E-10	6.58E-10
PK008310bCL	> 50 μ M	5.64E-08	> 50 μ M	1.49E-09	2.10E-09
KF01353a	7.87E-08	4.47E-08	1.70E-06	3.25E-09	3.91E-09
LENA159	n.d.	1.41E-07	4.27E-07	1.62E-08	7.55E-09
KF01037a	7.99E-07	> 50 μ M	4.32E-07	3.50E-09	8.07E-09
KF01038a	6.13E-07	7.40E-07	3.55E-07	1.71E-08	1.53E-08
LENA158	n.d.	5.73E-07	n.d.	1.43E-08	1.75E-08
KF01406a	n.d.	n.d.	n.d.	4.04E-08	2.66E-08
KF01516a	1.96E-05	2.88E-08	1.08E-08	3.14E-08	3.41E-08
LENA143	1.07E-06	6.72E-07	5.98E-07	2.82E-08	3.69E-08
KF01351a	n.d.	2.80E-08	6.17E-06	2.58E-08	3.70E-08
KF01046a	1.09E-06	7.02E-07	> 50 μ M	6.30E-08	4.46E-08
KF01210a	1.22E-05	n.d.	2.02E-05	2.14E-08	4.57E-08
KF01148a	n.d.	n.d.	4.57E-06	1.73E-07	5.73E-08

LENA127	> 50 μ M	n.d.	1.86E-06	1.45E-07	7.47E-08
KF01364a	n.d.	n.d.	7.66E-06	1.05E-07	8.63E-08
LENA83	n.d.	1.44E-07	2.89E-05	2.07E-08	9.47E-08
KF01428a	n.d.	n.d.	n.d.	1.63E-07	9.73E-08
PK007133e	n.d.	n.d.	n.d.	1.74E-07	1.06E-07
LENA174	n.d.	n.d.	n.d.	7.51E-08	1.13E-07
KF01497a	n.d.	n.d.	n.d.	1.50E-07	1.32E-07
KF01346a	4.38E-05	4.98E-07	> 50 μ M	1.59E-07	1.36E-07
PK016528a	n.d.	n.d.	n.d.	2.81E-07	1.37E-07
KF01445a	n.d.	n.d.	n.d.	1.37E-07	1.61E-07
KF01212a	n.d.	n.d.	n.d.	2.04E-07	1.66E-07
KF01188a	n.d.	n.d.	2.80E-05	1.19E-07	1.69E-07
KF01513a	n.d.	n.d.	n.d.	7.28E-07	1.74E-07
PK006169f	n.d.	n.d.	1.90E-05	8.21E-07	1.76E-07
KF01403a	n.d.	7.78E-07	n.d.	3.89E-07	1.77E-07
KF01382a	n.d.	n.d.	4.04E-05	3.41E-07	1.82E-07
PK006099c	n.d.	7.80E-07	n.d.	1.13E-07	1.86E-07
KF01538a	n.d.	n.d.	1.96E-06	9.11E-08	1.90E-07
KF01106a	n.d.	n.d.	n.d.	2.24E-07	2.01E-07
KF01138a	> 50 μ M	n.d.	n.d.	1.03E-07	2.02E-07
LENA168	n.d.	n.d.	n.d.	5.85E-07	2.20E-07
PK007313b	n.d.	n.d.	n.d.	1.68E-07	2.25E-07
LENA132	n.d.	1.07E-06	n.d.	1.64E-07	2.29E-07
KF01350a	n.d.	2.88E-08	1.16E-05	3.10E-07	2.35E-07
KF01042a	n.d.	n.d.	2.80E-06	3.52E-07	2.56E-07
ZZ000951a	> 50 μ M	n.d.	n.d.	2.07E-07	2.62E-07

KF01411a	n.d.	n.d.	n.d.	6.54E-07	2.87E-07
KF01122a	n.d.	n.d.	n.d.	3.72E-07	2.90E-07
KF01475a	n.d.	n.d.	n.d.	4.66E-07	2.95E-07
PK009758b	n.d.	n.d.	n.d.	3.46E-07	4.26E-07
KF01530a	n.d.	n.d.	n.d.	9.13E-07	4.73E-07
KF01087a	n.d.	1.13E-06	n.d.	5.08E-07	5.05E-07
LENA181	n.d.	n.d.	n.d.	6.47E-07	5.11E-07
KF01352a	n.d.	4.83E-08	4.98E-06	4.26E-07	5.32E-07
LENA22	n.d.	n.d.	n.d.	1.70E-06	5.63E-07
LENA42	n.d.	3.74E-07	n.d.	6.10E-07	5.66E-07
PK001363hCL	n.d.	n.d.	n.d.	4.32E-07	5.90E-07
LENA96	> 50 µM	n.d.	n.d.	1.13E-07	6.10E-07
PK010852b	n.d.	n.d.	n.d.	9.38E-07	6.18E-07
KF01540a	n.d.	n.d.	n.d.	1.92E-06	6.21E-07
LENA178	n.d.	2.32E-07	n.d.	1.13E-06	6.25E-07
LENA157	n.d.	7.13E-07	n.d.	6.17E-07	6.49E-07
LENA72	n.d.	n.d.	n.d.	1.41E-06	6.59E-07
KF01330a	n.d.	8.78E-07	n.d.	7.18E-07	6.67E-07
KF01401a	n.d.	2.15E-06	5.11E-06	9.81E-07	7.24E-07
KF01328a	n.d.	n.d.	n.d.	3.96E-07	7.41E-07
LENA94	n.d.	n.d.	n.d.	9.49E-07	9.02E-07
KF01503a	n.d.	n.d.	n.d.	4.87E-07	9.78E-07
KF01354a	n.d.	n.d.	n.d.	1.41E-06	1.03E-06
PK006016g	n.d.	n.d.	n.d.	9.26E-07	1.06E-06
LENA65	n.d.	n.d.	3.70E-05	2.82E-06	1.26E-06
KF01301a	n.d.	n.d.	n.d.	1.54E-06	1.27E-06

KF01529a	n.d.	n.d.	n.d.	1.16E-06	1.29E-06
LENA92	n.d.	n.d.	n.d.	1.20E-06	1.53E-06
LENA144	n.d.	n.d.	n.d.	2.54E-06	1.66E-06
LENA54	n.d.	1.29E-08	n.d.	1.38E-06	1.73E-06
LENA103	n.d.	n.d.	n.d.	1.68E-06	1.98E-06
LENA162	n.d.	n.d.	n.d.	2.46E-06	2.29E-06
KF01543a	n.d.	n.d.	n.d.	2.99E-06	2.59E-06
LENA136	n.d.	n.d.	n.d.	8.20E-06	4.04E-06
KF01142a	5.39E-06	8.78E-07	6.50E-06	1.34E-06	4.42E-06
KF01271a	n.d.	n.d.	n.d.	8.37E-06	1.05E-05
PK016465a	n.d.	n.d.	n.d.	3.81E-05	2.73E-05
KF01366a	n.d.	n.d.	n.d.	3.36E-05	3.86E-05
ZZ000726a	> 50 µM	n.d.	9.93E-07	> 50 µM	> 50 µM
KF01355a	8.19E-06	n.d.	6.75E-07	n.d.	n.d.
KF01115a	> 50 µM	n.d.	1.41E-06	n.d.	n.d.
ZZ000938aNA	1.80E-06	n.d.	1.63E-06	n.d.	n.d.
PK005950f	6.55E-06	n.d.	2.28E-06	n.d.	n.d.
XS037212gCL	n.d.	1.84E-06	2.71E-06	n.d.	n.d.
KF01140a	1.28E-05	n.d.	2.80E-06	n.d.	n.d.
KF01280a	n.d.	9.09E-07	3.49E-06	n.d.	n.d.
KF01185a	2.68E-05	n.d.	3.77E-06	n.d.	n.d.
KF01304a	n.d.	n.d.	4.47E-06	n.d.	n.d.
KF01281a	n.d.	6.41E-07	4.94E-06	n.d.	n.d.
KF01303a	n.d.	n.d.	6.74E-06	n.d.	n.d.
LENA69	n.d.	n.d.	8.76E-06	n.d.	n.d.
KF01452a	n.d.	n.d.	9.71E-06	n.d.	n.d.

KF01240a	n.d.	n.d.	1.06E-05	n.d.	n.d.
KF01286a	n.d.	n.d.	1.26E-05	n.d.	n.d.
LENA82	> 50 µM	n.d.	1.42E-05	n.d.	n.d.
KF01062a	n.d.	n.d.	1.42E-05	n.d.	n.d.
KF01292a	n.d.	n.d.	1.54E-05	n.d.	n.d.
KF01455a	n.d.	n.d.	1.55E-05	n.d.	n.d.
LENA73	n.d.	n.d.	1.56E-05	n.d.	n.d.
LENA87	n.d.	n.d.	1.63E-05	n.d.	n.d.
LENA133	n.d.	n.d.	1.86E-05	n.d.	n.d.
KF01466a	n.d.	n.d.	1.98E-05	n.d.	n.d.
KF01375a	n.d.	n.d.	2.21E-05	n.d.	n.d.
KF01377a	n.d.	n.d.	2.61E-05	n.d.	n.d.
PK000236e	> 50 µM	n.d.	2.88E-05	n.d.	n.d.
ZZ000936a	n.d.	5.46E-06	3.60E-05	n.d.	n.d.
KF01040a	n.d.	1.54E-06	n.d.	n.d.	n.d.
KF01052a	n.d.	n.d.	n.d.	n.d.	n.d.
LENA57	n.d.	n.d.	n.d.	n.d.	n.d.
KF01418a	n.d.	n.d.	n.d.	n.d.	n.d.
KF01068a	n.d.	n.d.	n.d.	n.d.	n.d.
PK000244i	> 50 µM	n.d.	> 50 µM	n.d.	n.d.
KF01094a	n.d.	n.d.	> 50 µM	n.d.	n.d.
KF01379a	n.d.	2.83E-09	n.d.	n.d.	n.d.
LENA29	n.d.	4.29E-09	n.d.	n.d.	n.d.
LENA126	n.d.	1.30E-08	n.d.	n.d.	n.d.
KF01316a	n.d.	1.38E-08	n.d.	n.d.	n.d.
LENA3	3.86E-07	1.74E-08	n.d.	n.d.	n.d.

KF01091a	2.24E-06	1.33E-07	n.d.	n.d.	n.d.
KF01410a	n.d.	1.50E-07	n.d.	n.d.	n.d.
LENA124	n.d.	1.68E-07	n.d.	n.d.	n.d.
KF01472a	n.d.	1.86E-07	n.d.	n.d.	n.d.
LENA1	n.d.	1.88E-07	n.d.	n.d.	n.d.
LENA191	n.d.	2.49E-07	n.d.	n.d.	n.d.
LENA184	n.d.	2.61E-07	n.d.	n.d.	n.d.
KF01257a	n.d.	3.00E-07	n.d.	n.d.	n.d.
LENA67	n.d.	3.00E-07	n.d.	n.d.	n.d.
LENA137	n.d.	3.00E-07	n.d.	n.d.	n.d.
LENA130	n.d.	3.23E-07	n.d.	n.d.	n.d.
LENA90	n.d.	3.37E-07	n.d.	n.d.	n.d.
PK015606a	n.d.	3.87E-07	n.d.	n.d.	n.d.
LENA89	n.d.	5.27E-07	n.d.	n.d.	n.d.
LENA120	n.d.	5.46E-07	n.d.	n.d.	n.d.
KF01093a	n.d.	5.46E-07	n.d.	n.d.	n.d.
KF01532a	n.d.	5.47E-07	n.d.	n.d.	n.d.
KF01160a	n.d.	6.74E-07	n.d.	n.d.	n.d.
KF01143a	n.d.	7.67E-07	n.d.	n.d.	n.d.
LENA31	n.d.	7.68E-07	n.d.	n.d.	n.d.
KF01526a	n.d.	8.96E-07	n.d.	n.d.	n.d.
KF01228a	n.d.	9.17E-07	n.d.	n.d.	n.d.
KF01092a	2.47E-07	9.19E-07	n.d.	n.d.	n.d.
KF01289a	n.d.	9.19E-07	n.d.	n.d.	n.d.
KF01253a	n.d.	1.00E-06	n.d.	n.d.	n.d.
KF01333a	n.d.	1.01E-06	n.d.	n.d.	n.d.

KF01136a	n.d.	1.23E-06	n.d.	n.d.	n.d.
KF01161a	n.d.	1.47E-06	n.d.	n.d.	n.d.
KF01557a	1.09E-06	n.d.	n.d.	n.d.	n.d.
ZZ000861a	7.85E-06	n.d.	n.d.	n.d.	n.d.
ZZ000928a	1.10E-05	n.d.	n.d.	n.d.	n.d.
KF01204a	1.11E-05	n.d.	n.d.	n.d.	n.d.
HD000029e	1.62E-05	n.d.	n.d.	n.d.	n.d.
XS035836e	1.93E-05	n.d.	n.d.	n.d.	n.d.
KF01519a	3.43E-05	n.d.	n.d.	n.d.	n.d.
ZZ000934a	4.07E-05	n.d.	n.d.	n.d.	n.d.
KF01219a	4.18E-05	n.d.	n.d.	n.d.	n.d.
LENA111	> 50 μ M	n.d.	n.d.	n.d.	n.d.

SI tables to chapter 5.3 Assessing the human kinome using the NanoBRET technology

SI Table 6 | FDA approved and clinical kinase inhibitors for the NanoBRET kinase panel.

Catalog Number	Product Name	Target	CAS Number	SMILES
S2922	Icotinib	EGFR	610798-31-7	<chem>C#CC1=CC(=CC=C1)NC2=NC=NC3=C2C=C4OCCOCCOCCO4=C3</chem>
S2161	RAF265 (CHIR-265)	Raf, VEGFR	927880-90-8	<chem>C[N]1C(=NC2=C1C=CC(=C2)OC3=CC=NC(=C3)C4=NC=C([NH]4)C(F)(F)F)NC5=CC=C(C=C5)C(F)(F)F</chem>
S2904	PF-477736	Chk	952021-60-2	<chem>C[N]1C=C(C=N1)C2=C3C=NNC(=O)C4=C3C(=CC(=C4)NC(=O)C(N)C5CCCC5)[NH]2</chem>
S1114	JNJ-38877605	c-Met	943540-75-8	<chem>C[N]1C=C(C=N1)C2=N[N]3C(=NN=C3C(F)(F)F)C4=CC5=C(C=C4)N=CC=C5)C=C2</chem>
S1055	Enzastaurin (LY317615)	PKC	170364-57-5	<chem>C[N]1C=C(C=CC=CC=C12)C3=C(C(=O)NC3=O)C4=C[N](C5CCN(CC5)CC6=NC=CC=C6)C7=CC=CC=C47</chem>
S1361	Glesatinib (MGCD265)	c-Met, Tie-2, VEGFR	875337-44-3	<chem>C[N]1C=NC(=C1)C2=CC3=NC=CC(=C3S2)OC4=CC=C(NC(=S)NC(=O)CC5=CC=CC=C5)C=C4F</chem>
S1008	Selumetinib (AZD6244)	MEK	606143-52-6	<chem>C[N]1C=NC2=C(F)C(=C(C=C12)C(=O)NOCCO)NC3=CC=C(Br)C=C3Cl</chem>
S7007	Binimetinib (MEK162, ARRY-162, ARRY-438162)	MEK	606143-89-9	<chem>C[N]1C=NC2=C1C=C(C(=O)NOCCO)C(=C2F)NC3=C(F)C=C(Br)C=C3</chem>
S7492	Uprosertib (GSK2141795)	Akt	1047634-65-0	<chem>C[N]1N=CC(=C1C2=C(Cl)OC(=C2)C(=O)NC(CN)CC3=CC(=C(F)C=C3)F)Cl</chem>

9. Appendix

S7521	Afuresertib (GSK2110183)	Akt	1047644-62-1	C[N]1N=CC(=C1C2=C(CI)SC(=C2)C(=O)NC(CN)CC3=CC=CC(=C3)F)Cl
S7014	Merestinib (LY2801653)	c-Met	1206799-15-6	C[N]1N=CC2=CC(=C(C=C12)C3=C[NH]N=C3)OC4=C(F)C=C(NC(=O)C5=CC=C(C)N(C5=O)C6=CC=C(F)C=C6)C=C4
S1065	Pictilisib (GDC-0941)	PI3K	957054-30-7	C[S](=O)(=O)N1CCN(CC1)CC2=CC3=NC(=NC(=C3S2)N4CCOCC4)C5=CC=CC6=C5C=N[NH]6
S2221	Apatinib?mesylate	VEGFR	1218779-75-9	C[S](O)(=O)=O.O=C(NC1=CC=C(C=C1)C2(CCCC2)C#N)C3=CC=CN=C3NCC4=CC=NC=C4
S8057	Pacritinib (SB1518)	FLT3,JAK	937272-79-2	C1CCN(C1)CCOC2=CC=C3NC4=NC=CC(=N4)C5=CC(=CC=C5)COC\C=C\COCOC2=C3
S8116	Acalabrutinib (ACP-196)	BTK	1420477-60-6	CC#CC(=O)N1CCCC1C2=NC(=C3[N]2C=CN=C3N)C4=CC=C(C=C4)C(=O)NC5=NC=CC=C5
S1526	Quizartinib (AC220)	FLT3	950769-58-1	CC(C)(C)C1=CC(=NO1)NC(=O)NC2=CC=C(C=C2)C3=C[N]4C(=N3)SC5=CC(=CC=C45)OCCN6CCOCC6
S1145	SNS-032 (BMS-387032)	CDK	345627-80-7	CC(C)(C)C1=CN=C(CSC2=CN=C(NC(=O)C3CCNCC3)S2)O1
S2807	Dabrafenib (GSK2118436)	Raf	1195765-45-7	CC(C)(C)C1=NC(=C(S1)C2=NC(=NC=N2)N)C3=C(F)C(=CC=C3)N[S](=O)(=O)C4=C(F)C=CC=C4F
S2784	TAK-285	EGFR,HER2	871026-44-7	CC(C)(O)CC(=O)NCC[N]1C=CC2=C1C(=NC=N2)NC3=CC=C(OC4=CC=CC(=C4)C(F)F)C(=C3)Cl
S2621	AZD5438	CDK	602306-29-6	CC(C)[N]1C=NC=C1C2=NC(=NC=C2)NC3=CC=C(C=C3)[S](C)(=O)=O)C
S2811	Sapanisertib (INK 128, MLN0128)	mTOR	1224844-38-5	CC(C)[N]1N=C(C2=CC3=C(OC(=N3)N)C=C2)C4=C(N)N=CN=C14
S1487	PHA-793887	CDK	718630-59-2	CC(C)CC(=O)NC1=N[NH]C2=C1CN(C(=O)C3CCN(C)CC3)C2(C)C
S7854	Ulixertinib (BVD-523, VRT752271)	ERK	869886-67-9	CC(C)NC1=NC=C(CI)C(=C1)C2=C[NH]C(=C2)C(=O)NC(CO)C3=CC(=CC=C3)Cl
S7083	Ceritinib (LDK378)	ALK	1032900-25-6	CC(C)OC1=C(NC2=NC(=C(CI)C=N2)NC3=C(C=CC=C3)[S](=O)(=O)C(C)C)C=C(C1)C4CCNCC4
S7121	MLN2480	Raf	1096708-71-2	CC(NC(=O)C1=C(CI)C(=NC=N1)N)C2=NC=C(S2)C(=O)NC3=NC=C(CI)C(=C3)C(F)F
S7694	AZD8186	PI3K	1627494-13-6	CC(NC1=CC(=CC=C1)F)C2=CC(=CC3=C2OC(=CC3=O)N4CCOCC4)C(=O)N(C)C
S1462	AZD6482	PI3K	1173900-33-8	CC(NC1=CC=CC=C1C(O)=O)C2=CC(=CN3C(=O)C=C(N=C23)N4CCOCC4)C
S2162	AZD1480	JAK	935666-88-9	CC(NC1=NC=C(CI)C(=N1)NC2=N[NH]C(=C2)C)C3=NC=C(F)C=N3
S2696	Apitolisib (GDC-0980, RG7422)	mTOR,PI3K	1032754-93-0	CC(O)C(=O)N1CCN(CC1)CC2=C(C)C3=NC(=NC(=C3S2)N4CCOCC4)C5=CN=C(N)N=C5
S1084	Brivanib (BMS-540215)	FGFR,VEGFR	649735-46-6	CC(O)COC1=C[N]2N=CN=C(OC3=C(F)C4=C([NH]C(=C4)C)C=C3)C2=C1C
S1068	Crizotinib (PF-02341066)	ALK,c-Met	877399-52-5	CC(OC1=C(N)N=CC(=C1)C2=C[N](N=C2)C3CCNCC3)C4=C(CI)C=CC(=C4Cl)F
S2193	GSK461364	PLK	929095-18-1	CC(OC1=C(SC(=C1)N)2C=NC3=C2C=C(CN4CCN(C)CC4)C=C3)C(N)=O)C5=CC=CC=C5C(F)F
S7144	BMS-911543	JAK	1271022-90-2	CC[N]1C(=CC2=C1N=C(NC3=N[N](C)C(=C3)C)C4=C2[N](C)C=N4)C(=O)N(C5CC5)C6CC6
S1113	GSK690693	Akt	937174-76-0	CC[N]1C(=NC2=C1C(=CN=C2C#CC(C)O)OCC3CCNC3)C4=NON=C4N
S2740	GSK1070916	Aurora Kinase	942918-07-2	CC[N]1C=C(C2=C3C=C([NH]C3=NC=C2)C4=CC=CC(=C4)CN(C)C)C(=N1)C5=CC=C(NC(=O)N(C)C)C=C5
S2718	TAK-901	Aurora Kinase	934541-31-8	CC[S](=O)(=O)C1=CC=CC(=C1)C2=CC(=C(C)C3=C2C4=C([NH]3)N=CC(=C4)C)C(=O)NC5CCN(C)CC5
S2851	Baricitinib (LY3009104, INCB028050)	JAK	1187594-09-7	CC[S](=O)(=O)N1CC(CC#N)(C1)[N]2C=C(C=N2)C3=NC=NC4=C3C=C[NH]4
S1124	BMS-754807	c-Met,IGF-1R,Trk receptor	1001350-96-4	CC1(CCCN1C2=N[N]3C=CC=C3C(=N2)NC4=N[NH]C(=C4)C5CC5)C(=O)NC6=CC=C(F)N=C6

S1018	Dovitinib (TKI-258, CHIR-258)	c-Kit,FGFR,FLT3,PDGFR,VEGFR	405169-16-6	CN1CCN(CC1)C2=CC3=C(C=C2)N=C([NH]3)C4=C(N)C5=C(NC4=O)C=CC=C5F
S2791	Sotrastaurin	PKC	425637-18-9	CN1CCN(CC1)C2=NC(=C3C=CC=CC3=N2)C4=C(C(=O)NC4=O)C5=C[NH]C6=C5C=CC=C6
S1048	Tozasertib (VX-680, MK-0457)	Aurora Kinase	639089-54-6	CN1CCN(CC1)C2=NC(=NC(=C2)NC3=N[NH]C(=C3)C)SC4=CC=C(NC(=O)C5CC5)C=C4
S2859	Golvatinib (E7050)	c-Met,VEGFR	928037-13-2	CN1CCN(CC1)C2CCN(CC2)C(=O)NC3=NC=CC(=C3)OC4=CC(=C(NC(=O)C5(CC5)C(=O)NC6=CC=C(F)C=C6)C=C4)F
S1490	Ponatinib (AP24534)	Bcr-Abl,FGFR,PDGFR,VEGFR	943319-70-8	CN1CCN(CC1)CC2=C(C=C(NC(=O)C3=CC(=C(C)C=C3)C#CC4=CN=C5C=CC=N[N]45)C=C2)C(F)(F)F
S1064	Masitinib (AB1010)	c-Kit,PDGFR	790299-79-5	CN1CCN(CC1)CC2=CC=C(C=C2)C(=O)NC3=CC(=C(C)C=C3)NC4=NC(=CS4)C5=CC=CN=C5
S2475	Imatinib (STI571)	PDGFR	152459-95-5	CN1CCN(CC1)CC2=CC=C(C=C2)C(=O)NC3=CC(=C(C)C=C3)NC4=NC=CC(=N4)C5=CC=CN=C5
S1006	Saracatinib (AZD0530)	Src	379231-04-6	CN1CCN(CCOC2=CC(=C3C(=NC=NC3=C2)NC4=C(C)C=CC5=C4OC05)OC6CCOCC6)CC1
S2726	PH-797804	p38 MAPK	586379-66-0	CNC(=O)C1=CC(=C(C)C=C1)N2C(=CC(=C(Br)C2=O)OCC3=CC=C(F)C=C3)C
S1178	Regorafenib (BAY 73-4506)	c-RET,VEGFR	755037-03-7	CNC(=O)C1=CC(=CC=N1)OC2=CC(=C(NC(=O)NC3=CC(=C(C)C=C3)C(F)(F)C=C2)F
S1040	Sorafenib Tosylate	PDGFR,Raf,VEGFR	475207-59-1	CNC(=O)C1=CC(=CC=N1)OC2=CC(=C(NC(=O)NC3=CC(=C(C)C=C3)C(F)(F)C=C2)CC4=CC=C(C=C4)[S](O)(=O)=O
S2783	Vistusertib (AZD2014)	mTOR	1009298-59-2	CNC(=O)C1=CC=CC(=C1)C2=CC=C3C(=N2)N=C(N=C3N4CCOCC4)N5CCOCC5C
S1005	Axitinib	c-Kit,PDGFR,VEGFR	319460-85-0	CNC(=O)C1=CC=CC=C1SC2=CC3=C(C=C2)C(=N[NH]3)\C=C\4=CC=CC=N4
S2751	Milciclib (PHA-848125)	CDK	802539-81-7	CNC(=O)C1=N[N](C)C2=C1C(C)CC3=CN=C(NC4=CC(=C(C4)N5CCN(C)CC5)N=C23
S2231	Telatinib	c-Kit,PDGFR,VEGFR	332012-40-5	CNC(=O)C1=NC=CC(=C1)COC2=NN=C(NC3=CC(=C(C)C=C3)C4=C2OC=C4
S2634	Rebastinib (DCC-2036)	Bcr-Abl	1020172-07-9	CNC(=O)C1=NC=CC(=C1)OC2=CC(=C(NC(=O)NC3=CC(=N[N]3)C4=CC5=C(C=C4)N=CC=C5)C(C)(C)C=C2)F
S2192	Sapitinib (AZD8931)	EGFR,HER2	848942-61-0	CNC(=O)CN1CCC(CC1)OC2=C(OC)C=C3N=CN=C(NC4=C(F)C(=CC=C4)C)C3=C2
S1010	Nintedanib (BIBF 1120)	FGFR,PDGFR,VEGFR	656247-17-5	COC(=O)C1=CC=C2C(=C1)NC(=O)C2=C(NC3=CC(=C(C3)N(C)C(=O)CN4CCN(C)CC4)/C5=CC=CC=C5
S1107	Danusertib (PHA-739358)	Aurora Kinase,Bcr-Abl,c-RET,FGFR	827318-97-8	COC(C(=O)N1CC2=C(C1)C(=N[NH]2)NC(=O)C3=CC=C(C=C3)N4CCN(C)CC4)C5=CC=CC=C5
S1133	Alisertib (MLN8237)	Aurora Kinase	1028486-01-2	COC1=C(C(=CC=C1)F)C2=NCC3=C(N=C(NC4=CC(=C(C=C4)C(=O)OC)N=C3)C5=C2C=C(C)C=C5
S1164	Lenvatinib (E7080)	VEGFR	417716-92-8	COC1=C(C=C2C(=CC=NC2=C1)OC3=CC(=C(NC(=O)NC4CC4)C=C3)C)C(N)=O
S1014	Bosutinib (SKI-606)	Src	380843-75-4	COC1=C(C)C=C(C)C(=C1)NC2=C(C=NC3=CC(=C(OC)C=C23)OCCCN4CCN(C)CC4)C#N
S1555	AZD8055	mTOR	1009298-09-2	COC1=C(CO)C=C(C=C1)C2=NC3=C(C=C2)C(=NC(=N3)N4CCOCC4)N5CCOCC5C
S1089	Refametinib (RDEA119, Bay 86-9766)	MEK	923032-37-5	COC1=C(N[S](=O)(=O)C2(CC2)CC(O)CO)C(=C(F)C(=C1)F)NC3=CC=C(I)C=C3F
S2727	Dacomitinib (PF299804, PF299)	EGFR	1110813-31-4	COC1=C(NC(=O)/C=C/CN2CCCC2)C=C3C(=NC=NC3=C1)NC4=CC(=C(F)C=C4)C1
S7284	Rociletinib (CO-1686, AVL-301)	EGFR	1374640-70-6	COC1=C(NC2=NC=C(C(=N2)NC3=CC=CC(=C3)NC(=O)C=C)C(F)(F)C=C(C=C1)N4CCN(CC4)C(C)=O

S2247	Buparlisib (BKM120, NVP-BKM120)	PI3K	944396-07-0	<chem>NC1=CC(=C(C=N1)C2=NC(=NC(=C2)N3CCOCC3)N4CCOCC4)C(F)(F)F</chem>
S1352	TG100-115	PI3K	677297-51-7	<chem>NC1=NC2=NC(=C(N=C2C(=N1)N)C3=CC(=CC=C3)O)C4=CC=CC(=C4)O</chem>
S7104	AZD1208	Pim	1204144-28-4	<chem>NC1CCCN(C1)C2=C(C=CC=C2C3=CC=CC=C3)\C=C\4SC(=O)NC4=O</chem>
S7563	AT13148	Akt,S6 Kinase,ROCK,PKA	1056901-62-2	<chem>NCC(O)(C1=CC=C(C1)C=C1)C2=CC=C(C=C2)C3=C[NH]N=C3</chem>
S2700	KX2-391	Src	897016-82-9	<chem>O=C(CC1=CC=C(C=N1)C2=CC=C(OCCN3CCOCC3)C=C2)NCC4=CC=CC=C4</chem>
S2158	KW-2449	Aurora Kinase,Bcr-Abl,FLT3	1000669-72-6	<chem>O=C(N1CCNCC1)C2=CC=C(C=C2)/C=C/C3=N[NH]C4=C3C=CC=C4</chem>
S7036	XL019	JAK	945755-56-6	<chem>O=C(NC1=CC=C(C=C1)C2=CC=NC(=N2)NC3=CC=C(C=C3)N4CCOCC4)C5CCCN5</chem>
S7605	Filgotinib (GLPG0634)	JAK	1206161-97-8	<chem>O=C(NC1=N[N]2C(=N1)C=CC=C2C3=CC=C(CN4CC[S](=O)(=O)CC4)C=C3)C5CC5</chem>
S1134	AT9283	Aurora Kinase,Bcr-Abl,JAK	896466-04-9	<chem>O=C(NC1CC1)NC2=C[NH]N=C2C3=NC4=CC(=CC=C4[NH]3)CN5CCOCC5</chem>
S2219	Momelotinib (CYT387)	JAK	1056634-68-4	<chem>O=C(NCC#N)C1=CC=C(C=C1)C2=NC(=NC=C2)NC3=CC=C(C=C3)N4CCOCC4</chem>
S2753	Tivantinib (ARQ 197)	c-Met	905854-02-6	<chem>O=C1NC(=O)C(C1C2=C[NH]C3=C2C=CC=C3)C4=C[N]5CCCC6=CC=CC4=C56</chem>
S2770	MK-5108 (VX-689)	Aurora Kinase	1010085-13-8	<chem>OC(=O)C1(CCC(C1)OC2=C(F)C(=CC=C2)C)CC3=CC=CC(=N3)NC4=NC=CS4</chem>
S1100	MLN8054	Aurora Kinase	869363-13-3	<chem>OC(=O)C1=CC=C(NC2=NC3=C(CN=C(C4=C(C=C(C34)C)C5=C(F)C=CC=C5F)C=N2)C=C1</chem>
S2248	Silmitasertib (CX-4945)	Casein Kinase	1009820-21-6	<chem>OC(=O)C1=CC=C(C=C1)C3=CN=CC=C3C(=N2)NC4=CC(=CC=C4)C1</chem>
S8041	Cobimetinib (GDC-0973, RG7420)	MEK	934660-93-2	<chem>OC1(CN(C1)C(=O)C2=C(NC3=CC=C(I)C=C3F)C(=C(F)C=C2)F)C4CCCCN4</chem>
S2864	IMD 0354	IκB/IKK	978-62-1	<chem>OC1=C(C=C(C1)C=C1)C(=O)NC2=CC(=CC(=C2)C(F)(F)F)C(F)(F)F</chem>
S7960	Larotrectinib (LOXO-101) sulfate	Trk receptor	1223405-08-0	<chem>OC1CCN(C1)C(=O)NC2=C3N=C(C=C[N]3N=C2)N4CCCC4C5=CC(=CC=C5F)O[S](O)(=O)=O</chem>
S1475	Pimasertib (AS-703026)	MEK	1236699-92-5	<chem>OCC(O)CNC(=O)C1=CC=NC=C1NC2=C(F)C=C(I)C=C2</chem>
S1036	PD0325901	MEK	391210-10-9	<chem>OCC(O)CONC(=O)C1=C(NC2=CC=C(I)C=C2F)C(=C(F)C=C1)F</chem>
S1094	PF-04217903	c-Met	956905-27-4	<chem>OCC[N]1C=C(C=N1)C2=NC3=C(N=C2)N=N[N]3CC4=CC5=CC=CN=C5C=C4</chem>
S1244	Amuvatinib (MP-470)	c-Kit,FLT3,PDGFR	850879-09-3	<chem>S=C(NCC1=CC=C2OCOC2=C1)N3CCN(CC3)C4=NC=NC5=C4OC6=CC=CC=C56</chem>

SI Table 7 | Small molecules that were excluded from the final evaluation due to assay interference.

Compound	SMILES	MW	Color	ALogP	Supplier Catalog No
IMD 0354	<chem>OC1=C(C=C(C)C=C1)C(=O)NC2=CC(=CC(=C2)C(F)(F)F)C(F)(F)F</chem>	383.67		4.921	S2864
Linifanib (ABT-869)	<chem>CC1=CC(=C(F)C=C1)NC(=O)NC2=CC=C(C=C2)C3=C4C(=N[NH]C4=CC=C3)N</chem>	375.41		4.169	S1003
GSK-1059615	<chem>C1=CC2=NC=CC(=C2C=C1C=C3C(=O)[N-]C(=O)S3)C4=CC=NC=C4.O</chem>	333.36			S1360
Varlitinib	<chem>CC1COC(=N1)NC2=CC3=C(C=C2)N=CN=C3NC4=CC(=C(OCC5=NC=CS5)C=C4)Cl</chem>	466.94		4.577	S2755
AZD5438	<chem>CC(C)[N]1C(=NC=C1C2=NC(=NC=C2)NC3=CC=C(C=C3)[S](C)(=O)=O)C</chem>	371.46		2.966	S2621
Sorafenib Tosylate	<chem>CNC(=O)C1=CC(=CC=N1)OC2=CC=C(NC(=O)NC3=CC=C(C)C(=C3)C(F)(F)F)C=C2.CC4=CC=C(C=C4)[S](O)(=O)=O</chem>	637.03		5.824	S1040
Ceritinib (LDK378)	<chem>CC(C)OC1=C(NC2=NC(=C(C)C=C2)NC3=C(C=CC=C3)[S](=O)(=O)C(C)C=C(C)C(=C1)C4CCNCC4</chem>	558.14		6.479	S7083
Bosutinib (SKI-606)	<chem>COC1=C(C)C=C(C)C(=C1)NC2=C(C=NC3=CC(=C(O)C=C23)OCCCN4CCN(C)CC4)C#N</chem>	530.45		4.883	S1014
Orantinib (TSU-68, SU6668)	<chem>CC1=C(CCC(O)=O)C(=C([NH]1)/C=C/2C(=O)NC3=CC=CC=C23)C</chem>	310.35	yellow	2.868	S1470
Amuvatinib (MP-470)	<chem>S=C(NCC1=CC=C2OCOC2=C1)N3CCN(CC3)C4=NC=NC5=C4OC6=CC=CC=C56</chem>	447.51		4.867	S1244
R05126766 (CH5126766)	<chem>CN[S](=O)(=O)NC1=NC=CC(=C1F)CC2=C(C)C3=CC=C(OC4=NC=CC=N4)C=C3OC2=O</chem>	471.46		2.473	S7170
BI-847325	<chem>CCNC(=O)C#CC1=CC=C\2C(=C1)NC(=O)C2=C(NC3=CC=C(CN(C)C)C=C3)/C4=CC=CC=C4</chem>	464.56	yellow	4.041	S7843
Nintedanib (BIBF 1120)	<chem>COC(=O)C1=CC=C\2C(=C1)NC(=O)C2=C(NC3=CC=C(C=C3)N(C)C(=O)CN4CCN(C)CC4)/C5=CC=CC=C5</chem>	539.62	yellow	2.965	S1010
Pexidartinib (PLX3397)	<chem>FC(F)(F)C1=NC=C(CNC2=NC=C(C3=C[NH]C4=NC=C(C)C=C34)C=C2)C=C1</chem>	417.81		4.811	S7818
Erdafitinib (JNJ-42756493)	<chem>COC1=CC(=CC(=C1)N(CCNC(C)C)C2=CC3=NC(=CN=C3C=C2)C4=C[N](C)N=C4)OC</chem>	446.54	yellow	3.943	S8401
Enzastaurin (LY317615)	<chem>C[N]1C=C(C2=CC=CC=C12)C3=C(C(=O)NC3=O)C4=C[N](C5CCN(CC5)CC6=NC=CC=C6)C7=CC=CC=C47</chem>	515.61	orange	4.32	S1055
CI-1033	<chem>C=CC(=O)NC1=C(C=C2C(=C1)C(=NC=N2)NC3=CC(=C(C=C3)F)Cl)OCCCN4CCOCC4</chem>	485.94			S1019
Rebastinib (DCC-2036)	<chem>CNC(=O)C1=NC=CC(=C1)OC2=CC(=C(NC(=O)NC3=CC(=N[N]3C4=CC5=C(C=C4)N=CC=C5)C(C)C(C)C=C2)F</chem>	553.59		5.14	S2634
Sunitinib Malate	<chem>CCN(CC)CCNC(=O)C1=C(C)[NH]C(=C1C)/C=C/2C(=O)NC3=CC=C(F)C=C23.OC(CC(O)=O)C(O)=O</chem>	532.56	orange	-1.049	S1042
Netarsudil	<chem>CC1=CC(=C(C=C1)C(=O)OCC2=CC=C(C=C2)[C@@H](CN)C(=O)NC3=CC4=C(C=C3)C=NC=C4)C</chem>	526.45			S8226
Axitinib	<chem>CNC(=O)C1=CC=CC=C1SC2=CC3=C(C=C2)C(=N[NH]3)\C=C\C4=CC=CC=N4</chem>	386.47		4.492	S1005

9.2 List of publications and collaboration partners

1) Kinase Panel paper

Link: N/A

Authors: Lena M. Berger, Martin P. Schwalm, Andreas Krämer, Susanne Müller, Benedict-Tilman Berger and Stefan Knapp

Status: *manuscript in preparation*

2) Evaluation of current chemogenomic candidates for splicing kinase subfamily

Link: N/A

Authors: Lena M. Berger, Benedict-Tilman Berger, Amelie Tjaden, Lewis Elson, Martin Schröder, Andreas Krämer, Susanne Müller and Stefan Knapp

Status: *manuscript in preparation*

Contribution: First authorship. Design of study. Assay development for all constructs in cellular target engagement assay NanoBRET. Tracer Titration of all constructs. Determination of cellular potency in lysed and intact mode for all tested molecules. Evaluation of the data and interpretation/discussion of the data. Preparation of manuscript.

3) A Toolbox for the Generation of Chemical Probes for Baculovirus IAP Repeat Containing Proteins

Link: <https://www.frontiersin.org/articles/10.3389/fcell.2022.886537/full>

Authors: Martin P. Schwalm, Lena M. Berger, Maximilian N. Meuter, James D. Vasta, Cesear R. Corona, Sandra Röhm, Benedict-Tilman Berger, Frederic Farges, Sebastian M. Beinert, Franziska Preuss, Viktoria Morasch, Vladimir V. Rogov, Sebastian Mathea, Krishna Saxena, Matthew B. Robers, Susanne Müller and Stefan Knapp

Status: accepted on 29 April 2022 in Front. Cell Dev. Biol.

Contribution: *Shared first authorship*. Design of study. Assay development for all constructs in cellular target engagement assay NanoBRET. Tracer Titration of all constructs.

Determination of cellular potency in lysed and intact mode for all tested molecules.
Evaluation of the data and interpretation/discussion of the data.

4) Donated Chemical Probes reveal tumour specific and normal behaviour in patient-derived organoids

Link: N/A

Authors: Claudia Tredup Benardina Ndreshkjana, Natalie S. Schneider, Amelie Tjaden, Aurino M. Kemas, Sonia Youhanna, Volker M. Lauschke, Benedict-Tilman Berger, Andreas Krämer, Lena M. Berger, Sandra Röhm, Stefan Knapp, Henner Farin and Susanne Müller

Status: *in revision process*

Contribution: Support of all chemical probe projects with cellular NanoBRET data. Evaluation of the data and interpretation/discussion of the data.

5) Chemogenomic tool compounds targeting mammalian STE20-like protein kinases 1-4

(MST1-4)

Link: N/A

Authors: Marcel Rak, Amelie Tjaden, Lena M. Berger, Susanne Müller, Stefan Knapp and Thomas Hanke

Status: *manuscript in preparation*

Contribution: Assay development for all constructs in cellular target engagement assay NanoBRET. Determination of cellular potency in lysed and intact mode for all tested molecules against all MSTs and SIK family. Evaluation of the data and interpretation/discussion of the data.

6) Discovery of 3-amino-1H-pyrazole-based kinase inhibitors to illuminate the understudied PCTAIRE family

Link: <https://www.mdpi.com/1422-0067/23/23/14834>

Authors: Jennifer A. Amrhein, Lena M. Berger, Amelie Tjaden, Andreas Krämer, Lewis Elson, Tuomas Tolvanen, Daniel Martinez-Molina, Astrid Kaiser, Manfred Schubert-Zsilavecz, Susanne Müller, Stefan Knapp and Thomas Hanke

Status: published on 27 November 2022 in Int. J. Mol. Sci.

Contribution: Assay development for all constructs in cellular target engagement assay NanoBRET. Tracer Titration of all constructs. Determination of cellular potency in lysed and intact mode for all tested molecules against the whole subfamily. Evaluation of the data and interpretation/discussion of the data.

7) Pharmacokinetic Optimization of Small Molecule Janus Kinase 3 Inhibitors to Target Immune Cells

Link: <https://pubs.acs.org/doi/full/10.1021/acsptsci.2c00054>

Authors: Julian Laux, Michael Forster, Laura Riexinger, Anna Schwamborn, Jamil Guezguez, Christina Pokoj, Mark Kudolo, Lena M. Berger, Stefan Knapp, Dieter Schollmeyer, Jan Guse, Michael Burnet and Stefan A. Laufer

Status: published on 14 July 2022 in ACS Pharmacol. Transl. Sci.

Contribution: Determination of intact and cellular target engagement of compounds against main target JAK3 and determination of cell permeability of compounds. Evaluation of the data and interpretation/discussion of the data.

8) Illuminating the Dark: Highly Selective Inhibition of Serine/ Threonine Kinase 17A with Pyrazolo[1,5-a]pyrimidine-Based Macrocycles

Link: <https://pubs.acs.org/doi/10.1021/acs.jmedchem.2c00173>

Authors: Christian G. Kurz, Franziska Preuss, Amelie Tjaden, Martin Cusack, Jennifer Alisa Amrhein, Deep Chatterjee, Sebastian Mathea, Lena Marie Berger, Benedict-Tilman Berger, Andreas Krämer, Michael Weller, Tobias Weiss, Susanne Muller, Stefan Knapp and Thomas Hanke

Status: published on 24 May 2022 in J. Med. Chem.

Contribution: Determination of cellular target engagement of macrocyclic pyrazolo[1,5-a]pyrimidines on DRAK1 (STK17A) and potential off-targets CK2a1, CK2a2, GAK, BIKE, and DRAK2. Evaluation of the data and interpretation/discussion of the data.

9) Single tracer-based protocol for broad-spectrum kinase profiling in live cells with NanoBRET

Link:

<https://www.sciencedirect.com/science/article/pii/S2666166721005281?via%3Dihub>

Authors: Matthew B. Robers, Jennifer M. Wilkinson, James D. Vasta, Lena M. Berger, Benedict-Tilman Berger and Stefan Knapp

Status: accepted on 17 December 2021 in STAR protocols

Contribution: Contribution to the design and validation of the profiling assay and optimization of general assay protocol. Evaluation of the data and interpretation/discussion of the data.

10) Inhibitors of the Hippo Pathway Kinases STK3/MST2 and STK4/MST1 Have Utility for the Treatment of Acute Myeloid Leukemia

Link: <https://pubs.acs.org/doi/10.1021/acs.jmedchem.1c00804>

Authors: Nicole Bata, Apirat Chaikuad, Nicole A. Bakas, Allison S. Limpert, Lester J. Lambert, Douglas J. Sheffler, Lena M. Berger, Guoxiong Liu, Cunxiang Yuan, Li Wang, Yi Peng, Jing Dong, Maria Celeridad, Fabiana Layng, Stefan Knapp and Nicholas D. P. Cosford

Status: published on 22 November 2021 in J. Med. Chem.

Contribution: Determination of cellular target engagement of compounds against possible off-target LRRK2. Evaluation of the data and interpretation/discussion of the data.

11) Design of a "Two-in-One" Mutant-Selective Epidermal Growth Factor Receptor Inhibitor That Spans the Orthosteric and Allosteric Sites

Link: <https://pubs.acs.org/doi/10.1021/acs.jmedchem.1c00848>

Authors: Florian Wittlinger, David E. Heppner, Ciric To, Marcel Gunther, Bo Hee Shin, Jaimin K. Rana, Anna M. Schmoker, Tyler S. Beyett, Lena M. Berger, Benedict-Tilman Berger, Nicolas

Bauer, James D. Vasta, Cesear R. Corona, Matthew B. Robers, Stefan Knapp, Pasi A. Jänne, Michael J. Eck and Stefan A. Laufer

Status: published on 20 October 2021 in J. Med. Chem.

Contribution: Tested the inhibitors in cellular target engagement assay against EGFR. Evaluation of the data and interpretation/discussion of the data.

12) Structure-Based Design of Selective Salt-Inducible Kinase Inhibitors

Link: <https://pubmed.ncbi.nlm.nih.gov/34086472/>

Authors: Roberta Tesch, Marcel Rak, Monika Raab, Lena M. Berger, Thales Kronenberger, Andreas C. Joerger, Benedict-Tilman Berger, Ismahan Abdi, Thomas Hanke, Antti Poso, Klaus Strebhardt, Mourad Sanhaji and Stefan Knapp

Status: published on 4 June 2021 in J. Med. Chem.

Contribution: NanoBRET assays. Cellular Target Engagement for all tested chemical molecules against main targets SIK2 and SIK3 as well as off-target profiling in cells of lead structures and negative controls against various kinases determined by PanQinase activity assay. Evaluation of the data and interpretation/discussion of the data.

13) Design, Synthesis, and Evaluation of WD-Repeat-Containing Protein 5 (WDR5) Degraders

Link: <https://pubs.acs.org/doi/10.1021/acs.jmedchem.1c00146>

Authors: Anja Dölle, Bikash Adhikari, Andreas Krämer, Janik Weckesser, Nicola Berner, Lena-Marie Berger, Mathias Diebold, Magdalena M. Szewczyk, Dalia Barsyte-Lovejoy, Cheryl H. Arrowsmith, Jakob Gebel, Frank Löhr, Volker Dötsch, Martin Eilers, Stephanie Heinzlmeir, Bernhard Kuster, Christoph Sotriffer, Elmar Wolf and Stefan Knapp

Status: published on 13 May 2021 in J. Med. Chem.

Contribution: Assay Development for WDR5 with newly synthesized tracer molecule. NanoBRET assay for all molecules in intact and lysed assay mode. Evaluation of the data and interpretation/discussion of the data.

14) C81- evoked inhibition of the TNFR1- NFκB pathway during inflammatory processes for stabilization of the impaired vascular endothelial barrier for leukocytes

Link: <https://faseb.onlinelibrary.wiley.com/doi/10.1096/fj.202100037R>

Authors: G. Melissa Krishnathas, Benjamin Strödke, Laura Mittmann, Thomas Zech, Lena M. Berger, Christoph A. Reichel, Silvia Rösser, Tobias Schmid, Stefan Knapp, Susanne Müller, Franz Bracher, Robert Fürst and Iris Bischoff- Kont

Status: accepted on 26 April 2021 in FASEB J.

Contribution: Contribution to *in vitro/ in cellulo* experimental data. Cellular target engagement of C81 against off-targets. Evaluation of the data and interpretation/discussion of the data.

15) A Highly Selective Chemical Probe for Activin Receptor-like Kinases ALK4 and ALK5

Link: <https://pubs.acs.org/doi/10.1021/acscchembio.0c00076>

Authors: Thomas Hanke, Jong Fu Wong, Benedict-Tilman Berger, Ismahan Abdi, Lena Marie Berger, Roberta Tesch, Claudia Tredup, Alex N. Bullock, Susanne Muller, and Stefan Knapp

Status: accepted on 16 March 2020 in ACS Chem. Biol.

Contribution: Determination of cellular target engagement of compounds against main targets ALK4 and ALK5. Evaluation of the data and interpretation/discussion of the data.

9.3 Statutory declarations

Except where stated otherwise by reference or acknowledgment, the work presented was generated by myself under the supervision of my advisors during my doctoral studies. All contributions from colleagues are explicitly referenced in the thesis. The material listed below was obtained in the context of collaborative research. Detailed author contribution can be found in the respective publication which is cited.

Figure 5: Structure activity relationship (SAR) of a pyrazolo[1,5-a] pyrimidine series.

Own contribution: NanoBRET for SAR series and off-target characterization of CK156 (C and D)

Christian Kurz: Synthesis of compounds (A); Franziska Preuss, Deep Chatterjee and Sebastian Mathea: Expressed, purified and co-crystallized DRAK1 (E); Amelie Tjaden: Multiplex assay, cytotoxicity (F)

Figure 6: Design of focused series of PAK1 inhibitor G-5555 to optimized molecule MRIA9.

Own contribution: none

Selectivity of G-5555 was determined by commercial assay service.

Marcel Rak and Thomas Hanke synthesized the compounds; Roberta Tesch and Marcel Rak: Structural Design of compounds

Table 5: Selectivity profile of G-5555.

Own contribution: EC50 determination via NanoBRET assay

Percent of control (%) and IC50 (nM) was determined using commercial assay service

Figure 7: CDK selectivity determination.

Own contribution: NanoBRET evaluation of compound 21i; 42d and 43d against CDK family (C and D)

Jennifer Amrhein and Thomas Hanke: Compound design and synthesis

Figure 9: Viability assessment and live-cell high content screen of the splicing compounds.

Own contributions: none

Amelie Tjaden: Cytotox assay, Assay design conduction, figure preparation

Figure 10: Inhibitor profiling to access druggability of the splicing kinases.

Own contributions: NanoBRET assay, Figure preparation, Data evaluation

Lewis Elson: Conduction DSF assay for 96 kinase plus splicing kinases

Figure 11: Hits of an "Initial Screen" against understudied kinases PRP4, HIPK4, SRPK3 and DYRK3.

Own contribution: NanoBRET assay, Figure preparation, Data evaluation

Benedict-Tilman Berger: NanoBRET assays of initial screening library

Lewis Elson: Conduction of DSF assay PRP44, HIPK4, SRPK3 and DYRK3, against initial screening library

Figure 13: Comparison of data across multiple assay platforms.

Own contributions: NanoBRET assay, Figure preparation, Data evaluation

Lewis Elson: Conduction of DSF assay

Figure 16: Synthesis of design of WDR5 degraders based on two different literature WDR5 binders.

Own contribution: none

Anja Dölle: Compound design and synthesis

Figure 18: Phylogenetic tree of BIRC family.


Own contribution: none

Martin P. Schwalm: Sequence alignment and design of BIRC tree

Figure 19: NanoBRET Tracer Titration and full-length screening data of compound set.

Own contribution: Conducting NanoBRET assay, Figure preparation (A and B)

Stefan Knapp: Figure idea/ Martin P- Schwalm: Figure preparation (C)



Whenever a figure, table or text is identical to a previous publication (or close to the original publication), it is stated explicitly in the thesis that copyright permission and/or co-author agreement has been obtained:

Figure 5: Permission granted by ACS publications on 2023-01-12.

Figure 6/ Table 5: Permission granted by ACS publications on 2023-01-12.

Figure 7: Permission granted by MDPI on 2023-01-12. Licensee MDPI, Basel, Switzerland. This article is an open access article distributed under the terms and conditions of the Creative Commons Attribution (CC BY) license (<https://creativecommons.org/licenses/by/4.0/>).

Figure 16/ 17: Permission granted by ACS publications on 2023-01-12.

Figure 18/ 19: All Frontiers articles from July 2012 onwards are published with open access under the Creative Commons CC-BY license (the current version is CC-BY, version 4.0). This means that the author(s) retains copyright, but the content is free to download, distribute, and adapt for commercial or non-commercial purposes, given appropriate attribution to the original article.